RECRUITMENT OF p63-EXPRESSING DEEP AIRWAY STEM CELLS FOR LUNG REPAIR FOLLOWING H1N1 INFLUENZA INFECTION IN MICE

POOJA ASHOK KUMAR

NATIONAL UNIVERSITY OF SINGAPORE

2012

RECRUITMENT OF p63-EXPRESSING DEEP AIRWAY STEM CELLS FOR LUNG REPAIR FOLLOWING H1N1 INFLUENZA INFECTION IN MICE

POOJA ASHOK KUMAR

(*B.Tech, Anna University*)

A THESIS SUBMITTED

FOR THE DEGREE OF DOCTOR OF PHILOSOPHY

IN COMPUTATION AND SYSTEMS BIOLOGY

(CSB)

SINGAPORE-MIT ALLIANCE

NATIONAL UNIVERSITY OF SINGAPORE

2012

DECLARATION

I hereby declare that this thesis is my original work
and it has been written by me in its entirety.
I have duly acknowledged all the sources of
information which have been used in the thesis.

This thesis has also not been submitted for any degree in any university
previously

Pooja Ashok Kumar

9 November 2012

ACKNOWLEDGEMENTS

First and foremost I would like to express my deepest gratitude to my supervisors, Prof. Frank McKeon and A/Prof. Wa Xian for their support, scientific advice as well as constant encouragement throughout my PhD candidature. Their incredible passion for science and dedication to research has truly amazed me. They have not only provided me with advice and taught me how to ask the correct questions, but also been very patient and worked closely with me at each step giving me hands-on training in different techniques whenever I needed guidance. They supported me through all the failures and disappointments I encountered, brainstormed with me together, and have always motivated me to continue to work hard. They have gone out of their way to support me and provide me with great opportunities. Prof. Frank McKeon and A/Prof. Wa Xian have taught me to develop not only as a scientist but also as an individual with integrity and I am extremely grateful for having such wonderful people as my mentors during such a critical period in my life and career.

Dr. Yusuke Yamamoto, post doctorial associate at the Xian-McKeon lab has been my guide, critique and a very good friend throughout my time in the lab. I would like to sincerely thank him for his selfless help and contributions to my project. He was the person I went to with the smallest of doubts and he has always been there to guide me. He shared with me his expertise and both trained and helped me in mouse work and all the bioinformatics which is a part of this project. He has been persistently guiding me through the different aspects of working in the lab as well how to analyze and summarize data and present them. He has taught

me to think positively and make the most of every result we obtained during these past four years. I would also like to thank him for his critical reading of the research paper as well as my thesis and for valuable inputs. I look up to him as a knowledgeable and extremely hardworking researcher, as well as a very good friend. I wish him the best with all his endeavors in the future.

I would also like to thank Dr. Yuanyu Hu, post doctorial associate in the Xian-McKeon lab. It has been great, working collaboratively with her on the airways stem cells project and her contributions to the human airway stem cell field is remarkable. Dr. Hu has also been very supportive and has always given very useful suggestions and advice.

I would also like to show my gratitude to Dr. Yan Sun and Dakai Mu for all their efforts in developing very important hybridomas for the lab, which were essential tools for our projects. I would like to thank other members of the Xian McKeon laboratory including Tay Seok Wei for help and guidance on microarrays as well as Lim Siew Joo Tiffany and Audrey-Ann Liew for all their support and valuable friendship throughout my candidature. I am grateful to all members of the Xian-McKeon lab for making my time in the Xian-McKeon lab a memorable one.

I wish to extend my sincere thanks to my MIT co-supervisor Prof. Jianzhu Chen for accepting me as his graduate student and supporting me during my visit to MIT. Prof. Chen has been very understanding and supportive through-out my candidature. I would also like to thank members of the SMART lab in Singapore including Dr. Gino Limmon and Dr. Dahai Zheng and members of the Chen lab

in MIT for data on initial kinetics experiments as well as all the support and advice they provided during my candidature.

I also wish to extend my gratitude to A/Prof. Vincent Chow for providing us with Influenza virus, Dr. Thomas Lufkin and Dr. Petra Kraus for providing us with the reporter mouse strain and Dr. Bing Lim for advice in the initial stages of the project.

My thanks also goes out to Prof. R.B. Narayanan, Centre for Biotechnology, Anna University for giving me an opportunity to work in his lab during my undergraduate studies. This research experience motivated me to apply for graduate study and a career in science.

I would like to thank the Singapore MIT Alliance for providing me with the opportunity to do my PhD as well as the graduate student fellowship. I would like to thank the Genome Institute of Singapore and the Institute of Medical Biology for being very supportive to my research and providing a great working environment.

I am grateful to the efficient staff of the animal facility at Biological Resource Centre, the microarray unit of the Biopolis Shared Facility and Dr. Graham Wright at the IMB Microscopy Unit for technical help.

A special thank you to all my roommates and friends here in Singapore for their valuable friendship and for making my stay here in Singapore a fun experience. I also wish to thank my grandparents who have supported me at every step since

childhood, and whose loving memories I will cherish forever. Lastly, I would like to thank my parents, sister and Santhosh for the unconditional support and love they have given me through all the ups and downs of graduate study, and their unwavering faith in my abilities without which I would not be here.

TABLE OF CONTENTS

SUMMARY

Airway diseases including Chronic obstructive pulmonary diseases (COPD), Idiopathic pulmonary fibrosis (IPF) and Acute respiratory distress syndrome (ARDS), are listed as the third largest killer worldwide accounting for millions of deaths every year. Influenza virus infections have resulted in some of the most devastating pandemics in world history including the 1918 Spanish flu, which killed millions of people worldwide. Influenza-induced ARDS is characterized by massive infiltration of immune cells and cytokines along with widespread damage to the airway epithelium. The possible stem cell regeneration of the damaged epithelium post infection remains unexplored. While p63+ Krt5+ cells have been implicated as the stem cells of the upper airways, stem cells of the lower airways (which participate in oxygen exchange) is still questionable.

In this study, we developed a mouse model to study H1N1-induced lung damage and repair. A murine-adapted H1N1 influenza virus induced viral pneumonia similar to that observed in humans, with damage to the bronchial as well as alveolar epithelium. A sub-lethal dose of the virus induced sufficient damage in mouse lungs and allowed careful investigation of the repair process post infection. Detailed analyses revealed that p63+ Krt5+ basal stem cells are responsible for the repair of the upper airways mirroring several chemical lung injury model studies. Interestingly, we also observed p63+ Krt5+ pods in the damaged interstitial regions during the repair initiation phase. We demonstrate that this epithelial cell population is actively proliferating *in vivo* and also has

clonogenic ability *in vitro*. Further, *in vitro,* p63+ Krt5+ mouse lung stem cells differentiate into cell types of upper as well as lower airways. Morphological analysis and expression patterns of cell type-specific markers revealed a possible alveolar type I fate of the Krt5+ pods independent of an alveolar type II cell transition. Gene expression profiling of the pods during the course of the repair process also suggested an alveolar differentiation of the Krt5+ pods accompanied by the necessary development of endothelial capillary beds to form potentially functional alveolar units. We also employed genetic tracing systems to track the p63+ Krt5+ cells underlying the basal layer of the bronchial epithelium, migrating into adjacent interstitial regions during extreme damage conditions, to regenerate alveolar epithelium. This work was strongly supported by parallel studies in the Xian-McKeon lab on pedigree analysis of human airway stem cells illustrating that p63+ Krt5+ distal airway stem cells can differentiate into alveolar epithelium *in vitro*.

Overall, this study demonstrates the potential of p63+ Krt5+ stem cells to regenerate bronchial as well as alveolar epithelium post H1N1 induced lung damage. Gene expression analyses of the Krt5+ pods observed *in vivo* provides us with candidate genes and key pathways that can be targeted to understand and manipulate the proliferation, migration and differentiation potential of these cells. The ultimate goal will be to dissect out the underlying mechanisms participating in the synchronized regeneration of different aspects of the airways to develop novel therapeutic intervention to treat patients with life threatening ARDS.

LIST OF TABLES

LIST OF FIGURES

LIST OF ABBREVIATIONS

-	:	negative
%	:	percentage
+	:	positive
<	:	lesser than
>	:	greater than
°C	:	Degree Celsius
3D	:	three dimensional
3H-TdR	:	Tritiated thymidine
3T3	:	3-day transfer, inoculum 3 x 10^5 cells (mouse fibroblasts)
Al	:	alveoli
ALI	:	Acute lung injury
ANOVA	:	Analysis of variance
ARDS	:	Acute respiratory damage syndrome
BADJ	:	Bronchio alveolar duct junction
BALT	:	Bronchus assosciated lymphoid tissue
BASC	:	Bronchio alveolar stem cells
BCS	:	Bovine calf serum
bp	:	base pairs
Br	:	bronchus
BrdU	:	Bromodeoxyuridine
BSA	:	Bovine serum albumin
BSI-B4	:	Bandeiraea simplicifolia lectin I, isolectin B
Bv	:	blood vessel
C57/Bl6	:	C57 black 6
cDNA	:	Complimentary deoxyribonucleic acid
CFA	:	Cryptogenic fibrosing alveolitis
cm	:	centimeter
CO2	:	Carbon dioxide
COLD	:	Chronic obstructive lung disease
COPD	:	Chronic obstructive pulmonary disease

CORD	:	Chronic obstructive respiratory disease
DA	:	damaged alveoli
DAB	:	3, 3'-diaminobenzidine
DAPI	:	4',6-diamidino-2-phenylindole
DMEM	:	Dulbecco's modified media
DNA	:	Deoxyribonucleic acid
dNTP	:	Deoxyribonucleotide triphosphate
dp	:	double positive
dpi	:	days post infection
E	:	Embryonic day
e.g.	:	exempli gratia
ECM	:	Extra cellular matrix
EDTA	:	Ethylenediaminetetraacetic acid
ERt	:	Estrogen receptor T
ES	:	Enrichment score
ES cells	:	Embryonic stem cells
etc	:	etcetera
f	:	forward
FBS	:	Fetal bovine serum
Fig	:	figures
g	:	grams
G	:	gauge
GO	:	Gene ontology
GS I	:	Griffonia (bandeiraea) simplicifolia
GSEA	:	Gene set enrichment analysis
GSIB4	:	Griffonia simplicifolia-IB4
H&E	:	Hematoxylin and Eosin
HCL	:	Hydrochloric acid
Hr	:	hours
IACUC	:	Institutional Animal Care and Use Committee
IF	:	Immunoflourescence

IHC	:	Immunohistochemistry
IP	:	Intraperitoneal
IPF	:	Idiopathic pulmonary fibrosis
Kg	:	kilogram
LCM	:	Laser Capture Microdissection
LD50	:	Lethal Dose, 50%
MDCK	:	Madin Darby canine kidney
Mg	:	milligram
$MgCl_2$	:	Magnesium chloride
Min	:	minutes
ml	:	milliliter
mm	:	millimeter
mM	:	milli Molar
mm^2	:	milli meter square
n	:	sample size
NaCl	:	Sodium chloride
Ncbi	:	National Center for Biotechnology Information
ng	:	Nanogram
NIH	:	National Institute of Health
NO_2	:	Nitrogen dioxide
NP-40	:	Nonyl phenoxypolyethoxylethanol
O_3	:	Ozone
OCT	:	Optimal Cutting Temperature
P	:	Post natal
p	:	P-value
PANTHER	:	Protein ANalysis THrough Evolutionary Relationships
PBS	:	Phosphate buffer saline
PCA	:	Principal component analysis
PCR	:	Polymerase Chain Reaction
Pen/Strep	:	Penicillin/ Streptomycin
PFU	:	Plaque forming unit

pH	:	Potential Hydrogen
PMA	:	Phosphomolybdic Acid
PNE	:	Pulmonary neuroendocrine cells
Ppm	:	Particles per minute
PR	:	Puerto Rico
PTA	:	Phosphotungstic acid
PVDF	:	Polyvinylidine Fluoride
qRT-PCR	:	Quantitative real time Polymerase Chain Reaction
r	:	reverse
Rads	:	Radiation absorbed dose
RNA	:	Ribonucleic acid
Rpm	:	Revolutions per minute
RT	:	Room temperature
SARS	:	Severe acute respiratory syndrome
SDS	:	Sodium dodecyl sulphate
sec	:	seconds
SEM	:	Standard error of the mean
SO_2	:	Sulphur dioxide
Sop	:	Standard Operating procedure
sp	:	single positive
SPIA	:	Single Primer Isothermal Amplification
ss	:	single stranded
TBST	:	Tris-buffered saline with Tween
TPCK	:	L-1-tosylamido-2-phenylethyl chloromethyl ketone
U	:	Units
UEA I	:	Ulex europaeus agglutinin 1
UIP	:	Usual Interstitial pneumonia
USA	:	United States of America
UVA	:	Ultraviolet laser A
VIL	:	Ventilator-induced lung injury
WHO	:	World Health Organization

x	:	times
X-gal	:	5-bromo-4-chloro-indolyl-β-D-galactopyranoside
α	:	alpha
β	:	beta
γ	:	gamma
µg	:	microgram
µm	:	micrometer
µM	:	micro Molar

CHAPTER 1:INTRODUCTION

1.1 Lung architecture

The respiratory system of an organism performs the function of gas exchange. The lungs are a major component of the respiratory system for most mammals, and are responsible for exchange of oxygen from the atmosphere to the bloodstream and the release of carbon dioxide from the blood into the atmosphere. The lung is a complex organ with a heterogeneous cell population and is most commonly divided into two anatomically distinct epithelial domains, namely the conducting airways and the gas-exchanging airspaces. The conducting airways can further be divided into two compartments, namely the cartilaginous tracheobronchial airways and the bronchiolar airways while the gas exchange airspaces consist of alveolar networks (Fig. 1).

The trachea and the bronchi, together known as the conducting or upper or proximal airways, consist of a stratified columnar epithelium populated with mainly ciliated cells (identified by β tubulin IV) and secretory cells. In humans the secretory cell population in the upper airways is predominantly the Goblet cells (identified by Muc5ac, a mucous marker) while in mouse it is the Clara cells (identified by Clara cell 10 protein, CC10), and less frequently the pulmonary neuroendocrine cells (PNEC). This epithelium is underlined by relatively rare basal cells that are believed to be the progenitor cell population of the upper airways. The bronchi and bronchioles are comprised mostly of columnar Clara

cells interspersed with ciliated cells (in both human and mouse). The main function of the conducting airways is to conduct air to and from the alveoli and to protect the lungs from toxic substances and pathogens. The distal, small or lower airways comprise of small respiratory bronchioles and alveolar region. The alveolar network consists of alveolar type I cells (identified by Podoplanin, PDPN) and cuboidal alveolar type II cells (identified by surfactant protein C, SPC), (Bannister, 1999). The alveolar type I cells are thin walled cells where gas exchange takes place, and the alveolar type II cells release surfactants to maintain the surface tension at the air-water interface and also act as a progenitor cell population for alveolar type I cells (Fehrenbach, 2001; Liu et al., 2006; Mason and Williams, 1977; Rawlins and Hogan, 2006).

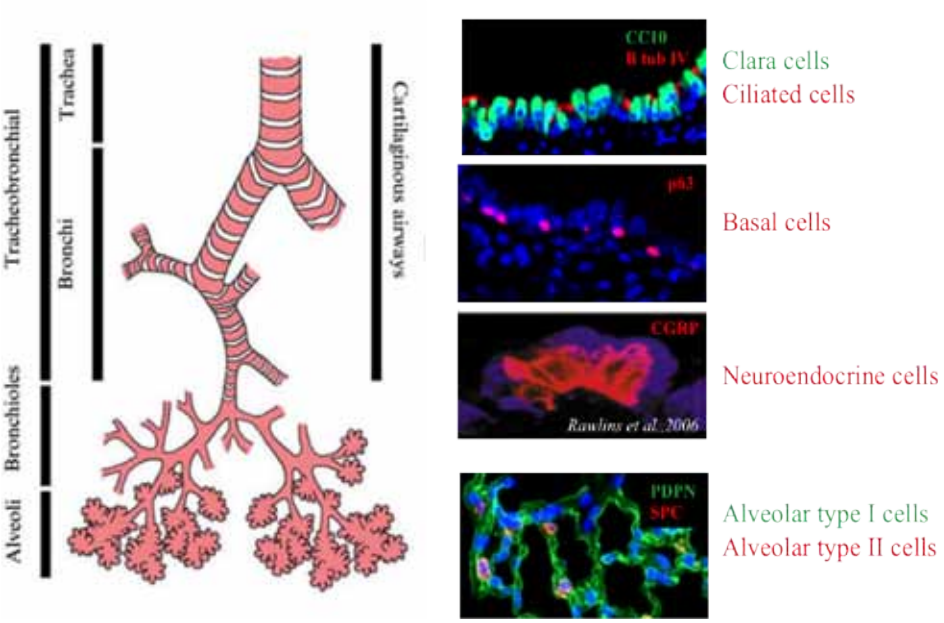

Figure 1 : Lung architecture
Clara cells (CC10, green) and ciliated cells (β tubulin IV red) line the tracheobronchial epithelium of the upper or proximal airways. Interspersed basal cells (p63, red) underlie the differentiated epithelium in the upper cartilaginous airways. Neuroendocrine cells (CGRP, red) are present in the neuroepithelial

bodies in the upper airways. Image adapted from Rawlins and Hogan, 2006). The lower or distal airways consist of the respiratory bronchioles opening up into alveolar sacs. The alveolar region consists of alveolar type I cells (PDPN, green) and alveolar type II cells (SPC, red). Architecture of the lung adapted from Liu et al., 2006.

1.2 Lung development

Human lung organogenesis and development consists of five distinct stages (Post and Copland, 2002). The early phases of development comprises of the first two stages namely the embryonic (day 26 to 52) and pseudoglandular (day 52 to end of 16 weeks of gestation) phases. During these initial phases the hierarchical structure of the system with conductive airways and visible acinar limits are visible. In the pseudoglandular phase, a combined development involving primitive airway epithelium differentiation consisting of neuroendocrine, ciliated and goblet cells as well as mesenchymal cell differentiation to form cartilage and smooth muscle cells is observed (Jeffery, 1998). In the following canalicular phase (17-26 weeks of gestation), the airway branching pattern with respiratory bronchioles are formed. The development of the lower airways is also initiated with increase in vascularization, and differentiation of alveolar type I and II cells releasing surfactants in prospective gas exchange regions (DiFiore and Wilson, 1994). In the following terminal sac phase (24-36 weeks to term), the important steps which occur are the growth of the pulmonary parenchyma, the thinning of the connective tissue between the airspaces and the further maturation of the surfactant system. At birth, the air spaces present are smooth-walled transitory ducts and saccules with primitive septa that are thick and contain a double

capillary network. Although fetal breathing movements are identified by only 8 weeks of development (De Vries et al., 1982), and the lungs are also functional at birth, structurally, the alveoli which are the functional gas exchange units of the adult lungs are not developed. The immature air spaces mature into alveoli through a septation process during the post natal alveolar phase, which is from 36 weeks to term and at least 36 months postnatal (Burri, 1984).

The development of mouse lung is relatively similar to that of human lung development and has been divided in four histological phases (Cardoso and Lü, 2006). Embryonic day (E) 10.5-16.5 is known as the pseudoglandular phase where branching morphogenesis takes place and the bronchiolar tree is formed. Further, the epithelium starts differentiating into Clara, neuroendocrine, and ciliated cells (Metzger et al., 2008). The next stage (E16.5-17.5) is the canalicular phase where the undifferentiated distal epithelium continues to branch and form terminal sacs. In the terminal sac phase (E17.5- postnatal day (P) 5), the number of terminal sacs continues to increase and the type I and II alveolar epithelial cells begin to develop. The terminal sac develops into mature alveoli during the alveolar phase (P5-30).

1.3 Airway diseases

Diseases of the airways such as asthma and chronic obstructive pulmonary disease (COPD), and parenchymal lung diseases such as idiopathic pulmonary fibrosis (IPF), pulmonary hypertension, pneumonia, and acute respiratory damage

syndrome (ARDS) are on the rise every year. After heart diseases and cancer, the US Centre for Disease control listed respiratory diseases including COPD, IPF and ARDS as the third largest killer, affecting about 600 million individuals worldwide in 2007 (Balkissoon et al., 2011; Tansey et al., 2007; Xian and McKeon, 2012).

COPD, also known as chronic obstructive lung disease (COLD), or chronic obstructive respiratory disease (CORD), is caused by the occurrence of chronic bronchitis or emphysemas. This leads to the narrowing of the airways, which subsequently limits the flow of air to and from the lungs resulting in dyspnea or shortness of breath (National Heart Lung and Blood Institute, 2010). Tobacco smoke is the most recognized cause for COPD globally. There are however other exposures that can cause COPD related to occupation or environment such as organic and inorganic dusts, chemical fumes, smoke, biomass fuels etc (Blanc et al., 2009). 20% - 30% of individuals who smoke develop evidence of COPD (Balkissoon et al., 2011), and COPD alone is amongst the leading five causes of death worldwide (Mathers and Loncar, 2006). Investigators have used several approaches to study COPD in animal models. For example, targeted disruption of the cystic fibrosis transmembrane receptor gene (CFTR) in pigs recapitulated human cystic fibrosis quiet accurately (Rogers et al., 2008a; Rogers et al., 2008b). Genetic approaches including over-expression or knock-down of COPD relevant human genes in mice (Baron et al., 2011) in combination with cigarette exposure models are more commonly used (Baron et al., 2011; Shapiro, 2007).

IPF, or cryptogenic fibrosing alveolitis (CFA), is a progressive and commonly fatal disease. It is characterized by sequential acute lung injury, and chronic inflammation with subsequent scarring due to extensive fibroblast proliferation and extracellular matrix remodeling (Fellrath and Bois, 2003; Gribbin et al., 2006). IPF is associated with a pathological lesion known as usual interstitial pneumonia (UIP). UIP shows a pattern of normal lung structure alternating with patches of dense fibrosis as a result of patchy fibroblast-myofibroblast foci. Exercise-induced breathlessness and chronic dry cough are the prevalent symptoms (Meltzer and Noble, 2008). This chronic disease affects an estimated 5 million people all over the world and during the last decade, the incidence of IPF appears to be on the rise (Gribbin et al., 2006; Meltzer and Noble, 2008) . The most common models to study IPF include that of bleomycin (Moeller et al., 2008), and Tgfβ1 transgenic mouse models (Zhou et al., 1996).

First described in 1967, ARDS, or acute lung injury (ALI) is a lung condition that leads to low oxygen levels in the blood (Ashbaugh et al., 1967). ARDS is caused mainly by extensive lung inflammation and small blood vessel injury due to sepsis (bacterial infection of the blood), trauma and/or severe pulmonary infection such as pneumonia. Pathologically, ARDS is characterized by diffuse alveolar damage and pneumonia. The massive infiltration in the lung parenchyma causes the alveolar sacs to be filled with inflammatory cells and cytokines which impairs normal gas exchange functions of the lungs. While the mortality rate of ARDS has improved over the years, the incidence of ARDS in the United Stated is

predicted to be 78.9/100,000 persons per year, with a mortality rate of approximately 40%-50% per year (Mancebo et al., 2006; Rubenfeld et al., 2005; Singer et al., 2006; Zambon and Vincent, 2008). In 2007, the National Heart, Lung and Blood Institute estimated that approximately 190,000 Americans are affected by ARDS annually (NIH, 2007). Although the histopathology of the survivors in human is not accessible, most patients that survive recover their normal lung function in terms of near-normal ranges of spirometry and oxymeter readings within a year of the disease (Tansey et al., 2007) suggesting a normal recovery process.

Mouse models of ARDS are commonly induced by ventilator-induced lung injury (VILI) and hyperoxia (Hosford et al., 2004). Bacterial infection models have also been used in the past in combination with genetically engineered mice involving knock-out or over-expression of different classes of genes including molecules involved in chemoattractant pathways, Toll like receptors and other inflammatory pathways (Albiger et al., 2007; Chen et al., 2001; Ye et al., 2001). Tissue and temporal specificity add additional control in these experiments. In VILI, mice are ventilated with high tidal volumes for 2–8 hours. This causes alveolar stretching which in return induces lung injury. Although the system is clinically very relevant, tidal volumes as high as 20–35 ml/kg would never be considered for human use. Short-term hyperoxic exposure models also result in ARDS in mice. However, a limitation to the use of this hyperoxia model is that the profound lung injury that mice exhibit is not observed in humans, making the system more

artificial (Matute-Bello et al., 2008). As a result, researchers have resorted to using "two-hit" models, which require sequential lung injuries as this reflects clinical disease more accurately (e.g., development of sepsis, followed by the need for mechanical ventilation). The disadvantages of these dual-injury models are that they are time intensive, complicated to reproduce, and the interpretations of the biological effects of these injuries become more complex.

One of the major causes of ARDS is viral pneumonia. Several serotypes of Influenza A virus including H1N1 and H5N1 have caused severe viral pneumonia which leads to patients dying of progressively complicated ARDS (Grose, 2004; Perez-Padilla et al., 2009); Centers for Disease Control and Prevention, 2004). In our study we investigate this influenza virus induced ARDS further.

1.4 Influenza virus

Influenza virus is a negative-sense ssRNA virus belonging to the Orthomyxoviridae family. This family consists of five genera, three of which include the influenza viruses namely Influenza virus A, Influenza virus B, and Influenza virus C (International Committee on taxonomy of Viruses). These three genera infect vertebrates and are characterized by the differences in their matrix proteins and nuclear proteins.

Influenza virus A is the most common and can infect human, mammals and birds while Influenza virus B and C are less common, and can infect humans as well as

seals and pigs respectively. Influenza virus causes flu, and is commonly misinterpreted as the common cold caused by rhinovirus. The Influenza A genome consists of eight single-stranded negative sense RNA molecules encoding a total of 11 proteins which include hemagglutinin (HA), neuraminidase (NA), nucleoprotein (NP), M1, M2, NS1, NS2 (NEP: nuclear export protein), PA, PB1 (polymerase basic 1), PB1-F2 and PB2 (Ghedin et al., 2005). Influenza A virus can be further classified based on the 16 hemagglutinin (HA or H) and nine neuraminidase (NA or N) serotypes.

Influenza viruses continue to evolve and give rise to several epidemics and pandemics (Hay et al., 2001). A phenomenon called antigenic drift occurs in Influenza A and B viruses due to the mutability of the RNA genome which leads to recurrent annual epidemics of the disease. Further, because of the segmented RNA genome of the Influenza A virus, they have the ability to undergo genetic reassortments during mixed infections resulting in a phenomenon called antigenic shift. This infrequent phenomenon leads to severe pandemics because of the low immunity of people to these novel strains.

Influenza viruses have the ability to cause sudden, pervasive illnesses in all age groups of the human population on a global scale. The virus has caused several pandemics like the 1918 Spanish flu (H1N1), the 1957 Asian Flu (H2N2), the 1968 Hong Kong flu (H3N2), and more recently the 2009 swine flu (H1N1) pandemic (Hilleman, 2002; Potter, 2001; WHO, 2005). The influenza pandemic

of 1918-1919 has been cited as the most devastating epidemic in recorded world history killing more people than the Great War (World War I), at somewhere between 50-100 million people (Johnson and Mueller, 2002). Even today influenza spreads around the world in seasonal epidemics, resulting in the deaths of between 250,000 and 500,000 people every year (WHO, 2010). Autopsy on 1918 patient samples revealed that there was an uncontrolled inflammatory response resulting in extensive tissue damage in the lung which ultimately led to lung failure and death of millions of people (Knobler, 2005). Investigations of recent influenza pandemics revealed that death was often associated with widespread viral antigen expression in, and damage to, respiratory epithelia in the tracheobronchial as well as alveolar regions, secondary bacterial infections and ultimately multiple organ failure (Gill et al., 2010; Lowy, 2003; Wu et al., 2011). Influenza virus A induces interstitial pneumonia, characterized by a rapid onset of inflammatory cytokines and immune cell infiltration resulting in, diffuse alveolar damage and associated hypoxemia (Berthiaume et al., 1999; Matuschak and Lechner, 2010; Ramsey and Kumar, 2011).

Although we understand the causes and terminal pathology of H1N1 influenza induced ARDS, the recovery processes from ARDS is still unclear. ARDS patients show improved lung function six to twelve months after the disease, but some patients still exhibit both pulmonary and extrapulmonary deficits in the long term (Herridge et al., 2003). Whether this recovery involves adaptive remodeling or stem cell induced regenerative process remains an area of intense study. It can be hypothesized that local stem cell populations are involved in the regenerative

process and this area of study could provide a new insight into airway recovery mechanisms.

1.5 Lung stem cells

Most adult tissues such as gastrointestinal tract, skin, and blood are believed to contain multipotent stem cells. These populations of cells are essential for maintaining normal self-renewal and homeostasis (Fuchs and Segre, 2000; Fuchs et al., 2004). They can undergo long-term self-renewal, as well as produce transit amplifying progenitor cells that can self-renew in the short term and also give rise to tissue-specific differentiated cell types. The lungs are constantly exposed to harmful pollutants and pathogens and yet they exhibit the capability to recover from the adverse effects. Hence it is critical to study the stem cell populations in the lung and elucidate the underlying pathways and key molecules involved. The time needed to replace all cells of a given population, termed cell turn-over time, is quite variable and depends on the specific tissue, developmental stage or age, and pathogenic conditions. At steady state, the airway epithelia have a very low turnover rate. The turnover rates can be as small as two to ten days for bronchial epithelium of adult mammals, and 4-5 weeks for the alveolar epithelium (Bowden, 1983). Owing to the low turn-over rate of the lung epithelium, stem cells in the lung have been most commonly studied using *ex vivo* systems like xenograft models, *in vivo* studies like chemical injury models, or *in vitro* culture systems (Liu et al., 2006).

Recently, Rawlins and colleagues (Rawlins et al., 2009a) identified an Id2+ self-

renewing, multipotent progenitor cell population in the pseudoglandular stage of mouse lung development that can contribute to all epithelial cell lineages, including the bronchial epithelium, alveolar epithelium and neuroendocrine cells. Thus, in the developing lung, a single stem cell has been identified which can differentiate into the entire lung epithelium. However, there is no evidence of these Id2+ progenitor populations in adult lungs. The field of stem cells in the adult lung is still controversial as some believe the region-specific progenitor cell model in which the trachea, bronchioles, and alveoli are maintained by distinct populations of epithelial progenitor cells (Rawlins et al., 2009b), while others believe a model in which the adult mouse lung contains a population of multipotent epithelial stem/progenitor cells whose descendants give rise to airway and alveolar epithelial cell lineages (Kim et al., 2005; McQualter et al., 2010). There are also some studies which demonstrate that bone marrow or umbilical cord derived stem cells can regenerate lung epithelium (Neuringer and Randell, 2004).

Local adult epithelial stem or progenitor cells identified in the lungs are discussed further in this chapter (Fig. 2).

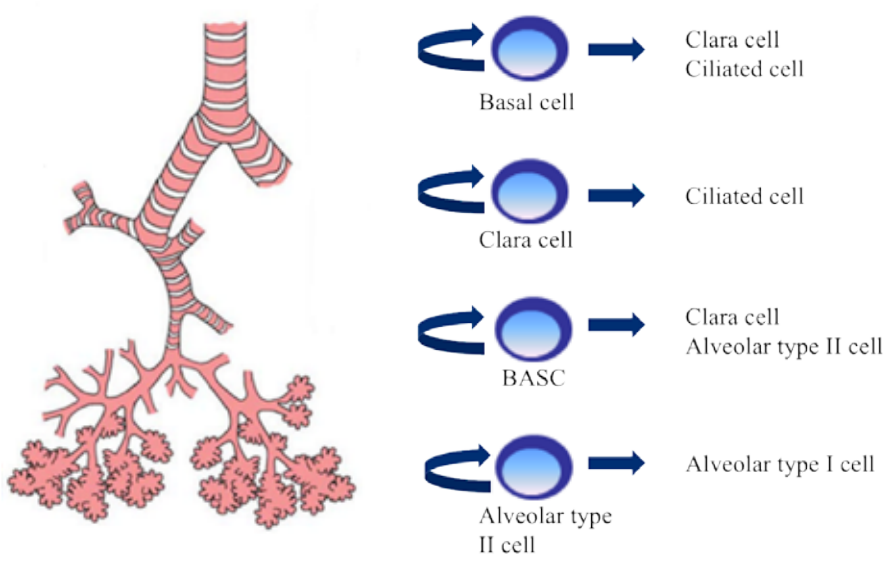

Figure 2 : Putative stem cells in the lung
Basal cells, Clara cells, Bronchioalveolar stem cells and alveolar type II cells have been proposed as putative stem or progenitor cell populations in the adult lung. Architecture of the lung adapted from Liu et al., 2006.

1.5.1 Clara cells

As early as 1978, it was speculated that Clara cells can self-renew and give rise to ciliated cells in the bronchioles in response to chemical injury (Evans et al., 1978). These early reports were supported later by experiments involving selective chemical depletion of Clara cells using naphthalene. It was observed that Neuroepithelial bodies (NEBs) (Reynolds et al., 2000b), and the bronchioalveolar duct junctions (BADJ) (Giangreco et al., 2002) sequester regenerative variant Clara cells, which contribute to bronchiolar regeneration. An interesting transgenic suicide gene ablation approach was employed to conclude that this variant Clara cell is both necessary and sufficient to restore the bronchiolar epithelium (Giangreco et al., 2002; Hong et al., 2001; Reynolds et al., 2000b). Proliferation and hyperplasia of pulmonary neuroendocrine cells (PNE) cells also

occurred in this system (Reynolds et al., 2000a) but they were unable to repopulate the ablated epithelium (Hong et al., 2001). More recently, the Scgb1a1-CreERTM transgenic mouse was used to clearly demonstrate that in the post-natal lung, majority of Clara cells could self renew in the trachea and bronchioles and also differentiate into ciliated cells (Rawlins et al., 2009b).

1.5.2 Bronchioalveolar stem cell

Bronchioalveolar stem cells (BASCs) were first identified in a lung tumor model study by (Jackson et al., 2001) in which a Lox–Stop–Lox-K-ras conditional mouse strain (referred to as LSL-K-ras G12D) was used to develop lung tumors. Expression of oncogenic K-ras was induced in this model by administration of AdenoCre virus into the lungs which removed the floxed stop element. This model gave rise to adenocarcinomas which contained a population of unique double positive cells (CC10+ SPC+) suggesting their role in tumor initiation. Kim and colleagues (Kim et al., 2005) further illustrated that these cells, renamed as Bronchioalveolar stem cells or BASCs were observed in the normal mouse lungs at the bronchioalveolar duct junction. BASCs are resistant to Napthalene and bleomycin injuries and also proliferate *in vivo* in response to these injuries. BASCs were characterized as Sca-1^{pos} $CD45^{neg}$ $Pecam^{neg}$ $CD34^{pos}$ cells and have tumor initiation potential as well as stem cell properties like self-renewal and multipotent differentiation to CC10+ and SPC+ cell types *in vitro*. These studies suggested their possible stem cell potential to regenerate the distal airways including the terminal bronchioles and the alveolar epithelium. Subsequent

studies illustrate the importance of Bmi1 for the self-renewal of these BASCs (Dovey et al., 2008; Zacharek et al., 2011). However the BASCs theory is not supported by single cell cloning assays, transplantation studies or lineage tracing experiments. Further, Rawlins and colleagues (Rawlins et al., 2009b) conducted lineage tracing experiments using a CC10 driven reporter system to clearly demonstrate that there is no special function of the BASCs cell population during postnatal growth, adult homeostasis, or repair.

1.5.3 c-kit+ stem cells

Kajstura and colleagues (Kajstura et al., 2011) recently reported a pool of resident multipotent cells in the human lung with stem cell potentials including self-renewal, clonogenicity, and multipotentiality *in vitro*. *In vivo*, these c-kit+ cells had the ability of creating human bronchioles, alveoli, and pulmonary vessels in immunosuppressant mice after cryo-injury. Their long term proliferation and self-renewal potential was also illustrated in serial-transplantation assays. This research has opened up a whole new avenue in the stem cell field arguing that there is one adult stem cell which can differentiate to cell types of different germ layers including epithelial cells of endodermal origin and pulmonary vessels derived from the mesoderm (Morrisey and Hogan, 2010). These results will need careful validation experiments to confirm the existence of such multipotent adult stem cell populations and their function in adult human lungs.

1.5.4 Alveolar type II cells

There is significant evidence suggesting that alveolar type II cells are the major progenitor cell population of the alveolar region and can differentiate to alveolar type I cells. Evans and colleagues used a nitrogen dioxide (48 hours of exposure to 15-17 ppm NO_2) chemical injury model in rats to demonstrate that alveolar type II cells may contribute to alveolar type I cell regeneration (Evans et al., 1973). Tritiated thymidine (3H-TdR), used to label dividing cells was detected in alveolar type II cells one hour after injury. The researchers followed the rats for several days to show an increase in labeled type I cells population with time thus suggesting that alveolar type II cells transform to type I cells. Around the same time, Adamson and Bowden reported similar results with the same 3H-TdR labeling system in mice exposed to 90% oxygen for 6 days to conclude that alveolar type II cells can transform into alveolar type I cells (Adamson and Bowden, 1974). Bleomycin injury models analyzed by light and electron microscopy as well as phospholipid analysis of the alveolar washings supported the hypothesis that alveolar type II cells divide and subsequently transform into type I cells during repair (Aso et al., 1976).

1.5.5 Basal cells

It has long been supposed that, by analogy to epidermal basal cells, basal cells in the trachea and bronchi play a pivotal role as stem cells in maintenance of the mucociliary epithelium of the upper airways. Back in the 1980s, Inayama and colleagues suggested that the basal cells are the major stem cell population of the

large airways in rabbits. They used centrifugal elutriation to isolate a majority fraction of rabbit basal cells (83-94%) and directly (Inayama et al., 1988) or after single cell cloning (Inayama et al., 1989) inoculated them in denuded tracheal grafts, which were transplanted in mice. In four weeks a fully differentiated epithelium consisting of basal cells, secretory cells, goblet cells and ciliated cells was obtained in these grafts. These studies were also supported by a numerous 3H-TdR labeling studies (Breuer et al., 1990) as well as morphometric studies (Evans et al., 1990; Evans and Plopper, 1988). Johnson and colleagues (Johnson et al., 1990a; Johnson et al., 1990b) used flow cytometry of rat tracheal cells to separate small, agranular cells (basal cells) from large, granular cells (secretory cells), and suggested that secretory cells are highly proliferative and multipotent whereas basal cells are more restricted in their ability to grow and differentiate.

Although these data were suggestive of a possible stem cell potential of basal cells, the above experiments were conducted based on rather non reliable parameters to identify basal cells including cell density, size, and granularity for cell. Secondly, a big problem in the field was the absence of functionally important unique markers which could be used to identify different populations of cells. Randell et al., 1991, used two biochemical markers, namely cell surface α-galactosyl end groups detected with a lectin from Griffonia (bandeiraea) simplicifolia (GS I) and secondly, the keratin 14-related protein using monoclonal antibodies. The GS I-negative fraction had a lower colony-forming efficiency than the GS I-positive fraction but, it too, was able to repopulate denuded tracheal

grafts with a complete mucociliary epithelium. These results show that both GS I-positive and -negative cells had the potential to proliferate and differentiate into the major tracheal cell types. Ford and Terzaghi-Howe, 1992a, b, used different markers namely Bandeiraea simplicifolia lectin I, isolectin B, ($BSI\text{-}B_4$) and Ulex europaeus agglutinin 1 (UEA I) lectins to sort out basal cells and secretory cells from rats. They observed that only the basal cell population was clonogenic *in vitro,* and when transplanted onto denuded tracheas or segments of inverted intestine, could repopulate the muco-ciliated epithelium. Thus these tracheal graft models demonstrated that both basal and secretory cell-enriched cell populations have the ability to regenerate a completely stratified muco-ciliary epithelium (Liu et al., 1994; Randell et al., 1991).

Researchers also started using chemical injury models such as SO_2 or detergent treatments in genetic tracing mouse models to demonstrate that basal cells are the BrdU label-retaining cells (Borthwick et al., 2001). Finally, Hong and colleagues (Hong et al., 2004a, b) illustrated that when all Clara cells are depleted using the transgenic suicide gene ablation system following naphthalene injury, the Griffonia simplicifolia-IB4, (GSIB4)+ , Keratin 14 (Krt14)+ basal cells are the progenitor cell population of bronchial airways. They also performed lineage tracing using the Krt14 promoter driver CreERt system to demonstrate that the basal cells are capable of either multipotent or unipotent differentiation *in vivo* to restore a fully differentiated tracheo-bronchial epithelium including basal cells, ciliated cells, goblet cells and granular secretory cells.

In vitro colony forming assays also demonstrated that Keratin 5 (Krt5) + basal cells are capable of forming large colonies *in vitro* and in the air liquid system can differentiate to give Clara cells and ciliated cells (Schoch et al., 2004). Basal cells implicated in the regeneration of the tracheobronchial epithelium are positive for stratified epithelial stem cell transcription factor p63. p63 is a member of the p53 family of transcription factors (Yang et al., 1998) and is the master regulator for all stratified epithelia including breast, skin, urothelia, and prostrate (Mills et al., 1999; Senoo et al., 2007; Yang et al., 1999). p63 is expressed in the basal layer of the tracheal and bronchial epithelium in the airways. In the p63 knock-out mouse, the complete absence of basal cells suggests that p63 is essential for the maintenance or survival of the progenitor cell population in the airways (Daniely et al., 2004). p63 is also observed in idiopathic pulmonary disorders in human samples (Chilosi et al., 2002) and non-small cell lung cancers like squamous carcinoma (Massion et al., 2003). Overall, basal cells are believed to be progenitor/stem cell populations of the upper airways and are generally identified with markers such as p63, Krt5 and Krt14.

1.5.6 Embryonic stem cells

Along with adult local stem cell populations, researchers have also studied the potential of embryonic stem (ES) cells in lung development and regeneration. Murine ES cells have been successfully differentiated into alveolar type II cells (Ali et al., 2002) and also the tracheobronchial airway epithelium (Coraux et al., 2005). Recently, human ES cells differentiated in culture into alveolar type II

cells improved survival and ameliorated lung inflammation and fibrosis in mice with experimentally-induced lung injury. This was the first demonstration that cells derived from ESCs can have beneficial effects in lung injury, and it provides a platform for potential therapeutic use of ESCs in a variety of lung diseases (Wang et al., 2010).

Research on adult stem cells has been growing rapidly and the findings have the potential to be applied vastly in regenerative medicine. Adult stem cells have less risk of teratoma formation as they are a more committed population (Ronaghi et al., 2010). This poses an important advantage for clinical purposes over the use of embryonic stem cells or induced pluripotent stem cells (iPS) cells. The lung is a vital organ, which is damaged in a variety of diseases and disorders like COPD, IPF, ARDS, asthma and lung cancers. In our study, we propose to investigate the role of p63+ stem cells in the lung in a physiologically relevant influenza virus infection lung injury model that damages both bronchial and alveolar epithelia and results in severe form of ARDS. The characterization of these stem cells gives us a tremendous opportunity to understand the molecular mechanisms driving lung stem cells and to exploit them in developing regenerative therapeutic strategies for life threatening airway diseases including ARDS.

CHAPTER 2: MATERIALS AND METHODS

2.1 Plaque assay

Plaque assay is a useful technique to measure the concentration of virus or the viral titre. A plaque is defined as an area of cells in a monolayer, which display a cytopathic effect, observed as white spots when visualized by eye. The plaque center may lack cells due to virus-induced lysis. Plaque-forming unit (PFU) is a virus or group of viruses which cause a plaque (Dulbecco and Vogt, 1953).

Plaque assay was performed on Madin Darby canine kidney cells (MDCK, ATCC, USA). MDCK cells were cultured in high glucose DMEM (Invitrogen, USA) with 1% L-Glutamine (Gibco, USA), 10% heat inactivated Fetal bovine serum (Hyclone Laboratories, INC, USA) and 1% Non-essential Amino Acids (Gibco, USA). 3 x 10^5 MDCK cells were seeded per well of a 24 well plate. Cells were incubated for 12-24 hours at 37°C to form confluent monolayer of cells for the plaque assay.

Influenza A H1N1 mouse adapted PR/8/34 (vr-95, ATCC, USA) was used for all the viral infections. The virus stock was amplified by our collaborator A/Prof. Vincent Chow's lab in chicken eggs. Virus dilutions were made from a range of 10^{-1}-10^{-6}x. For example, 50µl stock virus + 450µl DMEM medium containing 1µg/ml TPCK trypsin (Sigma-Aldrich, USA) were mixed together well. This is a 10^{-1}x dilution of the virus. For serial dilution, 50µl of the 10^{-1}x diluted virus was

added to 450µl DMEM containing 1µg/ml TPCK trypsin. This is a 10^{-2}x dilution. The virus was serial diluted until 10^{-6}x in this manner. All virus dilutions were made on ice.

A single monolayer of the MDCK cells in 24 well plates was used for the assay. After aspirating out the medium and washing the cells with PBS twice, the cells were incubated with a range of virus dilutions in 100µl DMEM containing 1µg/ml TPCK trypsin for one hour at 37°C. The assay was performed in triplicates for each dilution. After the incubation, medium containing the virus was aspirated out (and transferred to bleach) and the cells were coated with 1ml of sterilized 1.2% Avicel (FMCB biopolymers, USA) in 2x DMEM medium. The plates were then incubated in an incubator at 37°C for three days.

After three days the medium containing avicel was aspirated out and cells were washed with PBS twice. The cells were then fixed with 4% formaldehyde (Sigma-Aldrich, USA) in PBS for 20 min and then washed again with PBS twice. The wells were then stained with 1% crystal violet (Sigma-Aldrich, USA) in for 20 min, washed under running water and visualized. The number of plaques observed was counted, and the plaque forming unit (pfu) was estimated based on the average number of plaques observed for a particular virus dilution. For example if three plaques in average were observed in wells containing 100µl of 10^{-5} virus the pfu is $3x10^{5}$pfu/100µl.

2.2 Animal procedures

C57/Bl6 adult mice (> 6 weeks old) were infected with a sub-lethal dose of Influenza H1N1 A/PR/8/34 mouse adapted virus by intratracheal inhalation. Virus dilutions were always made in sterile PBS on ice. Mice were anesthetized with IP injection of Ketamine (150 mg/kg) + Xylazine (10mg/kg). The anesthetized mouse was rested on a stand with its front teeth hung over a suture. This causes the mouse airways to be relaxed and accessible. Using flat forceps the tongue of the animal was drawn out of its mouth so that the anatomy can be easily visualized. For viral infections, intratracheal aspiration was performed by pipetting the virus directly into the lungs. 4µl/g (of mouse bodyweight) containing 100pfu virus (diluted in PBS) was introduced into the animal. Sterile PBS 4µl/g (of mouse bodyweight) was administered to the control animals. The tongue of the mouse was held out and the virus was allowed to aspirate into the lungs.

For bleomycin (Sigma-Aldrich, USA) treatment intratracheal intubation was performed. The mouse was positioned on a stand as above and a small cool fiber optic light was placed directly under the animal's throat to illuminate the vocal cords. A 1ml syringe (BD biosciences, USA) fitted with a 30G blunt needle (BD Biosciences, USA) a 23 Gauge (OD) polyurethane catheter (.012"/0.3mm inner diameter and .025"/0.6mm outer diameter, Instech Laboratories, Inc. USA) was used to introduce the bleomycin into the animal. The catheter was gently slid down along the tongue towards the back of the throat into the trachea of the animal. 4µl/g (of mouse bodyweight) containing 6U/kg bleomycin in sterile PBS

was introduced into the animal. Due to respiration, the solution would enter the lungs of the animal. Once the bleomycin was inhaled the catheter was gently removed.

The virus or bleomycin treated mice were placed into the cage and monitored for distress regularly. Bodyweight of mice were also monitored for kinetics experiments after viral infections. If the mice looked very inactive and lost more than 20% of their bodyweight they were euthanized. The animals were euthanized (increasing concentrations of CO_2) and organs were harvested. For BrdU incorporation assays, 30 mg/kg BrdU in sterile PBS was administered IP. All procedures were conducted under IACUC guidelines and approved protocols.

Mice were euthanized by IACUC approved method of CO_2 overdose and tissues (lung, skin etc) were harvested. The mice were pinned down and dissected using standard procedures. After cutting open the skin and muscle layer the diaphragm was carefully cut open without touching the lungs. Once this is done, the lungs collapse immediately. For better histology (paraffin embedding only), the lungs were re-inflated using fixing solution (4% Formaldehyde in PBS). For lung inflation, a small incision was made in the proximal region of the trachea and adult lungs were inflated with approximately 1ml of fixing solution using a 30G needle. The inflated lungs were held by forceps at the trachea and carefully dissected out immediately and transferred to 40ml of fixing solution. Lungs and

other tissues were fixed over night at 4°C with gentle rocking and transferred to 70% ethanol until further processing.

2.3 Tissue/cells processing for cryo-embedding

Freshly harvested lungs (without inflation) or Matrigel embedded structures were embedded in OCT (Tissue-Tek, Japan) on dry ice/liquid nitrogen and placed in -80 °C. 10μm sections were then cut using a Cryotome (Leica Microsystems, Germany) with cryotome blades (Leica Microsystems, Germany) and the sections were placed on polylysine coated glass slides (Menzel Glaser, Thermo scientific, USA). Slides were stored at -80°C until further use.

2.4 Tissue processing for paraffin embedding

For paraffin embedding, lungs harvested from mice were inflated with 4% formaldehyde in PBS and fixed overnight at 4°C. Formaldehyde fixed tissues in cassettes were processed as follows in the Automatic tissue processor (Leica Microsystems, Germany).

Step 1 : 70% ethanol 30 min

Step 2 : 95% ethanol 15 min

Step 3 : 95% ethanol 15 min

Step 4 : 100% ethanol 1 hr

Step 5 : 100% ethanol 2 hr

Step 6 : 100% ethanol 2 hr

Step 7 : Histoclear 30 min

Step 8 : Histoclear 30 min

Step 9 : Histoclear 30 min

Step 10 : Paraffin vacuum 2 hr 20 min

Step 11 : Paraffin vacuum 3 hr

Tissues were then transferred to the Embedding machine (Leica Microsystems, Germany) and embedded into paraffin blocks. The blocks were cut using a microtome (Leica Microsystems, Germany) fixed with a microtome blade (S35 Type, Feather, Japan). 5μm sections were cut and transferred to a waterbath set to 37°C. The sections were flattened out and placed on polylysine coated glass slides (Menzel Glaser, Thermo scientific, USA). After draining the water from the slides, they were placed on a heating block set at 40°C overnight for drying. Slides were then stored at RT until further use.

2.5 Immunocytochemistry on frozen sections

Frozen sections were fixed with freshly prepared 4% formaldehyde in PBS for 20 min at RT. After washing away the fixing solution with PBS well (4x, 5min each), a PAP pen (Invitrogen, USA) was used to circle each tissue section. For Immunohistochemistry (IHC) staining alone, the sections were incubated with 3% hydrogen peroxide (Sigma-Aldrich, USA) for 20 min to block the endogenous peroxidases and washed away well with PBS (3x, 5min each). The sections were blocked and permeabilized with 3% BSA (Sigma-Aldrich, USA) and 0.05% TritonX-100 (Sigma-Aldrich, USA) in PBS for 1 hour at RT. For IF staining

permeabilization with detergent was avoided. After washing the sections with PBS (3x, 5min each), the sections were incubated with respective primary antibodies with appropriate dilution (in PBS) for 2 hr at RT or overnight at 4°C. The primary antibody was washed out well in PBS, 3x, 10min each on a shaker.

For IF staining, the sections were incubated with Alexa-conjugated secondary antibodies (1:300) and 1:500 Hoechst 33342 dye (Invitrogen, USA) in PBS, to counterstain nuclei for 1 hr at RT in the dark. After washing the sections well with PBS (3x, 10min each), the sections were mounted with Vectashield Mounting medium (Vector laboratories, USA) or Antifade (Invitrogen, USA). Cover slips were carefully placed on the sections while avoiding bubbles and sealed with nail polish. Stained slides were stored at 4 °C in the dark and images were taken using Zeiss fluorescence microscope (Observer.Z1, Carl Zeiss, Germany).

For IHC staining, after primary antibody incubation, sections were next incubated with biotinylated secondary antibody (1:300 in PBS) from the appropriate Vector ABC kit (Vector Laboratories, USA). After 30 min incubation at RT, and washing with PBS (3x, 10 min each) the sections were incubated with ABC solution (17µl of A and 17µl of B in 1000µl of water) from the same kit. The sections were washed well with PBS 3x, 5 min each, and incubated with DAB solution (in 2.5ml distilled water put 1 drop buffer, 2 drops DAB and 1 drop H_2O_2, Vector laboratories, USA) for 1-3 min. The reaction was stopped with water for 5 min. Nuclei were counterstained with hematoxylin (Sigma-Aldrich, USA) for

appropriate time (3-5 min) at RT. The slides were immersed in water for 5min and then dehydrated in increasing concentrations of ethanol (50%, 70%, 80%, 90%, and 100%) for 5 min each, and three series of xylene (Sigma-Aldrich, USA) for 5 min each. Sections were mounted using Vectamount mounting medium (Vector Laboratories, USA) and cover slips were placed on sections while avoiding bubbles. The slides were then air-dried and viewed using bright-field Zeiss microscope (Imager.Z1, Carl Zeiss, Germany) or Nikon Eclipse TS100 microscope (Nikon, Japan).

2.6 Immunocytochemistry on paraffin sections

5μm paraffin sections were first de-paraffinized in series of xylene (10min, 3x each) and rehydrated in decreasing concentrations of ethanol (100%, 90%, 80%, 70% and 50%) for 5 min each. Sections were then washed in PBS briefly and antigen retrieval was performed using freshly prepared 10mM sodium citrate, pH 6 (Dako, Denmark). Sections were heated for 20 min in cooker/microwave with the antigen retrieval solution and then cooled down for about 40 min. After briefly washing the sections with PBS, the sections were blocked and incubated with primary and secondary antibodies following similar protocol as that of frozen sections for IF or IHC respectively.

2.7 Primary antibodies

Antibodies used in this study included influenza virus A M2 protein (ab5416;

Abcam, UK), p63, 4A4 clone (Yang et al., 1999), alveolar specific hybridomas namely 13A1, 54D1, 11B6 and 1H8 clone; (Kumar et al., 2011), Krt5 (RM-2106; Neomarkers, USA, LS-c22715; Lifespan Biosciences, Inc. USA), β actin (sc130656; Santa Cruz Biotechnology, Inc. USA), Ecad (sc7870; Santa Cruz Biotechnology, Inc. USA), CC10 (sc-9772; Santa Cruz Biotechnology, Inc. USA), SPC (sc-7706; Santa Cruz Biotechnology, Inc. USA), Pdpn (sc-134483; Santa Cruz Biotechnology, Inc. USA), Aqp5 (sc-9891; Santa Cruz Biotechnology, Inc. USA), Cd45 (sc-53665; Santa Cruz Biotechnology, Inc. USA), BrdU (OBT0030; Accurate Chemicals, USA), p73 (3A6 clone), Krt14(PRB-155P; Covance, USA), Krt6 (ab24646; Abcam, UK), pan-Keratin (c5992; Sigma-Aldrich, USA), SMA (A5228; Sigma-Aldrich, USA), acetylated alpha tubulin (T7451; Sigma-Aldrich, USA), Ki67 (RM-9106; Neomarkers, USA). Murine monoclonal antibodies were generated to rat lung tissue obtained under IRB approval using standard methods (Köhler and Milstein, 1975) in the Xian-McKeon lab.

2.8 *In vitro* culture of mouse and rat lung cells

Lungs were harvested from mouse or rats and immersed in cold Wash buffer (F12 (Invitrogen, USA), 1% Pen/Strep (Gibco, USA), 5% FBS (Hyclone Laboratories, INC, USA), 50μg/ml Gentamycin (Gibco, USA). The trachea and two main bronchi were separated from the lungs and all the five lobes of the lungs were cut with a sterile surgical blade (Braun Aesculap Division, Germany) and digested with Dissociation Buffer (DMEM, 1mg/ml Pronase (Sigma-Aldrich, USA), 0.005% Trypsin (Gibco, USA), 10ng/ml Dnase I (Qiagen, Netherlands),

1%Pen/Strep, 100μg/ml Gentamycin, and 0.25μg/ml Fungizone (Gibco, USA)) overnight at 4°C with gentle rocking. The dissociated cells were then washed well with Wash buffer (atleast 4x, 40ml/lung) to remove any traces of the dissociation enzyme and passed through 40μm cell strainer (BD Biosciences, USA). The single cells are then counted and plated on irradiated 3T3 feeder layers.

3T3 J2 feeder cells (Senoo et al., 2007) were amplified using growth medium (DMEM, 10% Bovine calf serum (Hyclone Laboratories, INC, USA), 1% Pen/Strep and 1% L Glutamine). Amplified cells were lethally gamma irradiated (6000 rads, 1 hour) and evenly plated to form monolayer of irradiated cells.

Dissociated lung cells were plated on the irradiated 3T3 feeder layer and cultured in cFAD (Senoo et al., 2007) growth medium (DMEM : F12 - 3:1 (Invitrogen, USA), 10% FBS, 1% L-glutamine, 5μg/ml insulin (Sigma-Aldrich, Singapore), $2x10^{-9}$ M 3,3', 5-Triiodo-L-Thyronine (Sigma-Aldrich, Singapore), 0.4μg/ml hydrocortisone (Sigma-Aldrich, Singapore), 10^{-10} M cholera enterotoxin (MP Biomedicals, USA) 10ng/ml epidermal growth factor (Upstate biotechnology, Germany), 24 μg/ml adenine (Calbiochem, USA), 1% Pen/Strep). For clonogenic assays, lung cells from each mouse (control and infected) were plated in 10 cm plates each, and colonies obtained were counted after seven days in culture.

To obtain immature colonies, single cell suspensions of three-week-old mouse lungs were plated on 50% growth factor reduced Matrigel (BD Biosciences, USA)

coated plates with irradiated 3T3 feeder layers for two passages, 12 days each. Differential trypsinization of the fibroblasts and epithelial cells with 0.05% trypsin (Gibco, USA) was performed to collect majority p63+ Krt5+ immature epithelial stem cells for various assays.

For culture of rat lung epithelial stem cells, rat lungs were dissected similar to that of mouse using the following Dissociation buffer (DMEM/F12, 5% FBS, 1% Pen/Strep, 0.1mg/ml gentamycin, 2mg/ml, collagenase (Invitrogen , USA)) at 37°C for one hour with gentle rocking. Rat lung single cells obtained were cultured on irradiated 3T3 feeder layer with cFAD medium described earlier. Immature colonies were observed from 7-10 days in culture.

2.9 *In vitro* differentiation of mouse lung stem cells

Mouse lung cells were cultured on irradiated 3T3 for two passages to obtain p63+ Krt5+ colonies. The cells were then differentially trypsinized to obtain the p63+ Krt5+ cells and transferred to 8 chamber slides (BD Biosciences, USA) with 50µl growth factor reduced Matrigel in growth medium (DMEM/F12, 1:1, 15mM HEPES (Gibco, USA), 1% L-glutamine, 1% Pen/Strep, 10µg/ml insulin, 5µg/ml transferrin (Lonza BioScience, Singapore), 0.1µg/ml cholera enterotoxin, 25ng/ml epidermal growth factor, 30µg/ml bovine pituitary extract (Lonza BioScience, Singapore), 5% FBS, 50ng/ml fibroblast growth factor 10 (R&D systems, USA) and 30ng/ml hepatocyte growth factor (R&D systems, USA)) for 4 days. Differentiation was induced until day 12-15 with differentiation medium

(DMEM/ F12, 1:1, 15mM HEPES, 1% L-glutamine, 1% Pen/Strep, 5μg/ml insulin, 5μg/ml transferrin, 0.025μg/ml cholera enterotoxin, 5ng/ml epidermal growth factor, 30μg/ml bovine pituitary extract, 1mg/ml bovine serum albumin (Sigma-Aldrich, USA), 50ng/ml fibroblast growth factor 10 and 30ng/ml hepatocyte growth factor).

Medium was changed every alternate day.The structures tend to hollow out by day 10-15. For IF of the structures, after 15 days in culture the cells in Matrigel were embedded in OCT and placed in -80°C immediately. Cryo-molds containing embedded structures were cut using the cryotome and stained for several markers using standard procedures. For gene expression analysis structures were transferred to Trizol (Invitrogen, USA) after 15 days in culture and used for RNA isolation and cDNA conversion. qRT-PCR was performed with primers for several genes to study the expression profile of immature and differentiation genes.

2.10 *In vitro* differentiation of rat lung stem cells

For rat lung cell differentiation, the epithelial cells were cultured as mouse cells on irradiated feeder layers and were transferred to 8 chamber slides with 50μl growth factor reduced Matrigel in growth medium (cFAD) for 4-5 days and then in differentiation medium (DMEM/F12, 15mM HEPES, 1% L-glutamine, 1:1, 1% Pen/Strep, 10μg/ml insulin, 5μg/ml transferrin, 0.1μg/ml cholera enterotoxin, 25ng/ml epidermal growth factor, 30μg/ml bovine pituitary extract, 5% FBS,

0.01μM retinoic acid (Sigma-Aldrich, USA)) for 15-20 days. Medium was changed every alternate day. For IF of the hollow structures, after 15-20 days in culture the cells in Matrigel were embedded in OCT and placed in -80°C immediately. The cryo-molds containing embedded structures were cut using the cryotome and stained for several markers using standard procedures.

2.11 Immunofluorescence of cells in culture

For IF staining of cultured cells, medium was aspirated out and cells were washed well with PBS. The colonies were then fixed with 4% formaldehyde in PBS for 20 min at RT. After washing the fixing solution well with PBS, the cells were permeabilized and blocked with 0.01% TritonX-100 and 5% FBS for one hour at RT. Cells were incubated with primary antibodies with appropriate dilutions in PBS overnight at 4°C. After washing the primary antibody away with PBS (3x, 10 min each), the cells were incubated with Alexa fluor-conjugated secondary antibodies with appropriate dilutions in PBS for one hour at RT. The secondary antibodies were washed well with PBS (3x, 10 min each), and the nuclei were counterstained with Hoechst 33342. Cells were visualized with Zeiss fluorescence microscope (Observer.Z1, Carl Zeiss, Germany).

2.12 Histology

Hematoxylin and Eosin (H&E), the most popular staining technique for histology, was performed using standard procedures. Paraffin sections were dewaxed and

rehydrated and incubated with Hematoxylin for two minutes and Eosin Y (Sigma-Aldrich, USA) for 10 seconds. Sections were washed in water for the stain to develop. Sections were then dehydrated in series of ethanol and xylene and mounted using Vectamount and visualized under light microscope. Hematoxylin on oxidation results in haematein that combines with aluminium ions to form the active dye-metal complex. The Alum hematoxylin solution imparts a light transparent red stain to the nuclei of cells which rapidly turns blue on exposure to any neutral or alkaline liquid like water. Eosin is a fluorescent, acidic, red dye and binds to basic components of a cell namely, the cytoplasm imparting a pink color to the cytoplasm of cells.

Masson Trichrome staining was performed using the Trichrome Stain (Masson) Kit (Sigma-Aldrich, USA) following standard kit procedure. The kit involves sequential staining of the sections with Biebrich Scarlet-Acid Fuchsin, PTA/PMA and Aniline Blue. Nuclei are counterstained purple with hematoxylin, Cytoplasm and muscle fibers stain red whereas collagen displays blue coloration.

2.13 Western blot

Lungs from control or infected mice were homogenized using a hand held homogenizer and cells were lysed with Nonidet-P40 (NP40) buffer (150mM NaCl, 1.0% NP-40, 50mM Tris-HCl pH 8.0, Protease Inhibitors (Roche diagnostics)). 30µg of total protein for each sample was resolved on a 10% SDS polyacrylamide gel and transferred to methanol-activated PVDF membranes (GE healthcare).

After washing once with TBST (20mM Tris, pH 7.5, 500mM NaCl, 0.1% Tween 20), the membranes were blocked for 1 hour at RT in 5% bovine serum albumin (BSA) in TBST with mild shaking. The blots were then incubated with primary antibody at appropriate dilution in TBST with 2% BSA overnight with gentle shaking at 4°C, washed thrice for 20 minutes with TBST and incubated with horseradish peroxidase-conjugated secondary antibody for 1 hour at room temperature. The blots were washed with TBST 3 times for 5 minutes and visualized using a chemiluminescent substrate (Luminol reagent, Santa Cruz Biotechnologies).

2.14 Quantitative real time polymerase chain reaction

Total RNA was extracted from cells using Pico pure RNA extraction kit (Arcturus, USA) or RNeasy mini kit (Qiagen, Germany) and approximately 1μg RNA was converted to cDNA using the High capacity cDNA Reverse transcription kit (Applied Biosustems, USA). For primer designing, the cDNA sequences of genes from NCBI were imported into the Primer Express 3.0 software (Applied Biosystems, USA). Designed primers were tested by PCR using whole lung, trachea or skin cDNA. Relative transcript levels of different genes were quantified by SYBR green real time PCR (SYBR green PCR Master mix, Applied Biosystems, USA) using ABI Prism 7900HT Sequence Detection System 2.2 (Applied Biosystems, USA). The results were normalized to GAPDH and analyzed using SDS 2.2.2 software. The PCR cycle used for all PCR is as follows.
Step 1: 50°C, 2 min

Step 2: 95°C, 10 min

Step 3: 95°C, 15 sec

Step 4: 60°C, 1 min

Step 5: Repeat Steps 3, 4 40x

The primer sequences used in qRT-PCR are as follows:

Gene	Primer sequence (5'->3')
Sftpa1 f	AGGCAGACATCCACACAGCTT
Sftpa1 r	GCAGGCCTCCAACTTCAGATC
Sfptb f	TGCCCAGGTGCAGCTATCA
Sfptb r	CCAGAATTGAGGGCCTTGTG
SftpC f	GAGCAGACACCATCGCTACCTT
SftpC r	TAGGTTCCTGGAGCTGGCTTAT
Aqp5 f	TTCACCGGCTGTTCCATGA
Aqp5 r	CGATCGGTCCTACCCAGAAG
Ptgs2 f	TGCCTCCCACTCCAGACTAGA
Ptgs2 r	CAGCTCAGTTGAACGCCTTTT

Cftr f	CAGCTCAAACAACTGGAATCTGA
Cftr r	GCTCGAAGTGTCCAGAGTCCTT
CC10 f	ATTACAACATCACCCCACATCTACA
CC10 r	CTGCAGCAGATGGACAGCAT
Muc5ac f	GGTGTCGGCCGGAGAAA
Muc5ac r	GAGCGGTGTTCATGGTACGA
Krt10 f	CAGCTGGCCCTGAAACAATC
Krt10 r	CACGCAGTAGCGACCTTCTG
Krt5 f	CCCCTCTGAACCTGCAAATC
Krt5 r	TCGATGAAGGAGGCAAACTTG
Krt14 f	ACGAGAAGATGGCGGAGAAG
Krt14 r	CTCTGTCTTGCTGAAGAACCATTC
Krt6a f	TGACCCTGAAGAAGGATGTAGATG
Krt6a r	CTGCCTTGGCTTGCAGTTC
Vim f	GCTGCAGGCCCAGATTCA

Vim r	TTCATACTGCTGGCGCACAT
Gapdh f	ATCACTGCCACCCAGAAGAC
Gapdh r	CACATTGGGGTAGGAACAC

Table 1 : Primer list for gene set used for *in vitro* differentiation analysis (Fig. 20C)

Gene	Primer sequence (5'->3')
Fabp5 f	AACGACAGCTGATGGCAGAA
Fabp5 r	GACCAGGGCACCGTCTTG
Krt14 f	ACGAGAAGATGGCGGAGAAG
Krt14 r	CTCTGTCTTGCTGAAGAACCATTC
Pthlh f	GCCTGGGAAACGCAGAGA
Pthlh r	CCAGGCAGACCGAGTCCTT
F13a1 f	GGTCGCTACCCTCAGGAGAAC
F13a1 r	TTCCGCTTTGCAGCTCTTTC
Pf4 f	CGGTTCCCCAGCTCATAGC

Pf4 r	CCGGTCCAGGCAAATTTTC
F2r f	GGCAGTTCGGGTCTGGAAT
F2r r	GGCGTACATGTTCCCGTAAAA
CD36 f	GGACATACTTAGATGTGGAACCCATA
CD36 r	TGTTGACCTGCAGTCGTTTTG
Acvrl1 f	CCCCGAGTGGGTACCAAAA
Acvrl1 r	TCTGTGCGGATGTGCTCATC
Entpd1 f	GTGCGTACCTGGCCGAAT
Entpd1 r	TGATGCTTGGATGTTGGTATCAG
Acvr1b f	CCATGAAAACATCCTTGGCTTT
Acvr1b r	CTGGGTCCAGGTGCCATTAT
Inhba f	ACAAGAGCCGGCTGACAAAA
Inhba r	TAATCCAGCAACTTGCCAACAG
Mmp9 f	CACCTTCACCCGCGTGTAC
Mmp9 r	GCTCCGCGACACCAAACT

Krt6a f	TGACCCTGAAGAAGGATGTAGATG
Krt6a r	CTGCCTTGGCTTGCAGTTC
Gapdh f	ATCACTGCCACCCAGAAGAC
Gapdh r	CACATTGGGGTAGGAACAC

Table 2 : Primer list for microarray validation of mouse lung colonies (Fig.15C)

2.15 Laser capture microdissection

At 12 or 25 dpi mice were sacrificed and the harvested lungs were embedded in OCT and frozen on dry ice immediately to preserve RNA. 10µm cryosections were cut and stained with several antibodies including Krt5, SPC, 11B6 using standard protocols. Desired regions were marked out and the consecutive four sections on membrane slides were stained with Histogene staining solution (Arcturus Bioscience, Inc, USA) briefly and then used for LCM with the PALM® Robot Microbeam laser microdissection system (P.A.L.M. GmbH, Bernried, Germany) using the antibody stained slides as reference. The microdissected cells were collected from the adhesive Cap tubes (Carl Zeiss Microimaging GmbH, Germany) and used for RNA isolation using the PicoPure RNA Isolation Kit (Arcturus Bioscience, Inc, USA).

2.16 Microarray preparation and analysis

The RNA Amplification and cDNA conversion was performed using the WT-Ovation™ Pico RNA Amplification System (NuGEN, UK). This system uses the Ribo-SPIA™ technology, which starts from a minimum of 500pg RNA to get 3-5μg of cDNA. The sense transcript cDNA (ST-cDNA) was then synthesized using the WT-Ovation™ Exon Module (NuGEN, UK). The amplified, single-stranded cDNA was fragmented and labeled for microarray using the FL-Ovation™ cDNA Biotin Module V2 (NuGEN, UK). Fragments and labeled cDNA was then hybridized on GeneChip Mouse Exon 1.0 ST Array (Affymetrix, USA) using appropriate hybridization controls and the chips were scanned. The experiments were conducted in triplicates (each sample was taken from three mice lungs).

GeneChip operating software was used to process all the Cel files and calculate probe intensity values. To validate sample quality, probe hybridization ratios were calculated using Affymetrix Expression Console software. The intensity values were log2-transformed and imported into the Partek Genomics Suite 6.5(beta). Exons were summarized to genes and a 1-way ANOVA was performed to identify differentially expressed genes. p values and fold-change were calculated for each analysis. Heatmaps were generated using Pearson's correlation and Ward's method and Principal Component Analysis was conducted using all probe sets. Pathway analyses were performed using Gene Set Enrichment Analysis (GSEA) software and PANTHER database (Subramanian et al., 2005).

2.17 Genomic DNA extraction and genotyping PCR

Mice were ear-tagged and tail snips were cut following IACUC protocol and BRC SOP for genotyping. Tail snips (< 1cm) were digested at 55°C over night at 800 rpm shaker speed with 500µl proteinase K digestion buffer (50mM Tris pH 7-8, 5mM EDTA, 1% SDS, 0.2M NaCl, 200µg/ml proteinase K (Roche Diagnostics, USA). After cooling the samples to room temperature, equal volume of Phenol/Chloroform/Isoamyl alcohol, 25:24:1 (Sigma-Aldrich, Singapore) was added to each tube and samples were vortexed well (30 sec). Samples were spun down at 13,200 rpm for 10 min to separate out the organic and inorganic phases. The DNA from the top phase was transferred to a new tube while avoiding the interface contamination. Two volumes of 95% ethanol was added to the DNA and the tubes were vortexed and spun down at 13,200 rpm for 5 min to precipitate out the DNA. The DNA pellet was washed with 70% ethanol once and after air-drying the tubes to ensure complete removal of ethanol, the DNA pellet was re-suspended in 100µl water. 1µl of this sample containing a range of 50-100ng of DNA was used for genotyping PCR.

ROSA –LACZ mice were genotyped using the "Gt(ROSA)26Sortm1sor STD" protocol from Jackson Laboratories. Primers used for the PCR are as follows

Primer 1: 5'-GCG AAG AGT TTG TCC TCA ACC-3'

Primer 2: 5'-AAA GTC GCT CTG AGT TGT TAT-3'

Primer 3: 5'-GGA GCG GGA GAA ATG GAT ATG-3'

Expected band size: Mutant = 340 bp, Heterozygote = 340 bp and 650 bp,

Wild type = 650 bp.

Krt14 CreERt2 mice were genotyped using the "Gt(ROSA)26Sortm1(cre/Esr1)Nat" protocol from Jackson Laboratories. Primers used for the PCR are as follows

Transgene forward : 5'-GCG GTC TGG CAG TAA AAA CTA TC-3'

Transgene reverse : 5'-GTG AAA CAG CAT TGC TGT CAC TT-3'

Wildtype forward : 5'-CGT GAT CTG CAA CTC CAG TC-3'

Wildtype reverse : 5'-GGA GCG GGA GAA ATG GAT ATG-3'

Expected band size: Mutant = ~102 bp, Heterozygote = ~102 bp and ~400 bp, Wild type = ~400 bp.

Genotyping PCRs were performed using the Titanium Taq Polymerase enzyme and buffer (Clonetech Laboratories, Inc. USA), 10mM dNTP and 10μM primer mix. The PCR cycle used was as follows.

Step 1: 95°C, 3min

Step 2: 95°C, 30 sec

Step 3: 68°C, 1 min

Step 4: Repeat steps 2,3 for 30 cycles

Step 5: 68°C, 5min

Step 6: 10°C, hold

Samples were loaded on 2% agarose (Invitrogen, USA) gel with 1kb plus ladder (Invitrogen, USA) and visualized using a gel documentation machine (Syngene, USA).

2.18 X-gal staining of mouse lungs

Krt14CreERt2 x Rosa-STOP-Lacz mice were infected with a sub-lethal dose of influenza virus and treated with IP injections of 200mg/kg tamoxifen (Sigma-Aldrich, USA) dissolved in corn oil (Sigma-Aldrich, USA), at 5, 6 and 7 dpi. The mice were monitored regularly and sacrificed at 25 dpi. Mice were dissected and lungs were inflated with 1ml cold fixing solution (4% formaldehyde in PBS). The inflated lungs were incubated in fixing solution on ice for 20 min for the initial fixation of the tissue. After brief fixing, the lungs were washed in PBS two times, and reinflated with Wash buffer (0.2% NP-40, 0.01% sodium deoxycholate, 2mM $MgCl_2$ in PBS). The lungs were then washed in Wash buffer for 30 min, three times each to ensure the formaldehyde was washed off completely. Any remains of fixing solution will interfere with the X-gal enzymatic reaction. The lungs were then placed in the freshly prepared Staining solution (25mM Potassium ferricyanide, 25mM Potassium ferrocyanide, 1mg/ml X-gal (Invitrogen, USA) in Wash buffer) for up to 48 hours at 4°C in dark with gentle rocking. The lungs were then washed in PBS three times to wash away the Staining solution and fixed over night at 4°C in fixing solution. The lungs were then transferred to 70% ethanol and visualized for any blue color from the β galactosidase enzymatic reaction. Whole mount images of the tissues were taken using dissection

microscope (Leica Microsystems, Germany). Skin from the same mice was used as positive control to confirm that the mice were of the correct genotype as Krt14 is robustly expressed in the basal layer of the skin. Tail from Rosa-lacZ mice, which constitutively express β galactosidase was used as a positive control for the lacZ staining. Tissues were embedded in paraffin blocks and stained using standard procedures mentioned earlier. Histoclear (National diagnostics, USA) was used instead of xylene in the dewaxing steps to maintain the blue color obtained from the enzymatic reaction.

CHAPTER 3: INFLUENZA INFECTION MODEL OF LUNG DAMAGE AND IDENTIFICATION OF p63+ Krt5+ PODS DURING REPAIR

3.1 INTRODUCTION

Studies conducted in humans have provided detailed, descriptive information about the onset and progression of both inflammatory and physical changes in the lungs in disease conditions. This has led to various hypotheses about mechanisms of injury, which are difficult to test in humans in clinical settings due to the large number of clinical variables. An ideal animal model would reproduce the mechanisms and consequences of the human disease thus providing a bridge between clinical patient studies and the laboratory set up. These animal models provide an excellent platform to investigate as well as validate important hypothesis to understand human diseases better. There are small but potentially important differences between human and animal airway models on several issues such as variation in airway architecture, animal size, and factors of the immune system including Toll like receptors, mononuclear phagocyte system and chemokine signaling pathways (Matute-Bello et al., 2008). Extrapolation of data obtained from mouse models to the human disease system should be done with caution to account for these differences. Nevertheless mouse models have provided an indispensable tool for the advancement of research in the medical field.

In the past, several chemical injury models have been used to study lung damage and repair. These include oxidizing pollutants such as NO_2, O_3 (Evans et al., 1978; Evans et al., 1976), reducing pollutants such as l,l-Dichloroethylene (Forkert and Reynolds, 1982), 3-methylfuran (Haschek et al., 1984), SO_2 (Kavet and Brain, 1974; Lamb and Reid, 1968) and Naphthalene (Mahvi et al., 1977; Stripp et al., 1995). Bleomycin is a well established model for induced fibrosis in the lungs (Grande et al., 1998).

Influenza induced ARDS has lead to devastating pandemics causing millions of deaths worldwide. Animal models have been used in the past to study the immune response including viremia and pathogenicity post influenza virus infection (Mori et al., 1995). Mouse infection systems have also been utilized to test the efficiency of antiviral drugs such as Zanamivir as potential treatment for pandemic causing strains such as H5N1 Influenza virus A/HongKong/156/97 (Gubareva et al., 1998). Vaccine development against highly virulent vial strains of influenza also require preliminary studies in mice (Lu et al., 1999). In our study we use influenza virus infection as a physiologically relevant model of lung damage to explore the potential stem cell regeneration post infection. Mouse adapted H1N1 Influenza A/PR/8/34 strain (Narasaraju et al., 2010) which was originally isolated from a patient in Puerto Rico in 1934 (Vr-95, ATCC) was used for all our studies. C57/Bl6, a common inbred strain of laboratory mice were used for all experiments unless otherwise specified. This chapter describes the various parameters considered to establish an influenza virus infection lung damage and

repair model as well as the kinetics of the damage and repair process. It has been reported that some human influenza viruses can infect mouse lung epithelial cells (Ibricevic et al., 2006). We investigate the epithelial damage in mouse lungs post influenza virus infection and also report the first observation and characterization of p63+ Krt5+ cells during repair in the lungs post infection.

3.2 RESULTS

3.2.1 Optimization of parameters of viral infection to study lung damage and repair

The first step to establish the model of viral infection was to determine the optimal route of viral administration. Several routes of infection were tested with a colored dye to determine the route of infection which could best deliver most of the dye to all lobes of the lungs. The distribution of the dye to the distal airways was important to study damage and repair of upper as well as lower airways. Amongst several routes of delivery including intra nasal infection and intratracheal instillation, intratracheal aspiration (Fig. 3A) resulted in the best distribution of colored dye such as crystal violet (Fig. 3B). We also confirmed no aspiration of liquid in the stomach through the esophagus (data not shown).

After establishing the route of infection that would ensure efficient delivery of the virus to the lungs, we determined the dose of virus to be used for our study. The aim of our study was to cause sufficient damage to the mouse lungs while keeping

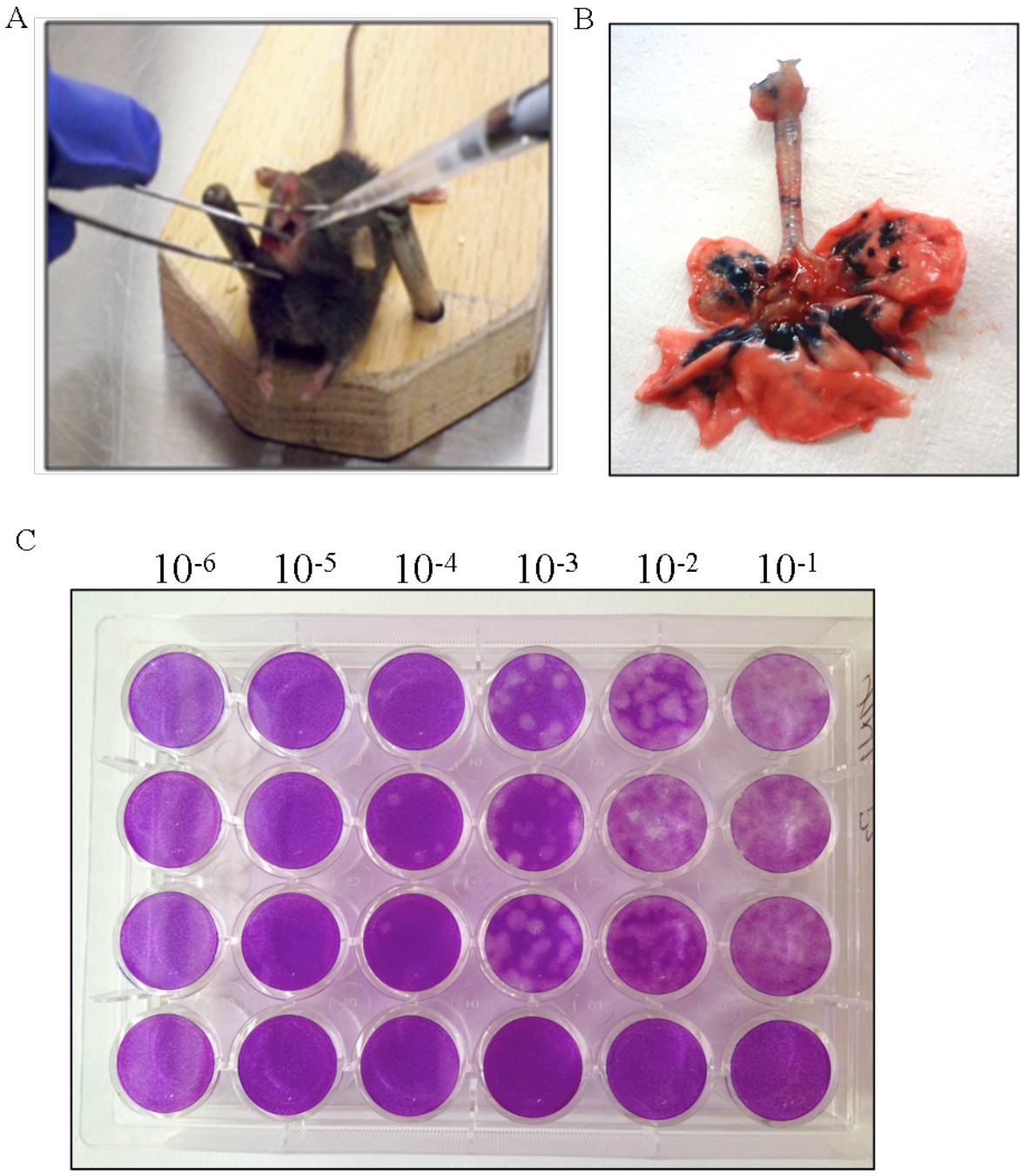

Figure 3 : Route of infection in mice and viral titer estimation
A. Intratracheal aspiration of H1N1 Influenza A/PR/34/8 virus. B. Image of rodent lungs after intratracheal aspiration with crystal violet dye. C. Representative image of plaque assay for H1N1 PR8 virus. An average of three plaques was counted in the three wells of 10^{-4} diluted virus. Thus the viral titer was calculated to be $3x10^4$ pfu/100µl.

the animal alive and able to recover and study the process of lung repair. Bearing this in mind, the sub-lethal dose or LD-50 of the virus, which is the dose of virus, at which at least half the mice survive the infection was first determined.

Plaque assay was performed to estimate the concentration of the virus stock. Fig. 3C represents an image of the plaque assay results using H1N1 stock virus. Since there are in average 3 plaques/well with 10^{-4} dilution of the virus, the concentration of the stock virus was calculated to be $3x10^4$ pfu/100µl. Knowing this initial virus concentration, we infected mice with a range of viral titers including 10^5pfu, 10^4 pfu, 10^3 pfu, 500 pfu, 250 pfu and 125 pfu to determine the LD-50. All virus dilutions were made in cold sterile PBS and the mock infected or control mice were always administered with PBS. 5 mice were used for each viral titer and they were monitored for survival until 23 dpi. As expected, at higher viral titers of 10^5-10^3 pfu all mice died within 6-12 dpi (Fig. 4A, upper panel). 500 pfu was determined to be the LD50 at which about 50% of the mice survived and at 250 and 125 pfu all mice survived (Fig. 4A, lower panel).

After determining the LD50 the next step was to ensure the mice fall sick with the low doses of virus infection. The "gold-standard" for evaluating morbidity in murine models of viral disease including influenza, is measuring the percentage of body weight lost during the course of infection (Mozdzanowska et al., 2005; van der Laan et al., 2008). Though the correlation of weight loss with the extent of lung pathology and the lung-specific immune response is unknown, trend in

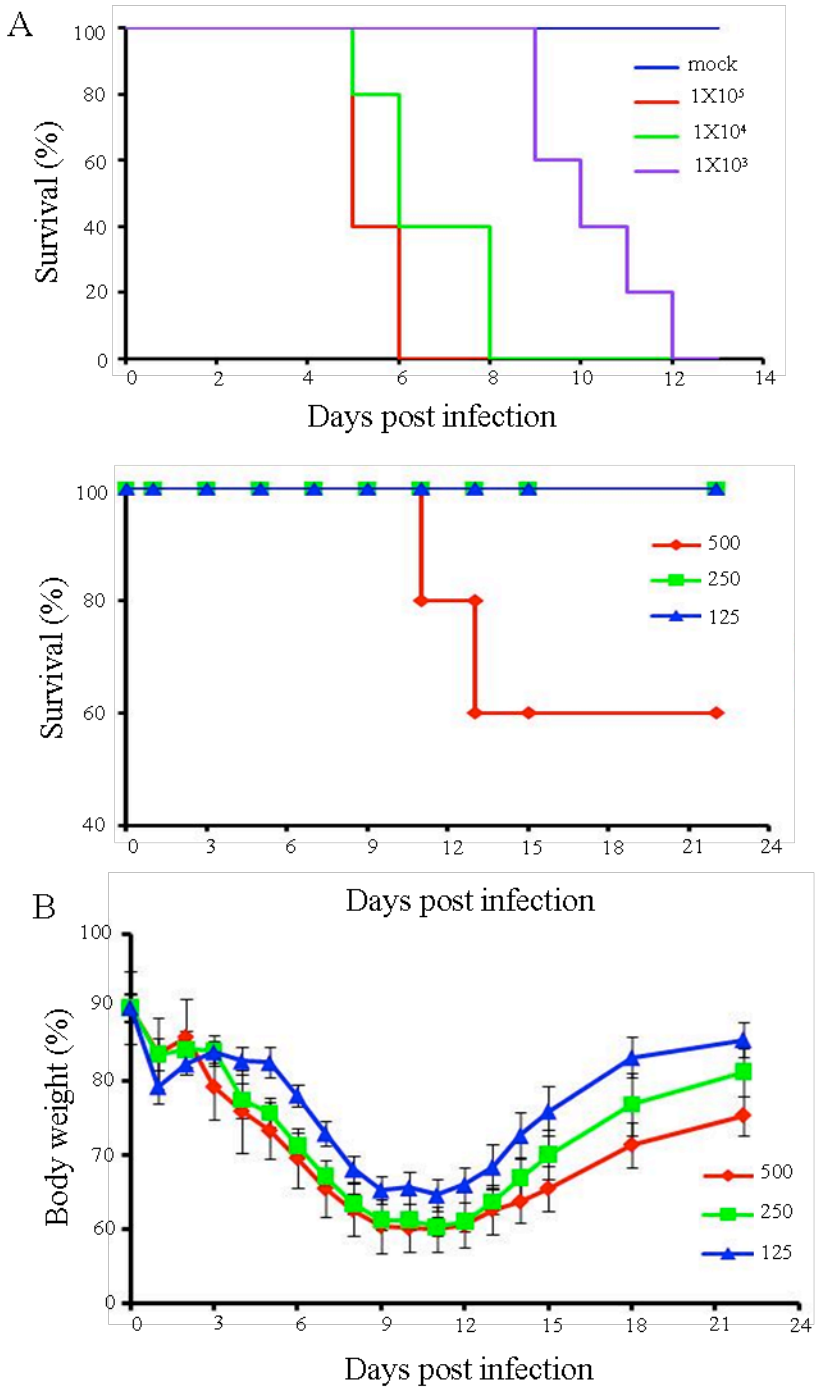

Figure 4 : Survival percentage and body weight kinetics
A. Mice were infected with a range of viral tires from 10^5pfu-10^3pfu (upper panel) and 500, 250,125 pfu (lower panel). Five mice were infected for each group including the mock infected group (PBS control). The mice were monitored for survival and % survival was plotted. B. Body weights of mice infected with 500, 250 and 125 pfu were tracked until 21 dpi and plotted. 5 mice per group were used for the analysis.

bodyweight has been used as a rough indication of animal injury and recovery. We analyzed the body weights of the mice periodically from 0-23 dpi. It was observed that at all three viral titers (500, 250 and 125 pfu) the mice lost at least 20% of their bodyweight (Fig. 4B). The maximum weight loss occurred between 9-12 dpi after which the mice started to regain their bodyweight and approached normal bodyweight by 23 dpi. This trend in bodyweight suggested that the mice fall sick post infection and also recover. In summary, from the survival percentage and bodyweight kinetics experiments, it was observed that at 250 pfu all the mice survived while still exhibiting significant loss of bodyweight. Hence a dose of 250 pfu was chosen for future infections.

Viruses used in all our experiments were propagated in chicken eggs in our collaborator's lab (A/Prof. Vincent Chow, NUS). To account for the variation of viral titer and virulence from each egg, the above mentioned experiments had to be repeated for each new batch of virus (from each egg) to identify the appropriate dose for our study.

3.2.2 H1N1 Influenza infection causes damage to mouse lung epithelium

Bodyweight kinetics studies were indicative of the mice falling sick post infection but were not conclusive of actual lung damage. Hence, we infected mice with 250 pfu of virus and sacrificed them at different time points post infection to harvest the lungs for histological analysis. From body weight kinetics studies it was observed that the mice lost most of their body weight around 9-12 dpi (Fig. 4B).

When we sacrificed mice at 11 dpi, it was observed that the infected lungs (without inflation) showed high degree of damage with hemorrhages and pulmonary edema compared to the lungs of normal, mock-infected mouse lungs (without inflation), (Fig. 5A).

To analyze the viral load in the lungs we used an Influenza A specific marker, M2, a viral proton-selective ion channel protein involved in virus assembly (Rossman et al., 2010; Wang et al., 1995). As seen in Fig. 5D, left panel, maximum viral load was observed at 4 dpi. Moreover, the viral staining was clearly observed in the alveolar region as well as in the bronchial epithelium 4 dpi. According to literature (Miao et al., 2010), the virus first encounters the innate immune response and by 5 dpi the adaptive immune response is induced. Correspondingly, a decrease in viral load was observed at 7 dpi when the adaptive immune response is active. By 11 dpi the viral load was very low and by 21 dpi the virus was completely cleared. This trend of viral staining is very similar to results obtained by Verhoeven and colleagues (Verhoeven et al., 2009) who demonstrated that even during infections with very high viral titers they were cleared completely by 12 dpi, indicated by lack of plaque forming units, confirming the absence of any replicating virions after 12 dpi.

We also analyzed the histology of the lungs at various time points post infection. Fig. 5D, right panel, shows lungs with clear alveolar spaces at 0 dpi. By 4 dpi an infiltration of immune cells was observed which gradually worsened and by 11

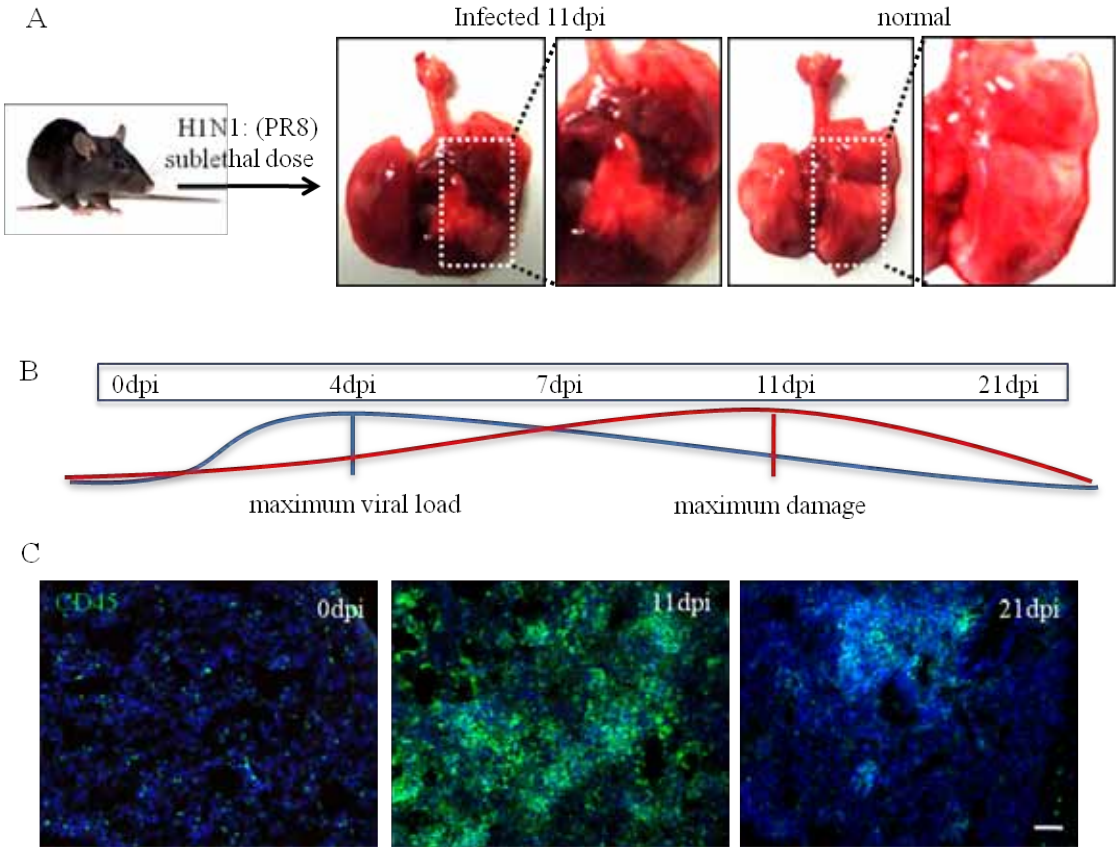

Figure 5 : Viral infection and kinetics
A. Representative image of damaged lungs 11 dpi infected with sub-lethal dose of H1N1 virus compared to mock infected (PBS) lungs. B. Pictorial representation of the trend of viral load and damage after a sub-lethal infection. Maximum viral load and maximum lung damage are estimated to be at 4 dpi and 11 dpi respectively. C. CD45 IF staining at 0, 11 and 21dpi infection showing an increase in immune cell population at 11 dpi. Scale bar represents 100µm. D. Image on next page. Left panel demonstrates the viral load in the lungs with IF staining for viral ion channel protein M2 (red) at 0 dpi, 4 dpi, 7 dpi, 11 and 21 dpi. Right panel depicts histology of the lungs at various time points post infection. Scale bar represents 200µm.

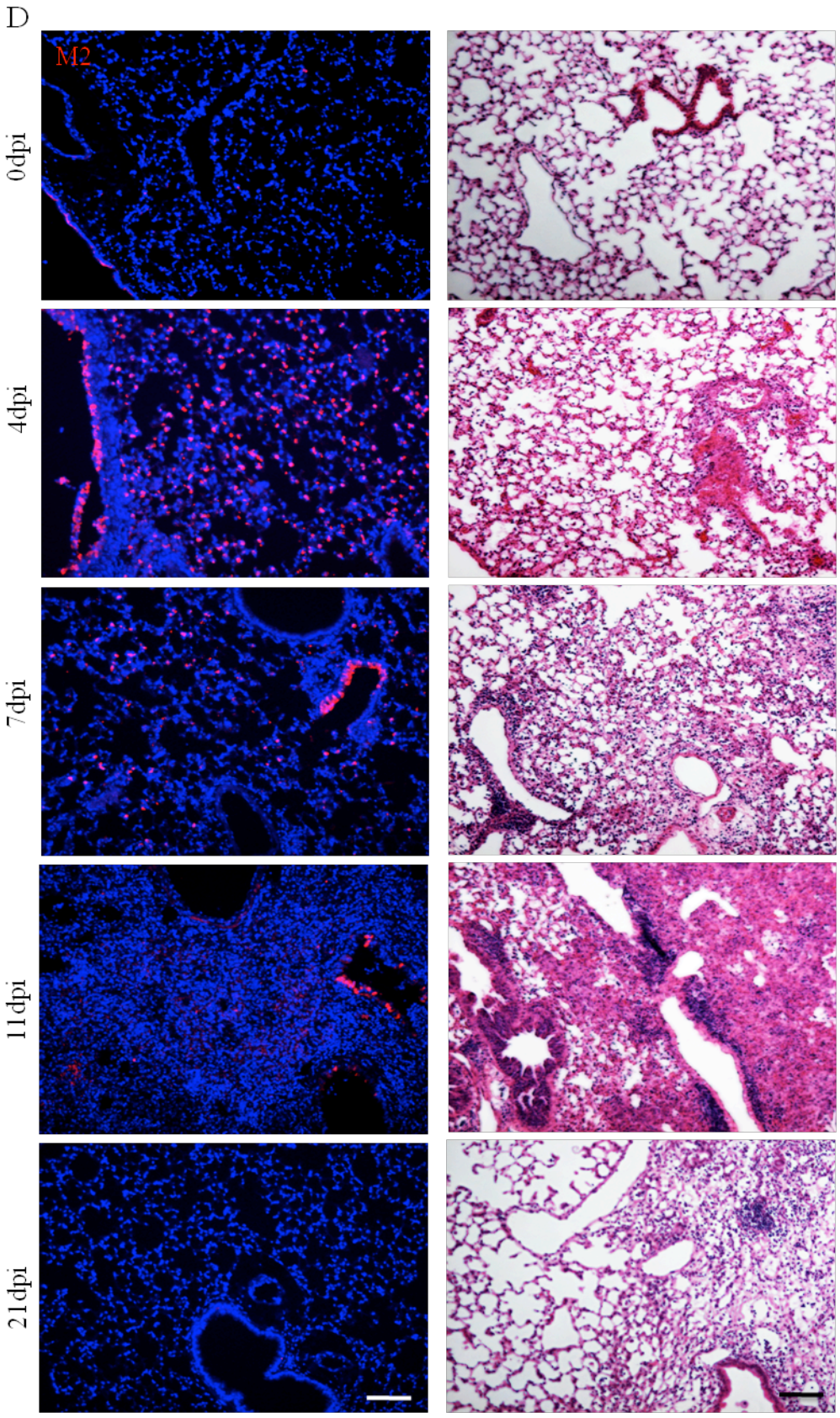
D
M2
0dpi
4dpi
7dpi
11dpi
21dpi

dpi a massive infiltration of immune cells accompanied with lung consolidation was observed. By 21 dpi however, the lungs looked relatively normal again. These histological results mirrored the body weight kinetics studies that indicated maximum damage in the lungs from 9-12 dpi and recovery nearing 21 dpi (Fig. 5B,D).

Influenza virus is controlled by both the innate and cell- mediated adaptive immune responses (Doherty et al., 2006; Thomas et al., 2006) and the infiltration of immune cells was further confirmed by using pan immune cell marker CD45 to stain sections at various time points post infection. Fig. 5C represents images of frozen sections of lung demonstrating a massive influx of immune cells at 11 dpi (middle panel) compared to normal lungs (left panel). Bronchus-associated lymphoid tissue or BALT (Sminia et al., 1989) which is commonly observed post influenza infection (Moyron-Quiroz et al., 2004) was also observed 21 dpi in mouse lungs as detected by CD45 positive staining in large regions of cells associated with a bronchus (right panel).

After observing viral load and corresponding immune responses by lung pathology, the possibility of epithelial cell damage was investigated. We probed for epithelial cell types of upper (Clara and ciliated cells) as well as the lower airways (alveolar type II cells) at 7 dpi compared to control (Fig. 6A). Clara cells marked by CC10 as well as ciliated cells marked by β tubulin IV and Tap73 were

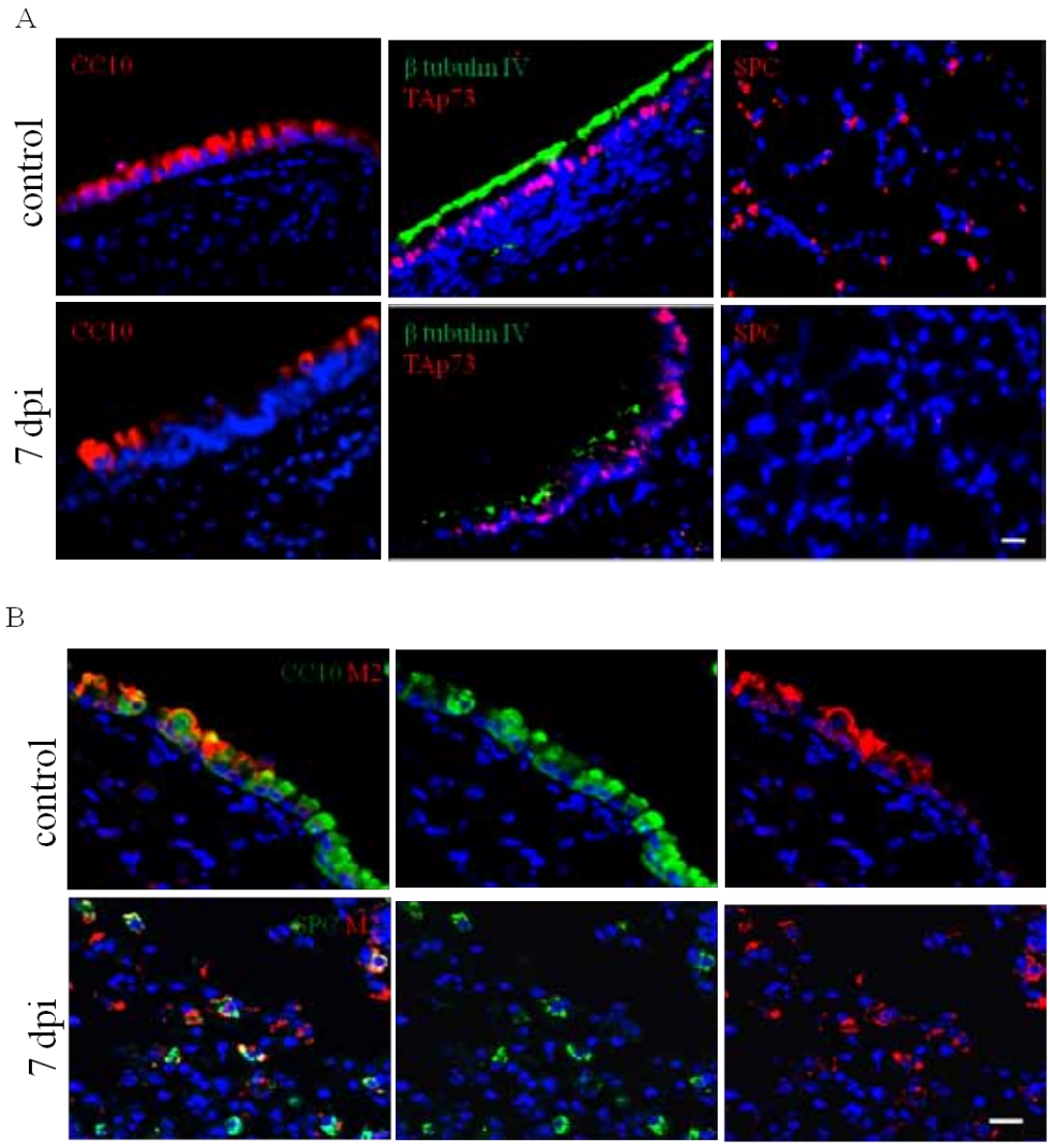

Figure 6 : Epithelial cell damage post H1N1 infection
A. IF staining of Clara cells (CC10, red) ciliated cells (β tubulin IV, green; TAp73, red) and alveolar type II (SPC, red) cells in mock infected and viral infected lungs 7 dpi. Scale bar represents 50µm. B. Upper panel shows co-staining of Clara cell marker CC10 (green) with viral ion channel protein M2 (red) at 7 dpi. Lower panel depicts co-staining of alveolar type II cell marker SPC (green) with viral ion channel protein M2 (red) at 7 dpi. Scale bar represents 20µm.

intact and distributed along the bronchial epithelium in normal mouse lung. However by 7 dpi there was widespread loss of marker expression of CC10 as well as β tubulin IV and Tap73. Similarly in the lower airways there was a loss of alveolar type II cell marker SPC, suggesting damage to these epithelial cell types of upper and lower airways.

To further prove the viral infection in these epithelial cell types, we co-stained Clara cells and alveolar type II cells with viral M2 ion channel protein markers. High magnification images of Clara cells and alveolar type II cells co-stained with viral marker revealed that the H1N1 influenza virus used in our experiments can infect epithelial cells thus directly or indirectly resulting in epithelial cell damage in addition to the substantial immune response elicited post infection (Fig.6B).

3.2.3 Increase in p63 expression during repair

p63 expression in the normal mouse lungs is restricted to the basal layer of the tracheobronchial epithelium (Fig. 7A). (Inset depicts a higher magnification of p63 nuclear staining in the basal layer). To examine if p63 plays a role during the damage and repair process, we next monitored the total expression level of p63 post influenza infection. Mice were infected with a sub-lethal dose of influenza virus and sacrificed at 7, 11 and 21 dpi. Protein from the entire lungs of mice was collected and western blot was performed for p63 using the monoclonal 4A4 hybridoma (Yang et al., 1999). Low levels of p63 was detected in normal

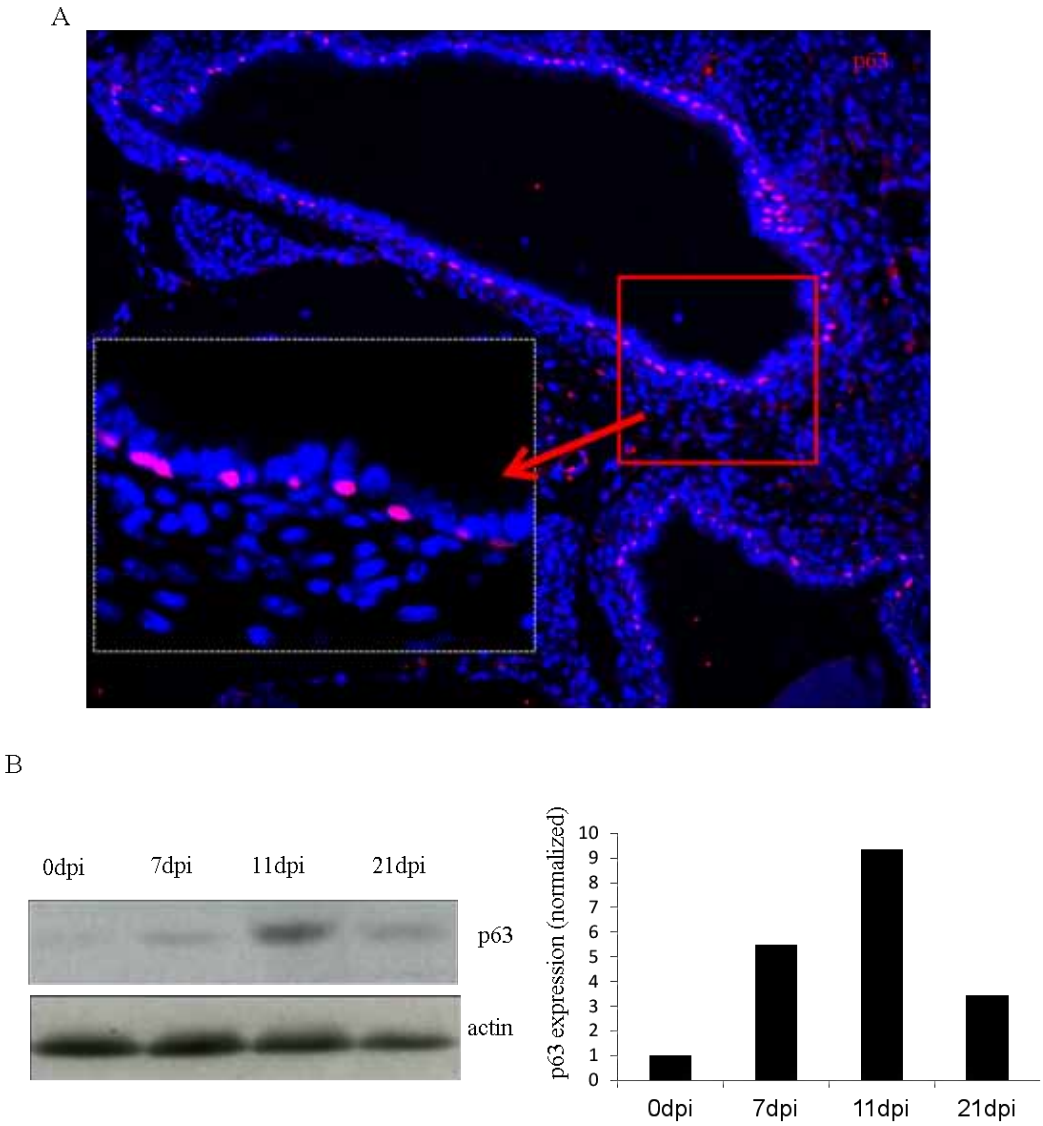

Figure 7 : Increase in p63 expression during repair
A. IF staining of p63 (red) expression in adult mouse lung. Inset shows higher magnification of p63 staining in bronchial epithelium. B. Western blot of p63 with whole lung lysate at 0, 7, 11 and 21 dpi. Actin was used as loading control (left panel). Right panel depicts the quantification of the band densities to estimate the normalized expression level of p63 at different time points post infection.

lungs (0dpi), (Fig. 7B). This was expected as p63 expression is restricted to the few basal cells lining the bronchial epithelium in the normal mouse lungs. After infection, levels of p63 protein expression increased and reached a maximum around 11 dpi. However by 21 dpi, which is the later recovery stages of the infection, the expression levels were near normal again. The density of the p63 bands normalized to the actin loading controls were quantified to further substantiate the elevated p63 expression levels at 11 dpi (Fig. 7B, right panel).

Once we established an increase in p63 expression during the damage and repair phase post infection, we wanted to localize the p63+ cells in the lungs. At 0 dpi, very few p63+ cells were detected underlying the bronchial epithelium only, and their intensity was not very high (Fig. 8A). The normal bronchial and bronchiolar epithelium was also lined with intact Clara cells (CC10, cytoplasmic) and ciliated cells (not stained here). Post infection, a loss of Clara cells was observed because of the viral infection as seen by the reduction of CC10 staining at 7 dpi. Corresponding to the loss in CC10 expression for Clara cells, we also detected an increase in p63+ cells in the bronchial epithelium (Fig. 8A). By 11 dpi, p63+CC10+ cells were observed in the bronchial epithelium illustrating that the p63+ basal cells give rise to the CC10+ Clara cells during regeneration of the bronchial epithelium. By 21 dpi most of the bronchial epithelium looked intact with uniform CC10 expression in bronchi and bronchioles, and p63 expression was also again restricted to very

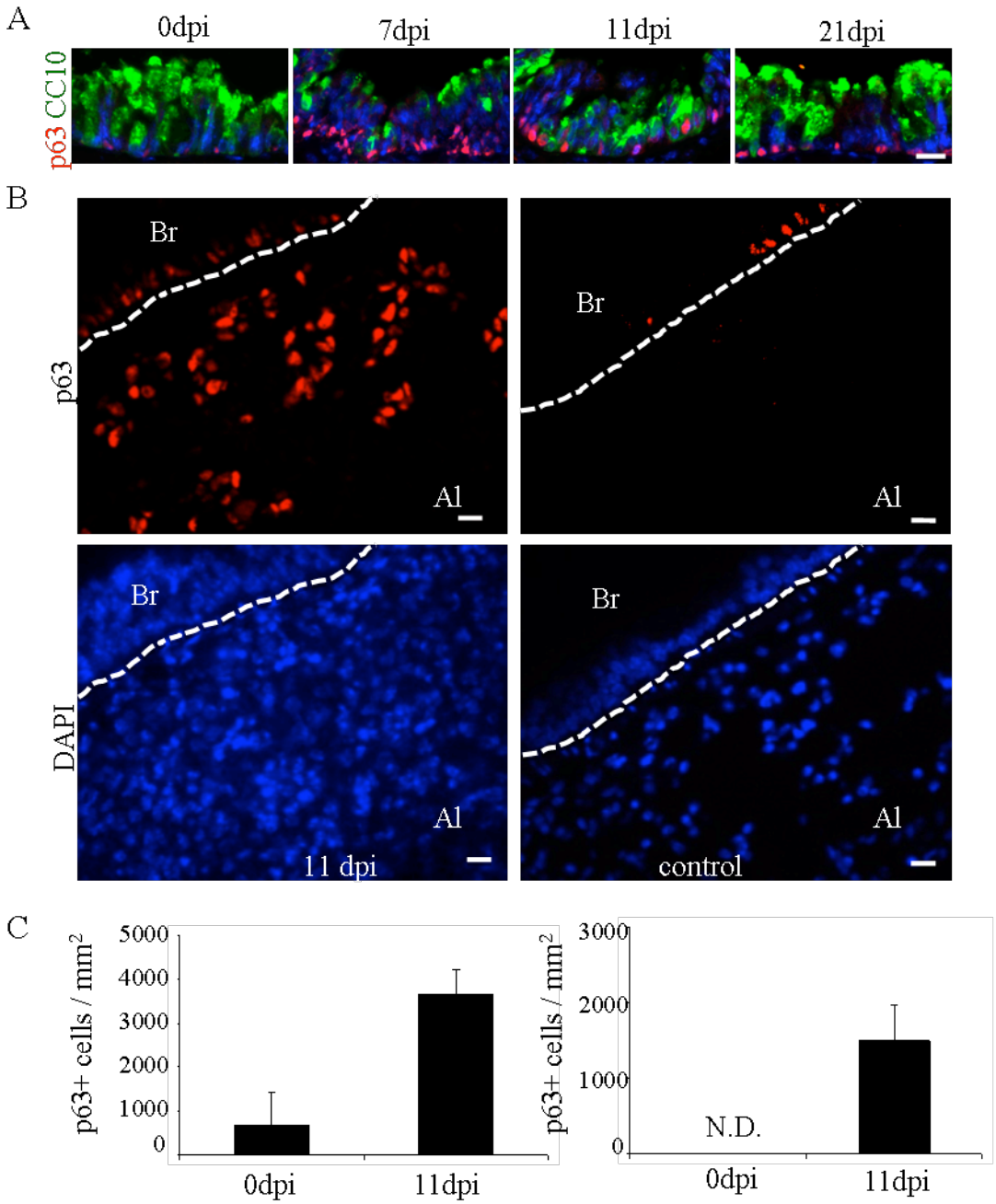

Figure 8 : Localization of p63+ cells in bronchial and damaged alveolar region

A. IF staining of basal cells marked by p63 (red) and Clara cells marked with CC10 (green) in bronchioles of lungs at 0, 7, 11 and 21 dpi. Scale bar represents 20µm. B. IF staining for p63 (red) of influenza infected (left panel) and mock infected (right panel) lungs at 11 dpi. Br: bronchi, Al: alveolar region. Dotted line marks the separation between bronchial and alveolar regions. Top panel shows p63 staining (red) and bottom panel shows nuclear counterstained DAPI staining of the same region as the respective top panel. Scale bar represents 20µm. C. Left

panel represents quantification of p63+ cells in bronchi and bronchioles at 0 and 11 dpi. Right panel represents quantification of p63+ cells in alveolar regions (deep lung). Error bar represents standard deviation about the mean. ND: Not detected. Sections from 3 control and infected mice were used for the quantification of p63+ cell number/mm^2 of positive staining.

few basal cells lining the bronchial epithelium. Thus Fig. 8A demonstrates that p63+ basal cells have the potential to differentiate into Clara cells in the bronchial epithelium mirroring the results of lung damage and repair using other chemical injury models like Naphthalene (Hong et al., 2004a).

In Fig. 7B we showed that the maximum expression of p63 was observed at 11 dpi but when we localized the expression in the bronchial epithelium, a maximum expansion of p63+ cells was detected at 7 dpi (Fig. 8A). Since these results did not correlate well we then considered if p63+ cells were also localized elsewhere in the lung to correspond to the maximum p63 protein expression observed at 11 dpi. Analyses of lungs at 11 dpi interestingly revealed an appearance of p63+ clusters in the damaged alveolar regions or interstitial regions along with the increase in p63+ cells in the bronchus and bronchiolar epithelium (Fig. 8B). These p63+ cells were not observed in the alveolar regions in mock infected mice.

To quantify the p63+ cells in bronchial and alveolar regions the number of p63+ cells /mm^2 in the lungs at 11 dpi compared to control (area focusing on positively stained regions) were counted. We observed an increase in p63+ cells in bronchial epithelium at 11 dpi compared to control (Fig. 8C, left panel) as also seen in the Fig. 8A, B. No p63+ cells were detected in the alveolar epithelium in mock

infected mice (0 dpi) where as regions of p63+ clusters of cells were observed in mouse lungs at 11 dpi (Fig. 8C, right panel).

To characterize these p63+ clusters in the alveolar region further, we sacrificed mice at later time points post infection such as 15 dpi and co-stained the p63+ clusters with Krt5, another basal cell marker. p63+Krt5+ cells were observed in the bronchial epithelium as well as in the alveolar region (Fig. 9A). Krt5 staining helped to visualize the p63+ cells as discrete pods in the alveolar region. Quantification of p63+ Krt5+ cells at 15 dpi revealed that most of the p63+ cells were also Krt5+ (Fig. 9B). Only 0.8% of stained cells were single positive for p63 while 50.7% of the cells were double positive for p63 and Krt5 and 48.4% cells were positive for Krt5 alone. These data point to a probable progression where initially at 11 dpi, p63+ Krt5+ cells are seen in the alveolar region. Eventually p63 expression is lowered and thus 48.4% of stained cells are only single positive for Krt5 with p63 expression very faint or nearly lost in them. Given the robust cytoplasmic staining of Krt5 for these p63+ cells, Krt5 was used as a marker for all staining at later time points to trace this population of cells even after p63 expression is decreased or lost. These p63+ Krt5+ cells will be called Krt5+ pods for simplicity from here on. We confirmed widespread expression of the Krt5+ pods in several mice at 15 dpi (Fig. 9C). Also an important point that will be addressed later is that these Krt5+ pods are always associated with a bronchus or a bronchiole as observed in Fig. 9 A, C.

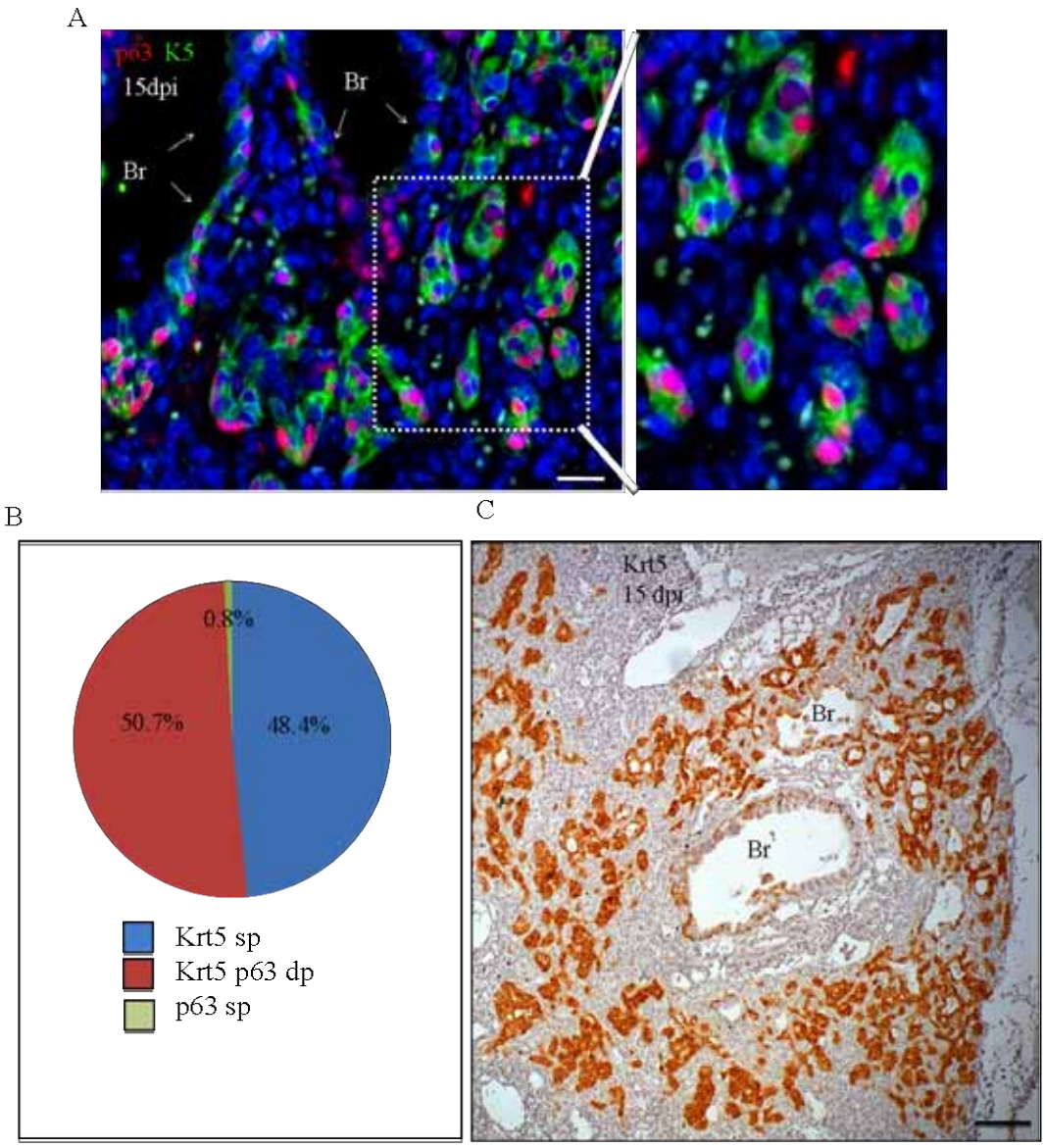

Figure 9 : p63+Krt5+ pods in repair of damaged lung
A. Double staining of mouse lungs 15 dpi with Krt5 (green) and p63 (red). Scale bar represents 20µm. Right panel shows high magnification of discreet p63+ Krt5+ pods. B. Pie chart represents quantification of p63+ Krt5+ cells at 15 dpi. Sections from three mice were used for the quantification. 0.8% of the stained cells are p63 single positive (p63 sp, green), 50.7% of the cells are p63 and Krt5 double positive (Krt5 p63 dp, red) and 48.4% of the stained cells are Krt5 single positive (Krt5 sp, blue). C. Low magnification IHC image of Krt5 staining on mouse lung 15 dpi. Scale bar represents 100µm. Br: bronchi.

3.2.4 Krt5+ pods are not involved in fibrosis

Fibrosis is one of the most common adverse outcomes of respiratory diseases including pneumonia (Yeldandl and Colby, 1994). To address this issue we explored the possibility of Krt5+ pods observed in mouse lungs post infection leading to fibrosis. Masson's trichrome staining is a common technique used to demonstrate fibrosis and stains red for keratin and muscle fibers, blue for collagen and bone, light red or pink for the cytoplasm, and dark brown to black for cell nuclei. Fibrotic collagen fibers are commonly observed as blue color in fibrotic lungs (Yu et al., 2001). Masson's trichrome staining in normal lung, stains all epithelial cells in bronchial and alveolar regions red while the cartilage and connective tissue surrounding the bronchus stains blue (Fig. 10A, right panel). We infected mice with H1N1 and stained the Krt5+ regions with Masson's trichrome stain to check if Krt5+ pods led to fibrotic lesions. Fig. 10A, left panel demonstrates Krt5 staining in the lungs at 15 dpi and the middle panel represents Masson's trichrome staining of the same region on a consecutive 5μm section. No blue colored collagen fibers were observed in regions of Krt5+ pods thus eliminating the possibility that Krt5+ pods lead to fibrosis in mouse lungs post H1N1 infection. Further, we also evaluated mouse lung sections at 50 dpi with Masson's trichrome staining and could not detect fibrotic collagen fibers (data not shown) suggesting that the system of H1N1 infection is a model for lung damage and repair unlike other chemical injury models such as bleomycin which lead to fibrosis.

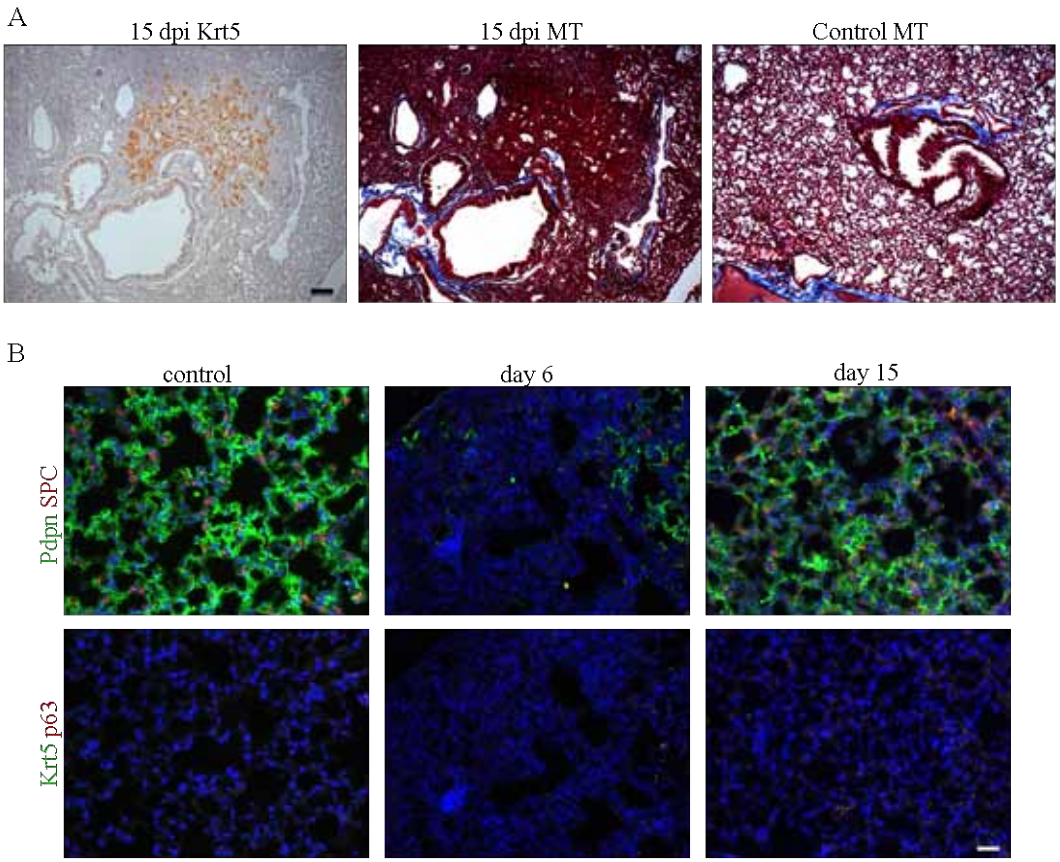

Figure 10 : Krt5+ pods are not involved in fibrosis
A. Left panel showing staining of Krt5 on mouse lung sections at 15 dpi. Middle panel shows Masson trichrome staining of consecutive section at 15 dpi. Right panel shows Masson trichrome staining in normal mouse lung. Scale bar represents 100µm. B. Top panel demonstrates alveolar type I cell staining with PDPN (green) and alveolar type II cells staining with SPC (red) at 0, 6 and 15 dpi post bleomycin treatment. Bottom panel shows p63 (red) and Krt5 (green) at 0, 6 and 15 dpi post bleomycin treatment. Scale bar represents 50µm.

To confirm these results we used the bleomycin model to test if Krt5+ pods are visible in mouse lungs using this fibrosis system. Mice were treated with 5U/kg bleomycin and lungs were harvested at different time points post treatment. The kinetics of bleomycin damage is different from infection, and by 6 days post treatment there is damage to the lungs as shown by loss of alveolar type I and type II cell markers (Fig.10B, top panel). By 15 dpi most of the regions in the lung have regained the marker staining. However during this phase no p63 or Krt5+ cells were detected in the alveolar regions suggesting that the repair/fibrosis taking place post bleomycin treatment does not involve widespread presence of p63 and Krt5+ cells. These data further confirm that p63+Krt5+ pods are not involved in fibrosis or repair in mouse lungs post bleomycin treatment.

3.2.5 Characterization of Krt5+ pods

To characterize the Krt5+ pods observed in the repair process post infection Krt5+ pods were co-stained with markers of different cell types. Krt5+ pods are not immune cells since they do not co-stain with pan immune cell marker CD45 (Fig.11A). We also eliminated the possibility that they are smooth muscle cells as they did not co-stain with smooth muscle actin (SMA) which stain muscle cells in the walls of blood vessels in the lungs (Fig. 11B). When Krt5+ cells were co-stained with pan-Keratin marker (which stains all epithelial cells) significant overlap was observed. Thus we confirm the epithelial nature of Krt5+ pods observed during repair *in vivo*.

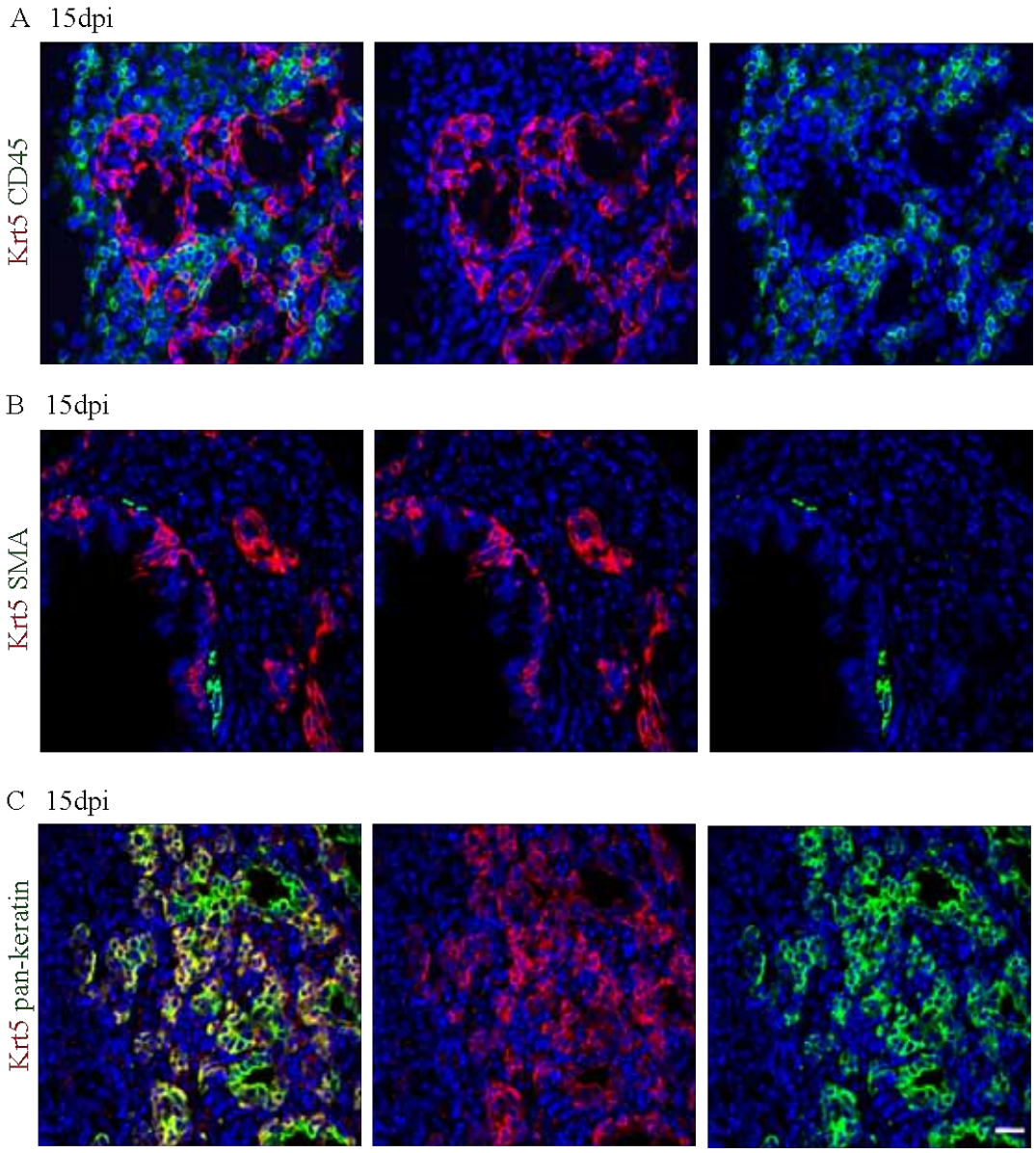

Figure 11 : Characterization of Krt5+ pods
A. Co-staining of pan immune cell marker CD45 (green) with Krt5 (red) on mouse lung frozen sections 15 dpi. B. Co-staining of smooth muscle marker SMA (green) with Krt5 (red) on mouse lung sections 15 dpi. C. Co-staining of epithelial cell marker pan-keratin (green) with Krt5 (red) on mouse lung sections 15 dpi. Scale bar represents 50µm.

3.2.6 Krt5+ pods are not BASCs

p63+Krt5+ cells are known to be stem cells for the upper airways. When they were first observed in the alveolar region during repair we wanted to determine if these cells have any relation to the recently identified putative stem cell marker of the upper and lower airways known as BASCs. These cells normally present at the BADJ are identified as CC10+ SPC+ cells (Kim et al., 2005). After infecting mice with H1N1 virus we stained lung sections 15 dpi for CC10 and SPC to identify BASCs at the BADJ. On the consecutive section, we stained with p63 and Krt5 to test if there was any overlap between these cell populations. As shown in Fig. 12A, no p63 or Krt5 staining was observed in the BADJ where CC10 and SPC staining was seen. Similarly, in damaged alveolar regions where p63+Krt5+ pods were observed, no significant CC10 and SPC staining was detected (Fig. 12B). Thus we conclude that Krt5+ pods are an independent cell population and may not be connected to BASCs .

3.3 CONCLUSIONS AND DISCUSSION

In this chapter we describe a novel physiologically relevant system established to study lung damage and repair. We identified the sub-lethal dose of H1N1 virus that could cause sufficient lung damage, yet also allow the mice to recover and regenerate the lungs. We used body weight studies as well as histological analysis to determine the kinetics for the damage and repair process. Further, we also showed that the virus is capable of infecting epithelial cells in the lung thus causing epithelial cell damage along with massive infiltration of immune cells

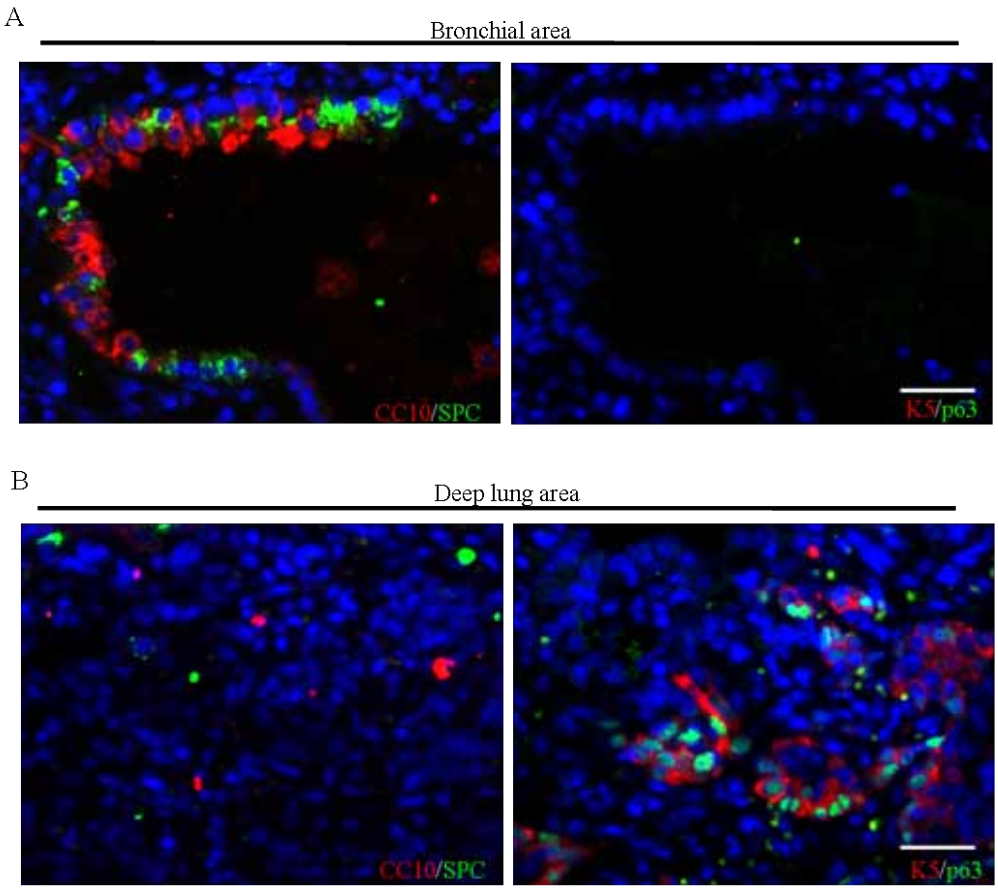

Figure 12 : Krt5+ pods are not Bronchio-Alveolar Stem Cells
A. Left panel shows IF co-staining of CC10 and SPC at a bronchioalveolar duct junction 15 dpi. Right panel shows IF staining on a consecutive sections for p63 (green) and Krt5 (red). B. Left panel shows CC10 and SPC staining in deep lung area 15 dpi. Right panel shows p63 (green) and Krt5 (red) staining on consecutive section in damaged deep lung areas 15 dpi. Scale bar represents 20µm.

reflecting viral pneumonia observed in humans. The advantage of this system over other chemical injury models is the ability of the virus to damage epithelial cells of the upper and lower airways, thus providing an ideal system to identify stem cells for the upper and lower airways.

After establishing the system we evaluated the role of p63+ cells during the repair process. We observed that p63+ cells in the bronchial epithelium are involved in regenerating the damaged Clara cells, thus restoring the bronchial epithelium (confirmed with lineage tracing in Chapter 7). These results mirror chemical injury models used in the past, which also demonstrate that p63+ basal cells are the stem cells for the upper airways.

In addition to this, we also observed an appearance of p63+ Krt5+ pods in the damaged alveolar regions at 11 dpi. These epithelial Krt5+ pods were observed in many damaged regions of the lung, and were mostly associated with a bronchus or bronchiole. It would be interesting to investigate the damage and repair pattern as well as the Krt5+ pods in lungs in response to a wide range of viral doses as well as different strains of mice. Moreover, the Krt5+ pods are also observed in mice infected with more pathogenic strains of Influenza virus such as the H5N1 virus (data not shown). Whether these results extend to other strains of Influenza virus (avian virus) or other viral infections remains an area to be explored.

We eliminated the possibility that Krt5+ pods could be contributing to fibrosis by reporting that our model does not result in fibrosis. We also used a known fibrosis model like bleomycin treatment and demonstrated that p63+ Krt5+ pods are not observed during the fibrotic process.

Considering that Krt5+ pods are not involved in fibrosis of the lower airways and that p63+ cells are the stem cells for the upper airways we next wanted to investigate if they were related to any known stem cells of the lower airways. BASCs are the only reported stem cells for the alveolar region in mice and we confirmed that the Krt5+ pods and BASCs are two mutually exclusive populations of cells in the lungs. While the contribution of BASCs in this process remains unknown, the widespread presence of epithelial Krt5+ pods in interstitial regions in the lung during repair is suggestive of a significant function. In the coming chapters we explore the possible functions of these Krt5+ pods during repair.

CHAPTER 4: *IN VITRO* CHARACTERIZATION OF MOUSE LUNG STEM CELLS

4.1 INTRODUCTION

The role of lung epithelial stem cells in maintenance and repair of the adult lung is ill defined, and their identity remains contentious because of the lack of definite markers for their prospective isolation and the absence of clonogenic assays to measure their stem cell potential. A stem cell is defined as a self-renewing cell population with the ability to differentiate into one or more cell types. Adult stem cells in the airways have the ability to generate highly proliferating transit amplifying cells by asymmetric cell division. This ability can be measured using an *in vitro* colony forming efficiency assay (McQualter et al., 2010; Schoch et al., 2004) or *in vivo* chemical injury models (Hong et al., 2004a, b).

Reports suggest that Krt5+ cells can differentiate into cells of the tracheobronchial epithelium *in vitro* (Rock et al., 2009; Schoch et al., 2004). Further, *in vitro* differentiation assays also illustrate that BASCs which are Sca-1^+ $CD34^+$ $CD45^-$ $Pecam^-$ can form CC10 and SPC+ cells *in vitro* (Kim et al., 2005) . McQualter and colleagues recently suggested that a subpopulation of EpCAM (hi), $CD49f^+$, $CD104^+$, CD24 (low) epithelial cells have the capacity for self-renewal and their descendants give rise to airway and alveolar epithelial cell lineages *in vitro* (McQualter et al., 2010).

While these studies have greatly contributed to our knowledge in the field, several key questions remain unanswered. It is still not defined if there is a common progenitor in the adult lung that can differentiate to form the bronchial and alveolar cell types. In our studies, we propose to culture mouse lung cells on 3T3 feeder layer to obtain stem cell populations that are capable of self-renewal and *in vitro* differentiation. This culture system was initially developed by Dr. Howard Green (Rheinwatd and Green, 1975) to culture human keratinocytes and it was first used in the field of regenerative medicine to treat burn patients in 1984 (Gallico III et al., 1984). Since then, this system has been employed for several clinical applications like skin engraftment and corneal epithelial grafting (Nishida et al., 2004).

p63+ keratinocytes and thymic epithelial stem cells from human and rats respectively have been cultured using this system (Barrandon and Green, 1985; Senoo et al., 2007). This *in vitro* culture system involves growing adult stem cells on feeder layers to form colonies which could be picked for expansion, molecular analysis, or differentiation assays after obtaining clonogenic cells from lungs. Detailed microarray analysis and Gene set enrichment analysis (GSEA), a powerful analytical method (Subramanian et al., 2005) was also used for interpreting gene expression data to reveal novel markers and pathway for potential targeting in various experimental systems. In parallel, *in vitro* differentiation assays were performed to determine the differentiation potential of the stem cells.

In this chapter we discuss the clonogenic ability of the p63+Krt5+ cells observed during repair post infection. We also performed detailed molecular analysis and differentiation assays *in vitro* to predict the fate of these cells and uncover novel pathways which could be involved in the regeneration process post infection.

4.2 RESULTS

4.2.1 p63+ Krt5+ pods proliferate during repair

From all the kinetics studies for damage and repair, our hypothesis was that from 11 dpi, when the maximum damage was observed, a repair process should have been initiated to regenerate the lung epithelium. This regeneration process would be enabled by actively proliferating stem cells. To determine if the p63+ cells we observed in the damaged regions were proliferating, we co-stained p63 with proliferation marker Ki67 (Fig. 13A). Nearly 30% of the p63+ cells co-stained with Ki67 suggesting they were proliferating, while about 40% of the cells positively stained in the alveolar region were single positive for Ki67 (Fig.13B). A major proportion of these were speculated to be immune cells.

To further confirm the active proliferation of p63+ Krt5+ pods, we performed BrdU incorporation assays. After infecting mice with sub-lethal dose of H1N1, the mice were injected with BrdU at 11 dpi. Lungs were harvested at several time points including several hours post injection at 11 dpi, and also at 15 and 19 dpi. Only cells actively proliferating at the time of injection and their daughter cells

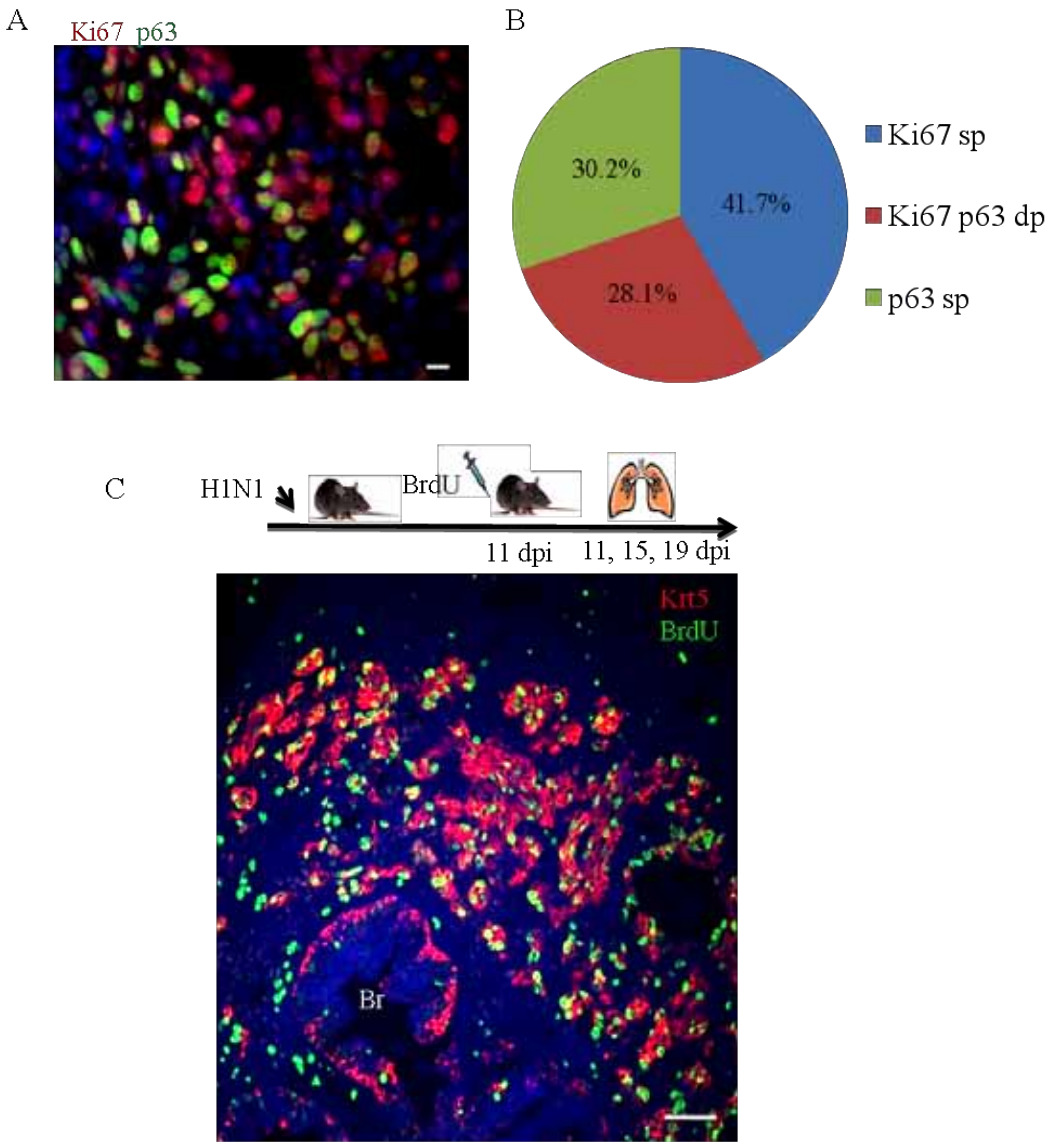

Figure 13 : p63+Krt5+ cells are proliferating
A. IF staining of p63 (green) and Ki67 (red) on mouse lung sections 11 dpi. Scale bar represents 20µm. B. Pie chart represents quantification of p63+ Ki67+ cells at 15 dpi. Sections from three mice were used for the quantification. 30.2% of the stained cells are p63 single positive (p63 sp, green), 28.1% of the cells are p63 and Ki67 double positive (Ki67 p63 dp, red) and 41.7% of the stained cells are Ki67 single positive (Krt5 sp, blue). C. Upper panel represents the schematic plan for the BrdU pulse chasing experiment. Mice were infected with a sub-lethal dose of the H1N1 virus and treated with BrdU at 11 dpi. The mice were then sacrificed at different time points including 11, 15 and 19 dpi. Lower panel shows a low magnification image of Krt5 (red) and BrdU (green) at 15 dpi. Scale bar represents 100µm. Br: bronchiole.

would be labeled with BrdU. Fig.13C represents an image of proliferating Krt5+ cells in bronchial as well as damaged alveolar regions surrounding a bronchus at 15 dpi, labeled with BrdU.

Next, we quantified the proliferating Krt5+ cells in the bronchial and alveolar epithelium. To analyze the percentage of Krt5+ BrdU+ cells amongst the Krt5+ cells in the bronchial epithelium we co-stained infected lung sections and quantified them across 11, 15 and 19 dpi (Fig. 14A). Maximum number of double positive cells in the bronchial or bronchiolar epithelium were observed at 11 dpi as seen in the representative IF image in the left panel. These data suggest that the labeled Krt5+ cells eventually differentiate into other cell types in the bronchial epithelium resulting in the decreased number of Krt5+ cells labeled with BrdU at later time points (right panel). Interestingly, when we quantified the percentage of Krt5+ BrdU+ cells amongst the Krt5+ cells in the alveolar epithelium, we observed maximum number of double positive cells at 15 dpi (Fig. 14B). About 30% of the Krt5+ cells were labeled with BrdU similar to the quantification data obtained with Ki67 staining in Fig.13A. This trend observed could be interpreted as a population of Krt5+ pods in alveolar region being labeled at 11 dpi which expand in number at 15 dpi to give an increase in double positive cells. This trend was represented in Fig. 14 C, which showed relatively small regions of Krt5+ pods in alveolar regions at 11 dpi, but by 15 dpi the Krt5+ regions were much bigger, and contain more double positive cells. Eventually, these cells start to

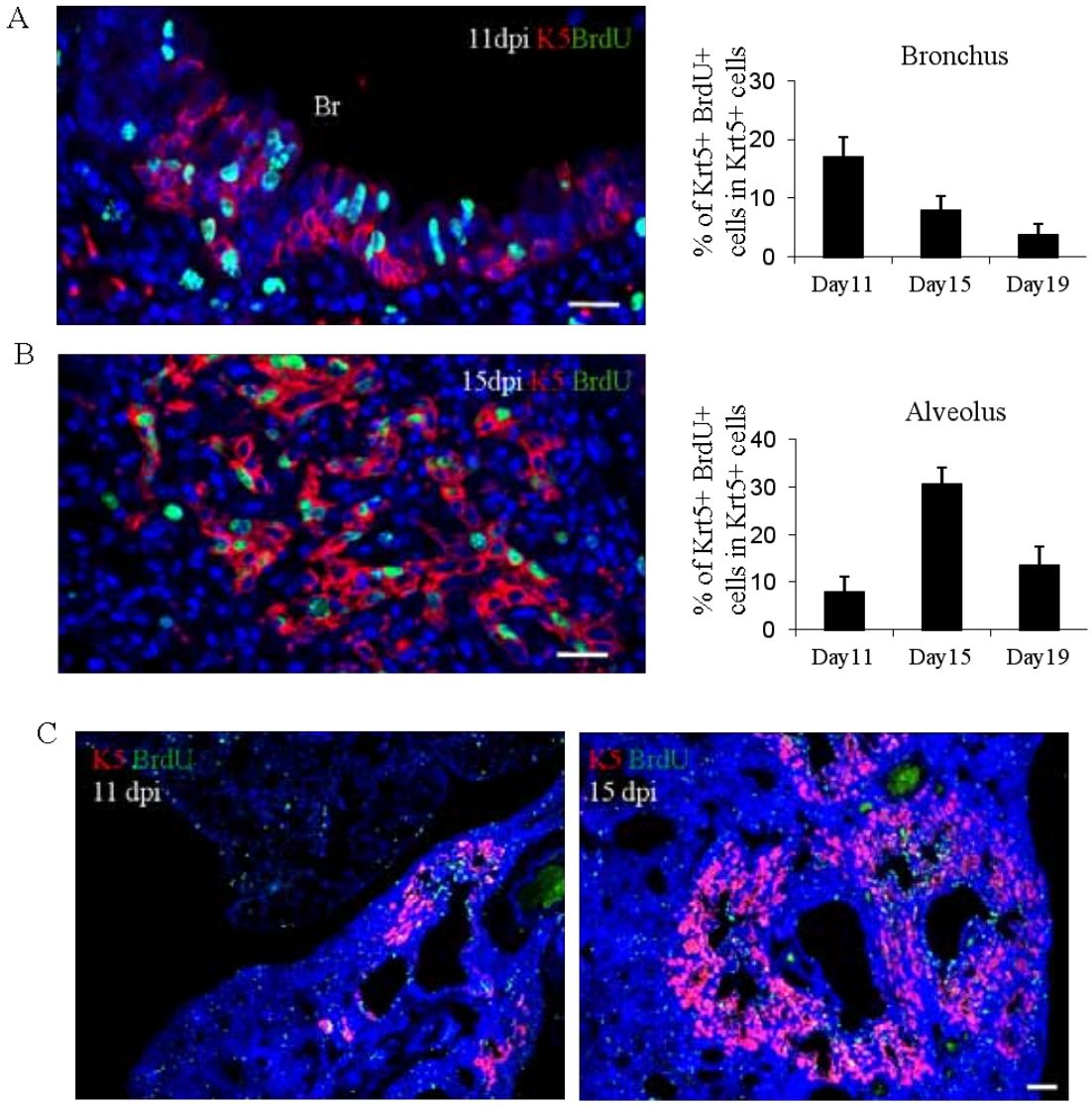

Figure 14 : Quantification of Krt5+ proliferating cells post infection
A. Left panel shows Krt5 (red) and BrdU (green) staining in bronchial regions of the lung 11 dpi. Scale bar represents 20µm. Right panel demonstrates % of Krt5+ BrdU+ cells of all the Krt5+ cells in the bronchus region at 11, 15 and 19 dpi. Three mice were used for each time point and error bar represents standard deviation from the mean. B. Left panel shows Krt5 (red) and BrdU (green) staining in damaged alveolar regions of the lung at 15 dpi. Scale bar represents 20µm. Right panel demonstrates % of Krt5+ BrdU+ cells of all the Krt5+ cells in the alveolar region at 11, 15 and 19 dpi. Three mice were used for each time point and error bar represents standard deviation from the mean. C. Krt5 (red) and BrdU (green) staining on mouse lung sections 11 and 15 dpi. Scale bar represents 100µm.

differentiate into other cell types, which was reflected in the decreased number of Krt5+ BrdU+ cells by 19 dpi. It has to be noted that with many multiplications, the BrdU signal is diluted out which could also be responsible for the decreased Krt5+BrdU+ cells with time.

4.2.2 Increase in clonogenic cells during repair

To confirm the presence of stem cell populations during repair, we conducted clonogenic assays of the lung cells *in vitro* post infection. We infected mice with sub-lethal dose of H1N1 virus and at 12 dpi, when p63+ Krt5+ proliferating cells were observed in the lungs, mice were sacrificed from mock infected and virus infected groups to harvest the lungs. Harvesting lungs at 12 dpi also ensured that the virus is completely cleared from the lungs, to avoid transferring any live virus to the *in vitro* culture experiments. Single cell suspension of cells from control and infected mouse lungs were seeded on irradiated feeder layers (Fig. 15A). Colonies first appear after five days in culture and the colony numbers obtained from control and infected lungs were counted at seven days. Interestingly, more than 20 fold increase in the number of clonogenic cells from infected lungs than control lungs was obtained (Fig. 15B). This data supports our hypothesis of stem cells actively proliferating during the repair period to regenerate the lungs.

A

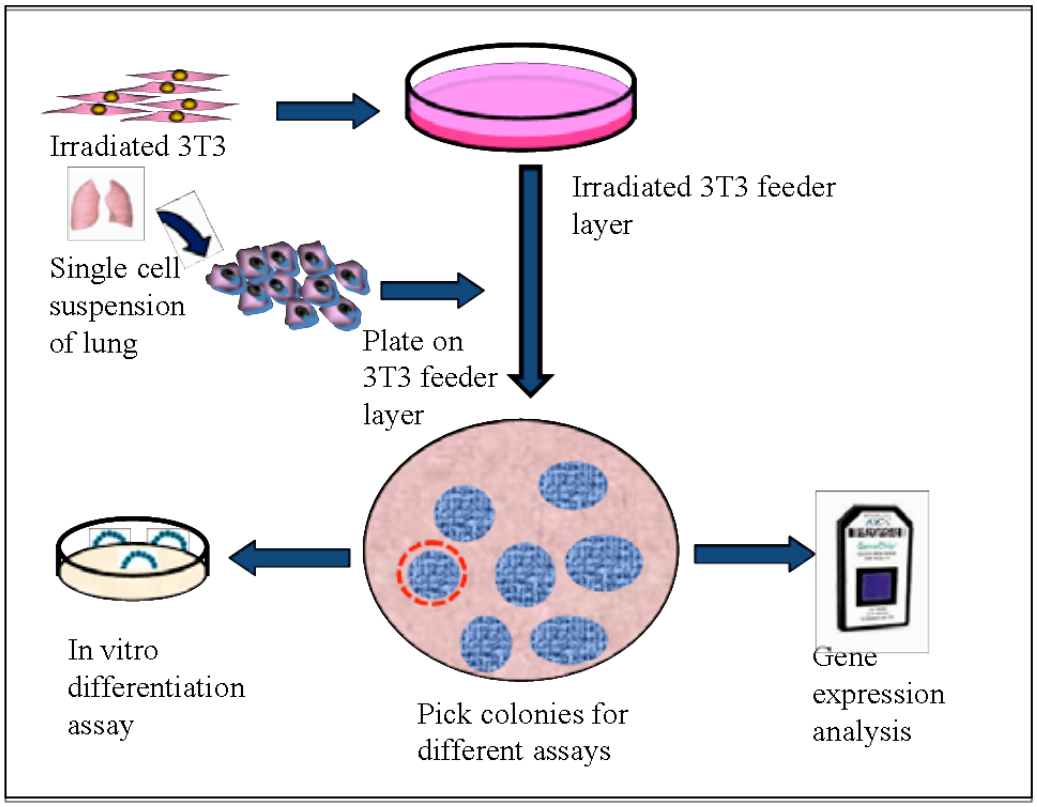

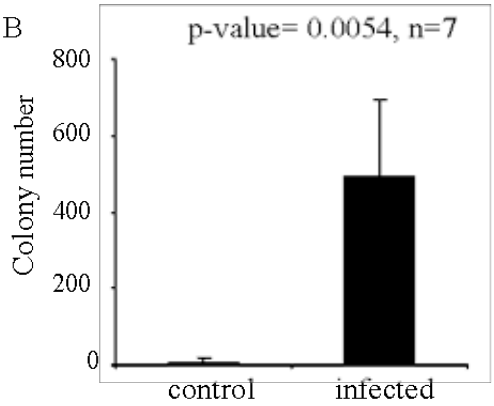

Figure 15 : Increase in clonogenic cell population during repair post H1N1 infection

Schematic represents the workflow followed for culturing mouse lung stem cells. Irradiated 3T3 cells are plated and the cells are allowed to settle down and form a monolayer feeder of cells. Mice (mock or virus infected) are sacrificed and lungs are dissociated using enzymatic digestion and the single cell suspension is then plated on the feeder layer. Colonies appear from 5-7 days in culture. Colonies can be picked and used for gene expression analysis or *in vitro* differentiation assays. B. Graph depicts number of colonies obtained from lungs of control and infected mice. Number of mice n=7 and p value<0.05. Error bar represents standard deviation from the mean.

4.2.3 Gene expression profiling of colonies from infected lung

Next we examined if the colonies obtained from control and infected mouse lungs were the same, or if we could separate them based on their gene expression profiles. After confirming the epithelial nature of these colonies by marking the cells with Ecad (Fig. 16B), we picked one colony each, from three mock and virus infected mouse lungs (Fig. 16A) for whole genome expression analysis. By means of unsupervised clustering of all the six colonies it was observed that the control and infected lung colonies cluster separately, demonstrating that the cells comprising those colonies were indeed different (Fig.16C). The PCA map shown in Fig. 16D further illustrates the same finding. The control colonies were very uniform and clustered very close together, while the infected colonies were more different in whole gene expression profile probably owing to the more dynamic state of the cells contributing to the repair post infection. 506 genes were differentially expressed in control and infected colonies and most of the genes had similar expression profile in the triplicates from control and infected lungs (Fig.16E).

We next performed GSEA analysis of the pathways that were differentially regulated because of the gene expression profiles from control and infected lung colonies . Genes involved in wound healing, tissue development and regulation of growth pathways were differentially enriched in the colonies from infected mouse lungs compared to control lungs (Fig. 17A). Fig.17B depicts the heat map of genes involved in these pathways. Important genes involved in each of the

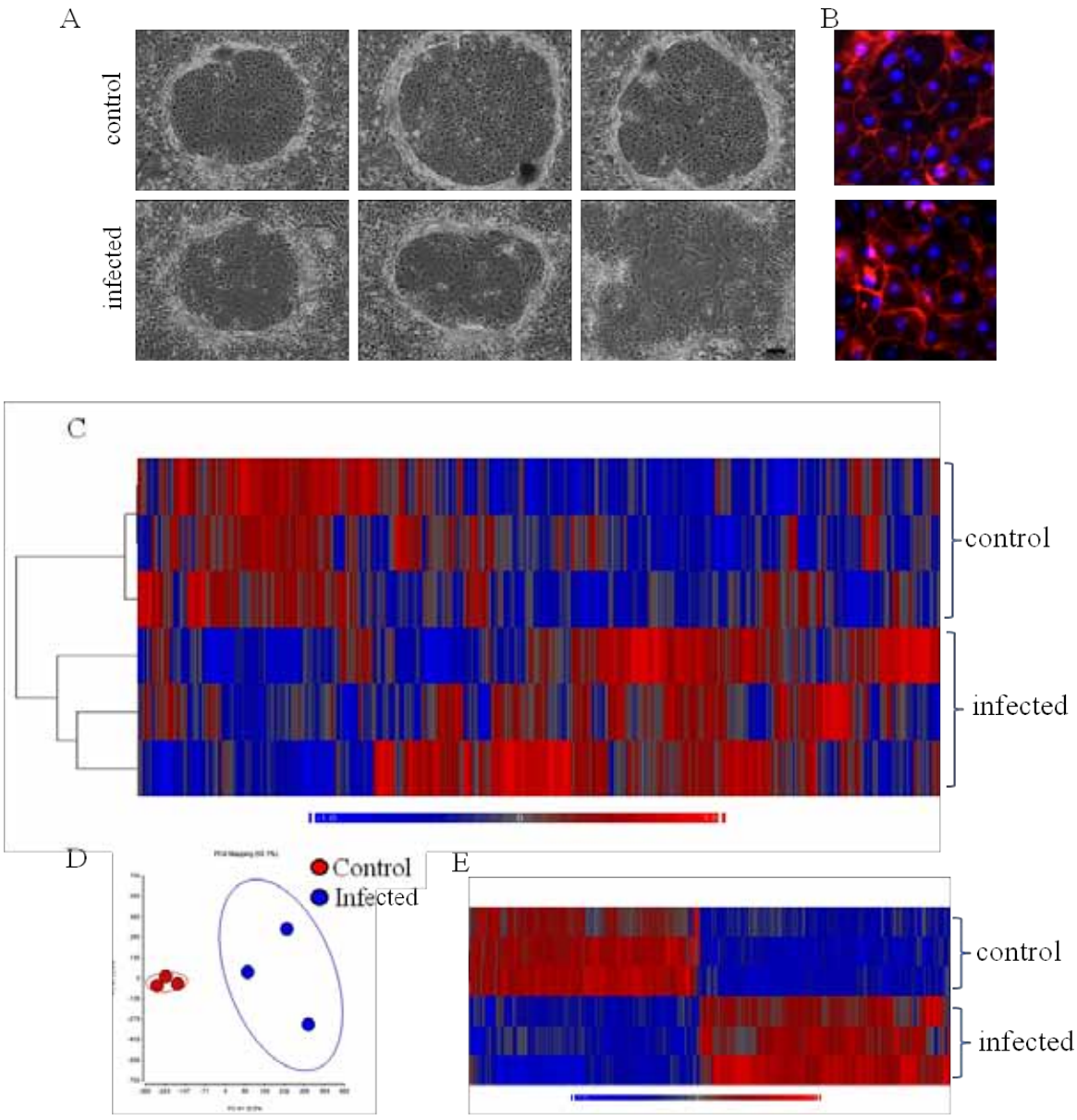

Figure 16 : Gene expression analysis of colonies from control and infected mice

A. Three colonies picked from control (top panel) and infected mouse lung (bottom panel) culture after 12 days in culture. Scale bar represents 200µm. B. Ecad (red) IF staining of mouse lung colonies from control and infected mice. C. Unsupervised clustering of control and infected lung colonies based on whole genome expression profiles. D. PCA analysis of colonies from control mouse lungs (red) and infected mouse lungs (blue). E. Heatmap of 506 differentially expressed genes between colonies from control and infected mouse lungs.

pathways were validated in three different colonies form control and infected mouse lungs and significantly different genes ($p<0.05$) were plotted (Fig. 17C).

Amongst the genes that were up-regulated in lung colonies, Matrix metalloproteinase (MMP)-9, a metalloprotease involved in migration was also detected. Interestingly, in normal adult lungs, MMP9 is expressed at low levels but is significantly elevated in several lung diseases, including asthma, IPF and COPD (Atkinson and Senior, 2003).

Other important genes up-regulated in infected compared to control lung colonies were Krt14 and Krt6a. Krt14 is another marker for p63 and Krt5+ basal cells and will be discussed more in the coming chapters. Krt6a is a keratin reportedly involved in wound healing (Wojcik et al., 2000). We noticed that Krt6a was highly up-regulated in infected colonies compared to control suggesting their role in lung regeneration. Moreover, Krt6a expression level was sufficient to separate the colonies derived from infected and control lungs as Krt6a high and low colonies respectively (Fig.18A). To validate this result with more number of colonies, we picked a total of 24 colonies from three control and infected lungs each (Fig.18B). We examined Krt6a expression in each of the 48 colonies and observed a statistically significant up-regulation of Krt6a in colonies from infected lung compared to control lung colonies (Fig.18C).

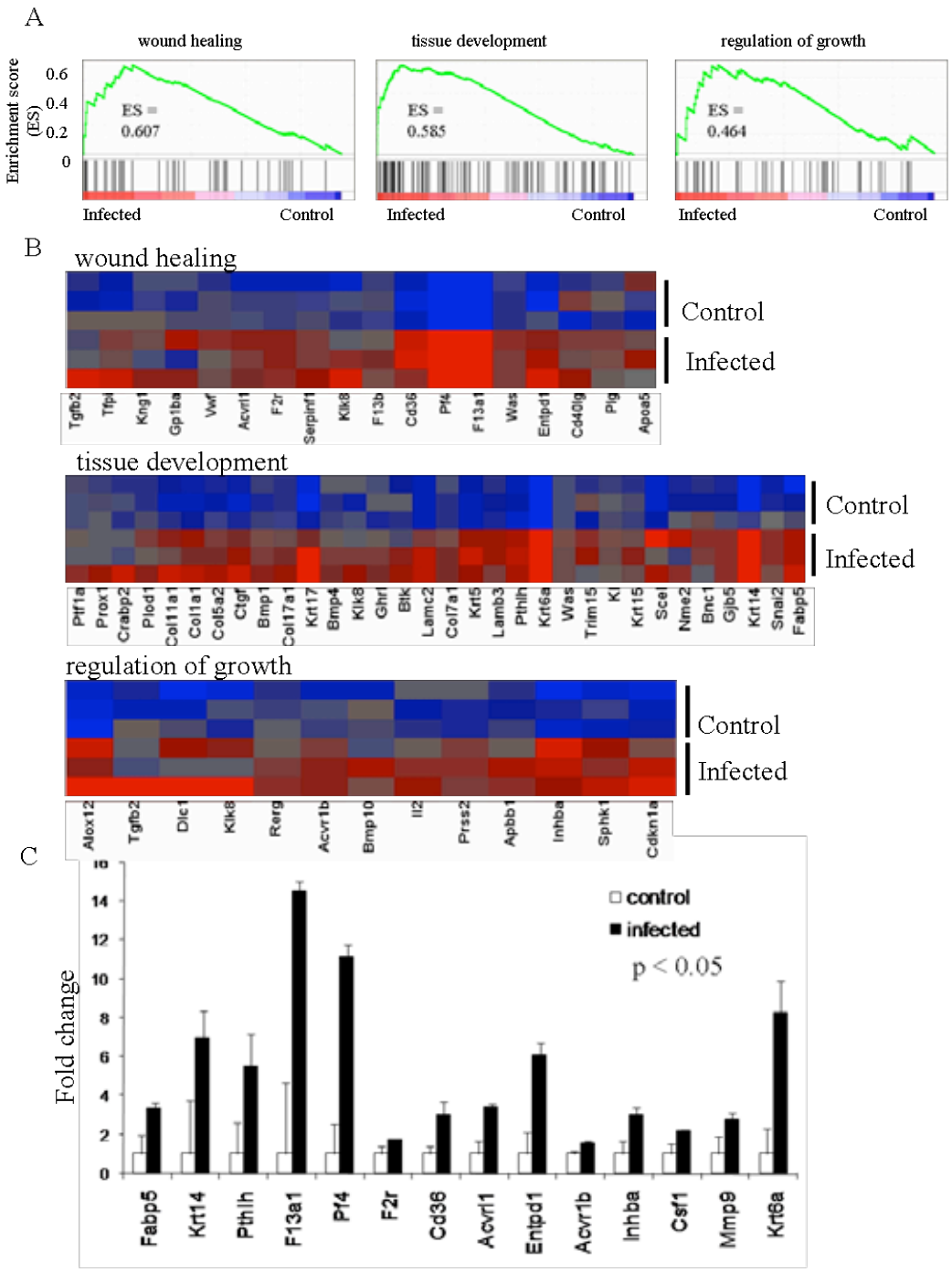

Figure 17 : Pathway analysis of mouse lung colonies post H1N1 infection
A. GSEA analysis of colonies from infected vs control colonies. Enrichment score (ES) for the wound healing, tissue development and regulation of growth pathways are 0.607, 0.585 and 0.464 respectively, p<0.001. B. Expression pattern of genes involved in differentially expressed pathways including wound healing, tissue development and regulation of growth in control and infected colonies. C. Fold change of genes involved in differentially enriched pathways validated by

qRT-PCR in three colonies from control and infected lungs. Error bar represents standard deviation from mean, $p<0.05$.

To validate Krt6a expression *in vivo* we stained normal and infected lung sections. Krt6a expression is absent in normal lungs and at 15 dpi is only detected in areas that have p63 expression (Fig.18E). About 50% of the p63+ cells co-stained with Krt6a at 15 dpi (Fig. 18D), suggesting Krt6a as a novel marker for the Krt5+ pods. Given that Krt6a+ cells are involved in wound healing in the skin we speculated that these p63+ Krt5+ Krt6a+ cells could also be involved in regenerating the lungs. These data also provide a possible link between the *in vitro* culture studies and *in vivo* infection data suggesting that the Krt6a+ cells that we cloned *in vitro* are the same as the p63+ Krt5+ pods we detected *in vivo* during the repair period.

Another gene that was up-regulated in colonies from infected lung was the transcription factor Sox2. Sox2 is commonly expressed in the bronchial epithelium of the mouse lung (Fig. 19C), and is important for cell proliferation and differentiation in the upper airways (Tompkins et al., 2011). During repair, Sox2 is present in regenerating bronchi as well as the alveolar regions where p63+ cells are present (Fig. 19A, B). About 40% of the cells are double positive for p63 and Sox2 in the alveolar regions (Fig. 19D). Generally Sox2 stains p63+ cells as well as the more differentiated cell types that eventually lose p63 expression 15 dpi. Sox2 is required to maintain a variety of stem cells and is known to play an important role in branching morphogenesis and epithelial cell differentiation during lung development (Gontan et al., 2008). Recently, Lu et al., 2010

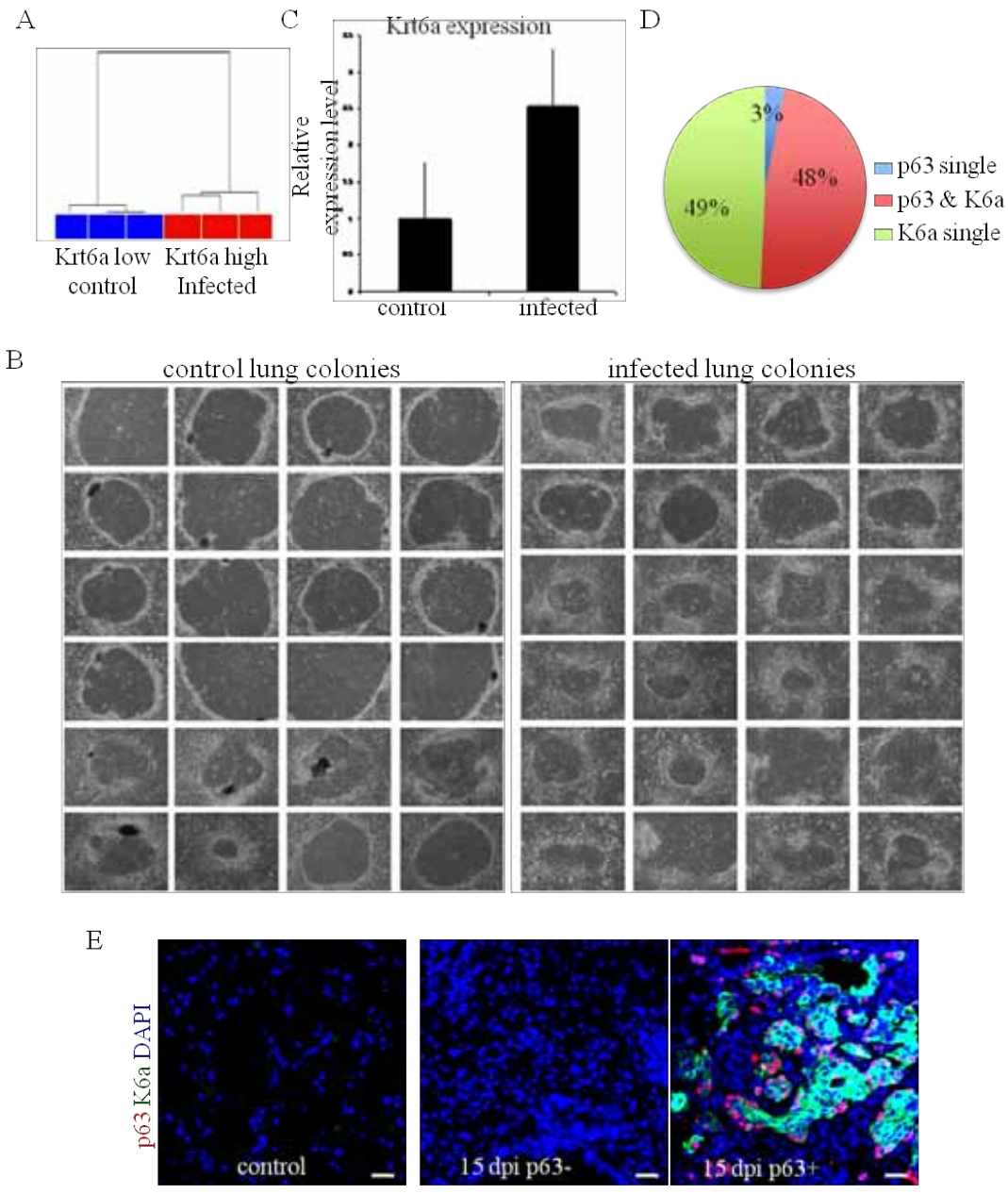

Figure 18 : 18 Krt6a expression pattern in mouse lungs colonies post H1N1 infection

A. Unsupervised clustering of control and infected colonies cluster out as Krt6a low and Krt6a high colonies respectively. B. Bright field images of 24 single colonies picked from control (left panel) and infected lungs (right panel) after 12 days in culture. C. Relative expression levels of Krt6a in 24 control and infected lung colonies by qRT-PCR. Error bar represents SEM. $p<0.05$. D. Quantification of p63+ Krt6a +cells in total stained cells from three mouse lungs 15 dpi. 3% of the stained cells are p63 single positive (blue), 48% stained cells are p63 Krt6a double positive (red) and 49% cells are Krt6a single positive (green). E. p63 (red) and Krt6a (green) staining in normal and infected lungs 15 dpi. Left panel shows

absence of p63 and Krt6a staining in alveolar regions of control lungs. Middle panel demonstrates absence of Krt6a staining in p63- damaged regions in lungs 15 dpi. Right panel shows Krt6a staining in regions which have p63+ clusters. Scale bar represents 100μm.

reported that over-expression of Sox2 is observed in squamous cell carcinomas and some adenocarcinomas in the lung.

4.2.4 *In vitro* culture and differentiation of mouse lung stem cells

We have established that during repair in the lungs post infection there is a massive increase in clonogenic cells. We also characterized these cells and identified novel markers that could be used for further characterization and molecular analysis.

The next step in the study was to determine the differentiation potential of the p63+ mouse lung stem cells from the lungs *in vitro*. In the clonogenic assays used above, the colonies obtained were quite differentiated because of the inherent problems of the culture system, which causes mouse stem cells to differentiate instead of staying immature.

In an effort to improve the conditions to obtain p63+ Krt5+ stem cells in culture we tested several culture conditions and concluded that Matrigel coating with feeder layer provided the best conditions to get p63+ Krt5+ colonies (Fig.20A). These colonies obtained from three-week mouse lungs in the second passage (P1) looked morphologically undifferentiated or immature and consisted of p63+

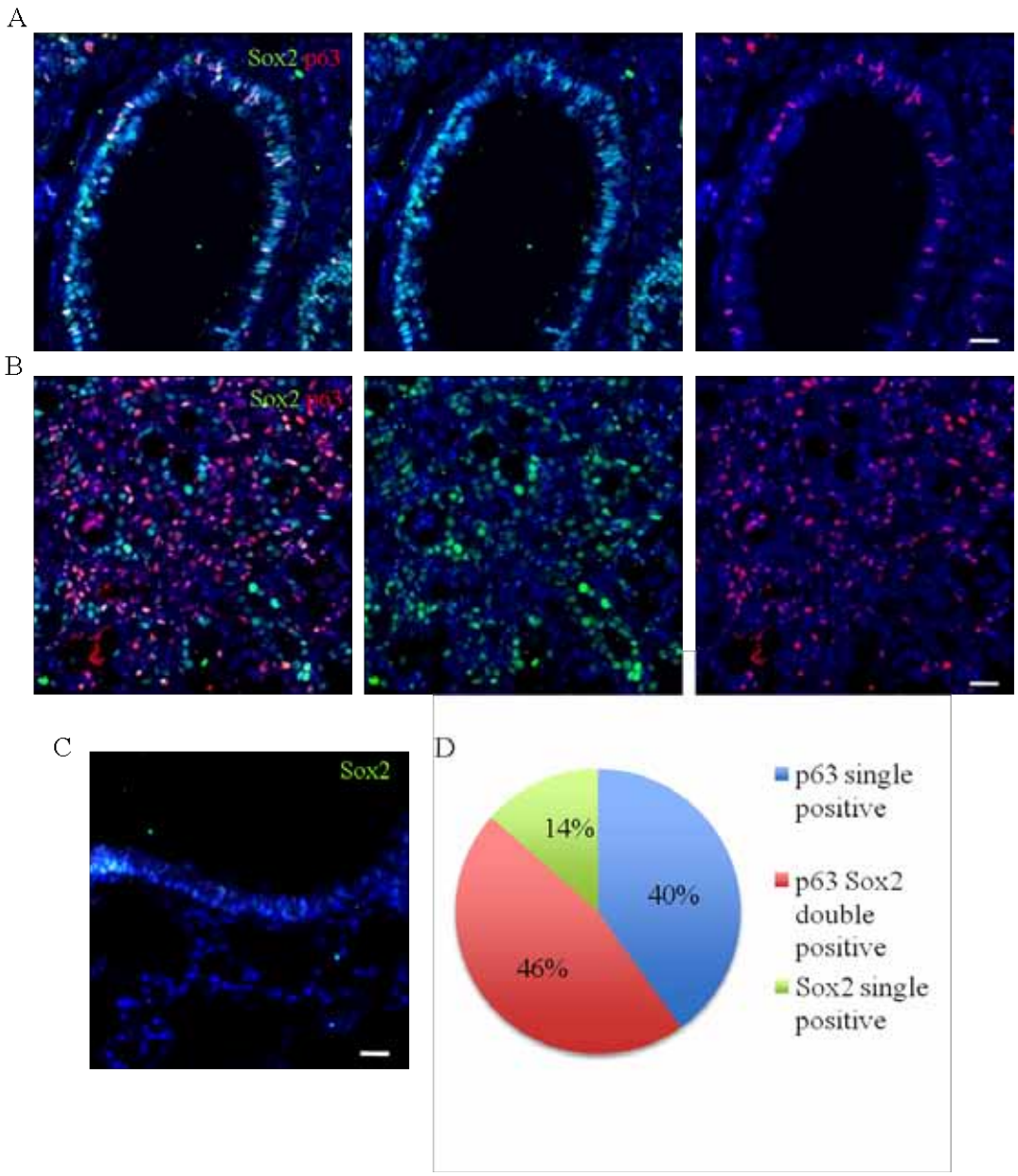

Figure 19 : Sox2 expression in mouse lungs
A.p63 (red) and Sox2 (green) staining in bronchiolar epithelium in lungs 15 dpi. Left panel shows overlapped image of p63 and Sox2 double staining while centre and right panel show Sox2 and p63 single staining respectively. Scale bar represents 50µm. B. p63 (red) and Sox2 (green) staining in alveolar epithelium in lungs 15 dpi. Left panel shows overlapped image of p63 and Sox2 double staining while centre and right panel show Sox2 and p63 single staining respectively. Scale bar represents 50µm. C. Sox2 (green) staining in bronchial epithelium of control mouse lungs. Scale bar represents 50µm. D. Quantification of p63+ Sox2+ cells in total stained cells from three mouse lungs 15 dpi. 40% of the stained cells are p63 single positive (blue), 46% stained cells are p63 Sox2 double positive (red) and 14% cells are Sox2 single positive (green).

Krt5+ cells. We picked three immature p63+ colonies for gene expression analysis and compared them with the gene expression analysis obtained form the differentiated colonies obtained from normal mouse lungs (Fig.20B, 16A).

The whole genome unsupervised clustering analysis grouped the differentiated and undifferentiated colonies separately (Fig. 20C) with about 3929 genes differentially regulated between them (Fig. 20D). For validation, we compared the gene expression of stem cell markers like p63, Krt5 and Krt14 in the immature colonies obtained from normal lungs compared to the differentiated mouse lung colonies and also mouse colonies from other tissues cultured in the Xian-McKeon laboratory including brain, ureter, pancreas, kidney and small intestine. Stem cell markers like p63, Krt5 and Krt14 were highly enriched in the immature colonies from mouse lungs compared to colonies obtained from differentiated colonies from mouse lungs as well as colonies from other tissues (Fig. 21A). We also confirmed that the differentiation markers like PDPN (alveolar type I cells), SPC (alveolar type II cells) and CC10 (Clara cells) were not up-regulated in the stem cell colonies confirming their immature status (Fig. 21B). This data also further illustrates that the p63+Krt5+ stem cell colonies are not the same as CC10+ SPC+ BASCs reported earlier (Kim et al., 2005).

Once we verified the immature status of the p63+Krt5+ colonies cultured, we further went on to perform differentiation assays to determine the differentiation potential of these cells. Fig. 22A represents a p63+ Krt5+ colony obtained from

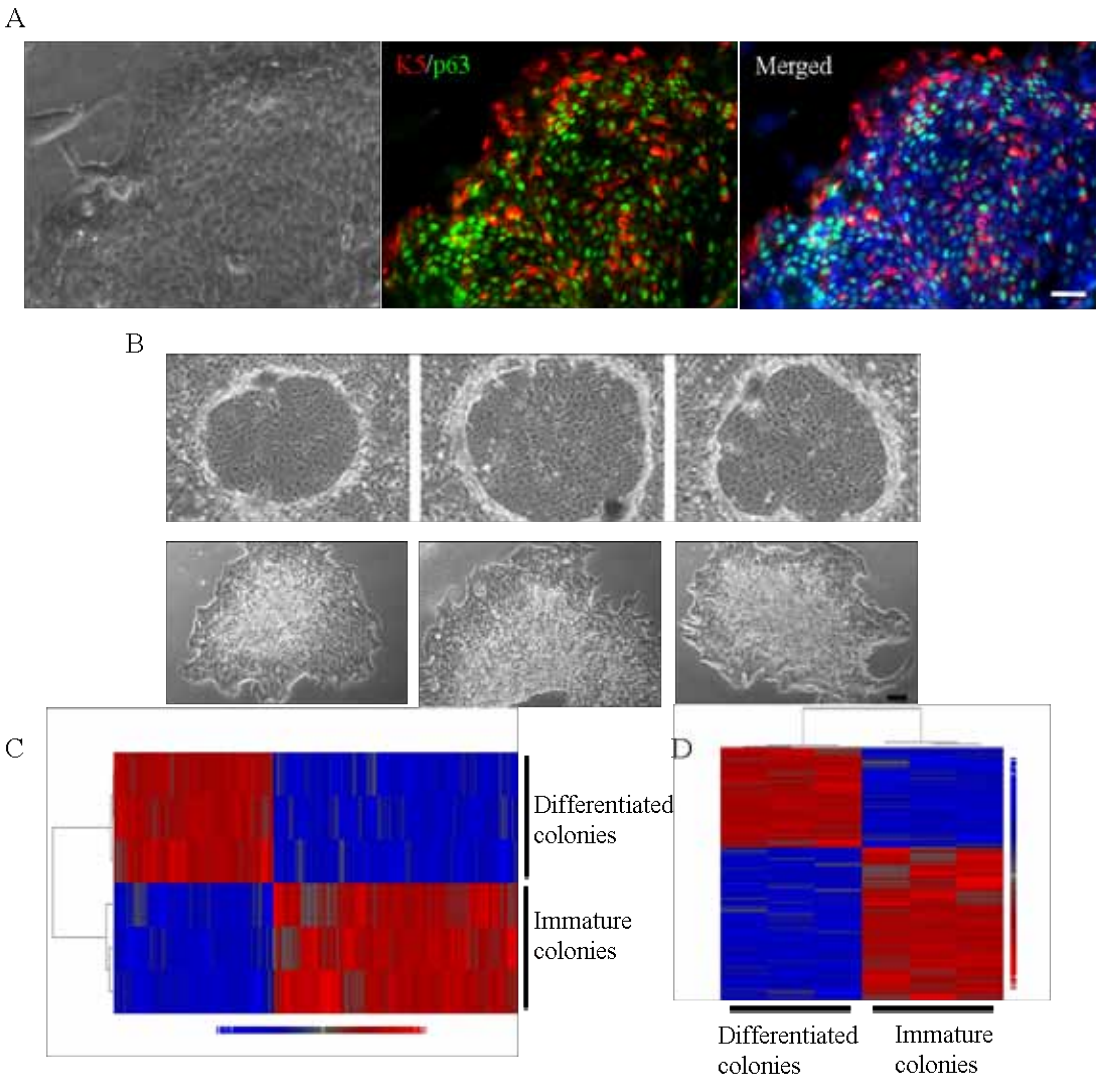

Figure 20 : Cloning p63+Krt5+ mouse lungs stem cells
A. High magnification image of p63+Krt5+ colonies colony obtained from three week old mouse lungs. Left panel shows bright field images of immature colonies. Middle and right panel shows p63 (green) and Krt5 (red) staining overlapped with nuclear stain DAPI (right panel). Scale bar represents 50µm. B. Image of colonies used for microarray analysis. Top panel represents the differentiated colonies and bottom panel represents the three immature (undifferentiated) colonies used for microarray analysis. Scale bar represents 200µm. C. Whole genome unsupervised clustering analysis of differentiated and immature colonies. D. 3929 differentially expressed genes (2 fold change, $p<0.05$) between differentiated and immature lung colonies.

three-week old mice after two passages on Matrigel coated 3T3 feeder layer. Colonies like these were pooled to get sufficient cells for differentiation assays in Matrigel. The immature cells were cultured in differentiation medium in Matrigel for 12-15 days to form hollow spherical structures (Fig. 22B). For detailed analysis, Matrigel with structures were embedded in OCT and 10μm frozen sections were cut through them. The hollow structures were single layered epithelial structures that stained positive for Ecad (Fig. 22B). Though the structures still expressed stem cell markers like Krt14, confirming they arose from the p63+Krt5+ immature colonies, they also stained positive for differentiation marker Aquaporin 5 (Aqp5). Aqp5 is a mercury-sensitive water channel and is expressed in mouse salivary gland acinar cells, lacrimal glands, eyes and alveolar type I cells in the airways. Although AQP5 is most commonly used as an alveolar type I cell marker it is also detected in alveolar type II cells as well as tracheal and bronchial epithelium in mice (Krane et al., 2001; Nielsen et al., 1997).

At the gene expression level we analyzed the expression levels of several differentiated cell markers including surfactants released by alveolar or bronchial epithelium like Sftpa1, Sftpb, Sftpc, other alveolar markers like Aqp5, Cftr, Ptgs2, Clara cell marker (CC10) and Goblet cell marker (Muc5ac), (Fig. 22C). Along with the up-regulation of these differentiation markers we also observed a down-regulation of the stem cell markers like Krt5, Krt14 and Krt6a suggesting that the p63+Krt5+ stem cells are capable of differentiating into terminally differentiated airway epithelium. No change in expression of squamous differentiation markers

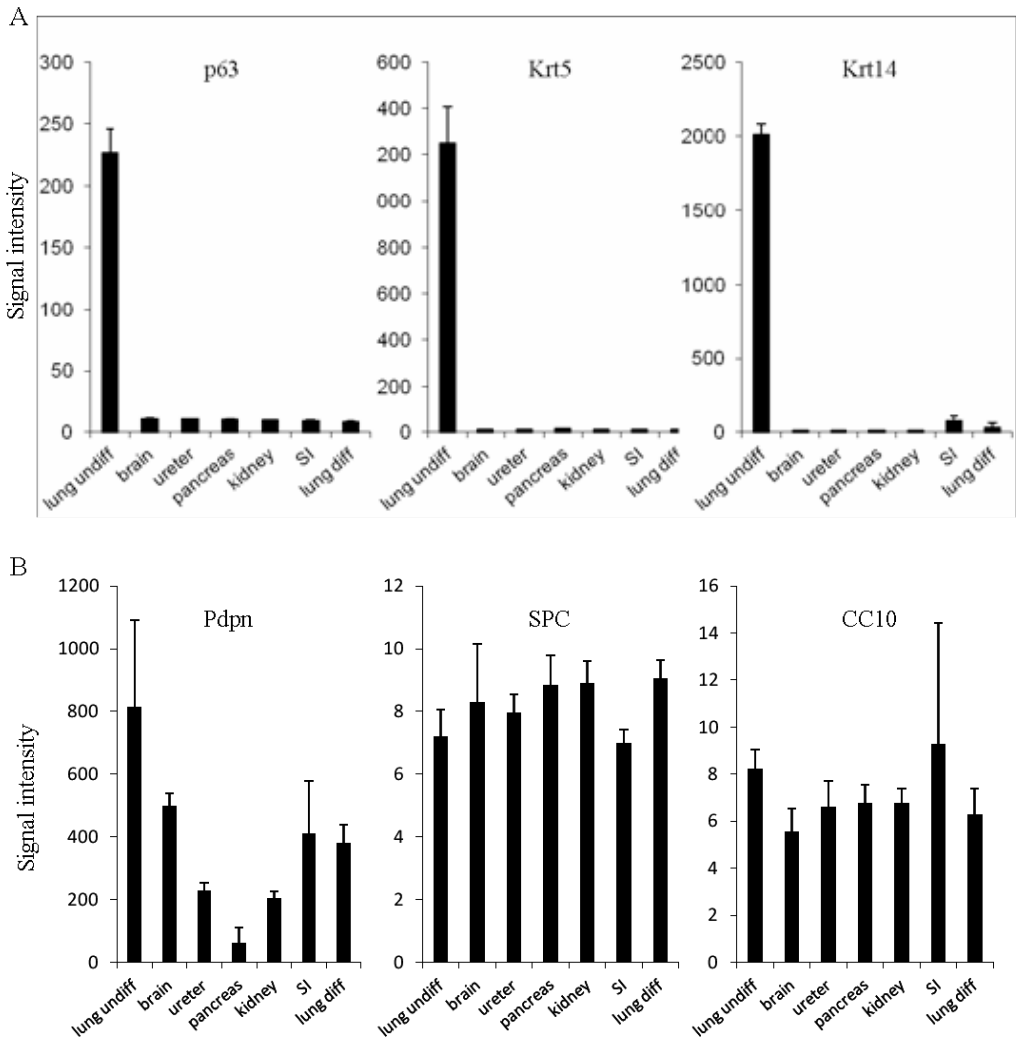

Figure 21 : Gene expression analysis of mouse stem cells colonies
A. Top panel represents signal intensity data obtained for p63, Krt5 and Krt14 form microarray data sets of different colonies including undifferentiated (immature) lungs colonies (lung undiff), colonies from brain, ureter, pancreas, kidney, small intestine (SI) and differentiated lung colonies (lung diff). Error bar represents standard deviation from mean. B. Signal intensity of differentiation markers Pdpn, SPC and CC10 from microarray data sets of different colonies including undifferentiated (immature) lungs colonies (lung undiff), colonies from brain, ureter, pancreas, kidney, small intestine (SI) and differentiated lung colonies (lung diff). Error bar represents standard deviation from mean.

such as Krt10 confirmed that the p63+Krt5+ were not differentiating into squamous cell types. We also evaluated the expression level of endothelial cell markers like Vimentin to ensure that the cells retained their epithelial nature on differentiation. All expression studies were done in triplicates and normalized to GAPDH expression levels in the cells.

In total we conclude that mouse lung stem cells in our culture system are p63 and Krt5+ and can be differentiated into epithelial structures with markers of alveolar and bronchial cells up-regulated.

4.2.5 *In vitro* culture and differentiation of rat lung stem cells

We also cultured lung stem cells from other rodents such as rats. Single cell suspension of adult rat lungs was plated on 3T3 feeder layer to obtain immature colonies (Fig. 23A) that are positive for stem cell markers such as p63. When these cells were transferred to differentiation conditions in Matrigel they formed 3D spherical structures that hollowed out after differentiation (Fig. 23B). These structures stained positive for alveolar markers like 13A1 and 54D1 (Fig. 23C). These two markers are hybridomas developed in the Xian-McKeon lab that react specifically to alveolar cell types in the rat lungs (Fig. 23D, E).

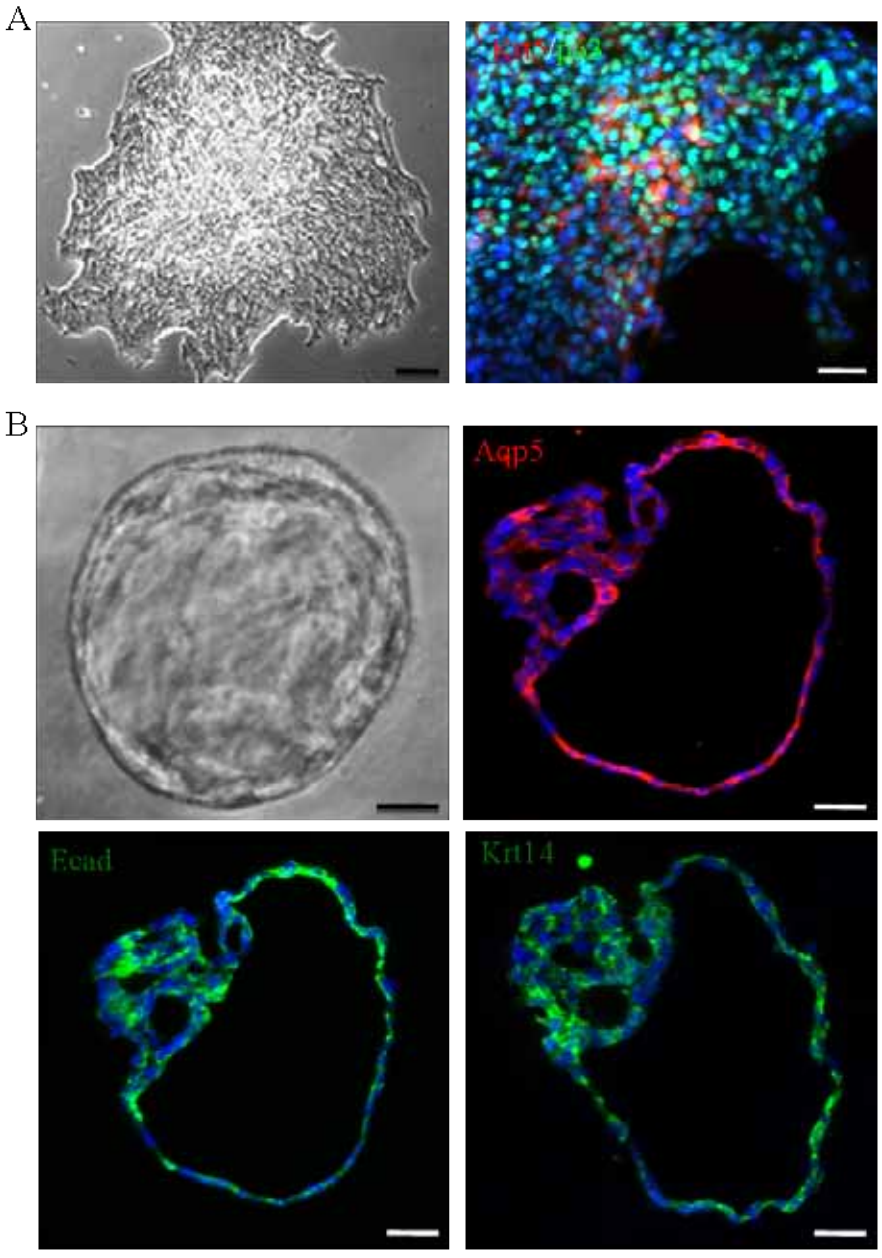
A
B
Aqp5
Ecad
Krt14
C
Sftpa1
Sftpb
Sftpc
Aqp5
Ptgs2
Cftr
CC10
Muc5ac
Krt10
Krt5
Krt14
Krt6a
Vim
Matrigel
Stem cell

Figure 22 : Differentiation potential of p63+Krt5+ mouse lung stem cells *in vitro*
A. Left panel shows low magnification image of immature colony obtained from mouse lungs which are positive for stem cell markers p63 (green) and Krt5 (red), right panel. Scale bar represents 200μm and 50μm respectively. B. 3D *in vitro* differentiation of p63+ Krt5+ mouse lung stem cells in Matrigel. Top left panel shows bright field image of differentiated hollow structures after 12 days in differentiation culture. Scale bar represents 50μm. The structures in Matrigel were embedded in OCT and 10μm frozen sections were cut and stained for Aqp5 (red, top right panel), Ecad (green, bottom left panel), Krt14 (green, bottom right panel) on consecutive sections. Scale bar represents 50μm. C. qRT-PCR analysis of selected genes in triplicates of stem cells and Matrigel structures.

4.3 CONCLUSIONS AND DISCUSSION

In this chapter, the stem cell potential of p63+Krt5+ cells was assayed. We observed about 30% of the Krt5+ pods were actively proliferating *in vivo* during repair. This pointed to a stem cell potential of the p63+Krt5+ pods and hence, we next assayed the clonogenic ability of these cells. Using a system developed by Dr. Howard Green in the 1970s to culture epidermal stem cells, we observed that the cells from infected lungs at 12 dpi were 20 fold more clonogenic than the control lungs. These cells had a differential gene expression pattern compared to colonies from control lungs and were enriched in pathways related to wound healing and tissue development.

Several genes including MMP9 and Krt6a were also up-regulated in the colonies from infected lungs. MMP9 is important for cellular migration in several tissues, and in the lungs has been reported to be involved in the migration of basal cells

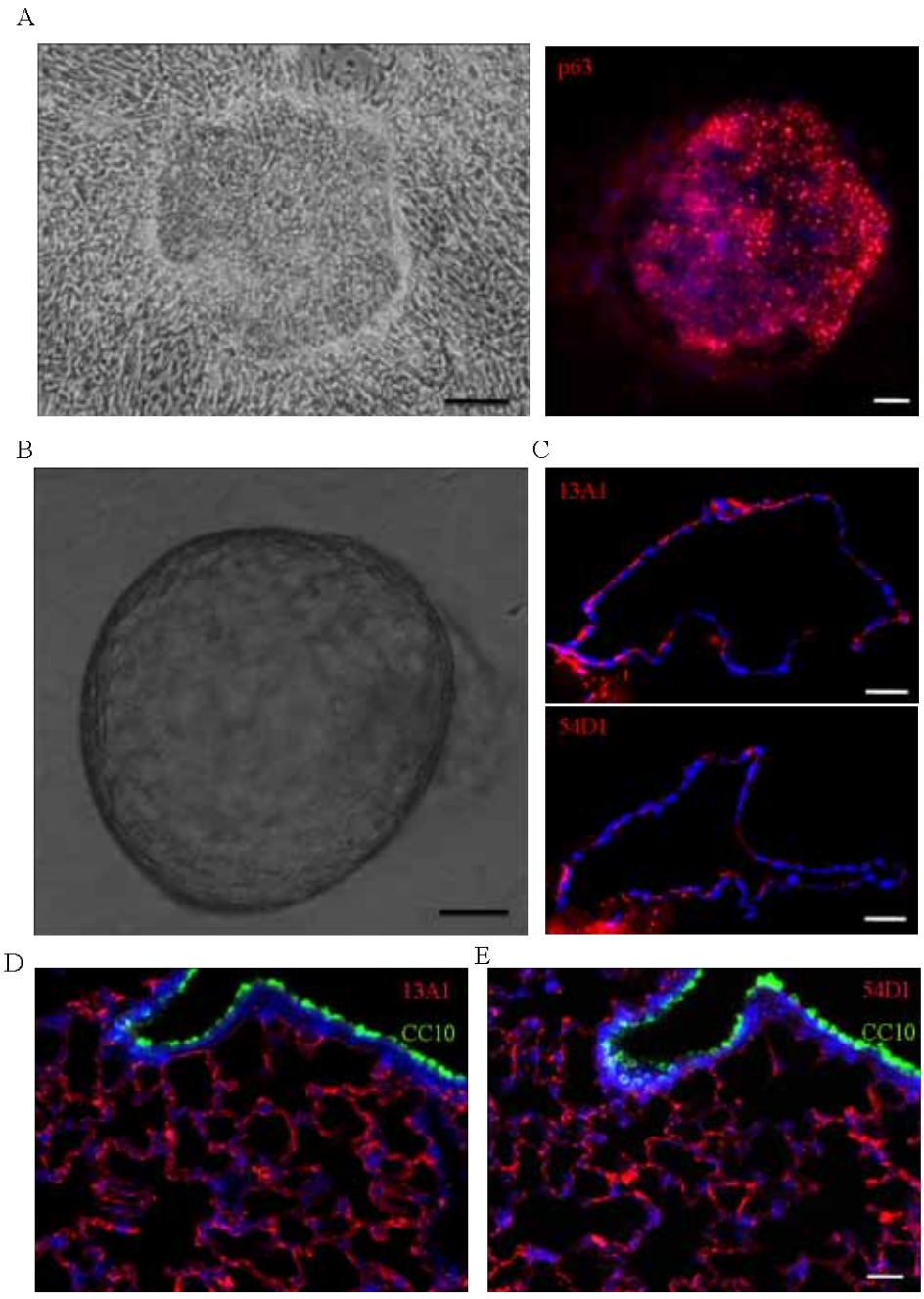

Figure 23 : Rat lung stem cell culture and differentiation
A. Top left panel represents colonies obtained from rat lung on 3T3 feeder layer. Scale bar represents 200µm. Top right panel demonstrates p63 (red) staining on the immature rat lung colonies. Scale bar represents 25µm B. Differentiation of p63+ rat lung colonies in Matrigel after 21 days in culture. Scale bar represents 100µm. C. The structures in Matrigel were embedded in OCT and 10µm frozen sections were cut and stained for 13A1 (red, top panel) and 54D1 (red, bottom panel). Scale bar represents 50µm. D. Rat lung sections stained with alveolar

markers 13A1 (red) and 54D1 (red) with CC10 (green). Scale bar represents 50μm.

after tracheal wounding and terminal airway epithelial cells after bleomycin. MMP-9 cleaves type IV collagen, and is thus hypothesized to contribute to the migration of epithelial cells through basement membranes (Atkinson and Senior, 2003).

Krt6a has also been studied extensively in stratified epithelia such as the skin and oral epithelium (Wojcik et al., 2000; Wong et al., 2000). While the Krt6a knock-out mouse has no significant developmental defects in the skin or airways, delayed wound healing was observed in the skin suggesting the importance of Krt6a+ cells in repair. In our studies, Krt6a was up-regulated in the p63+ Krt5+ pods *in vivo,* and also in the colonies obtained from the lungs of infected mice. Krt6a expression profile thus provided a crucial link between the *in vivo* studies and *in vitro* clonogenic cells suggesting that the increase in clonogenic cells post infection could be because of the increase in Krt5+ Krt6a+ cells *in vivo* 12 dpi. These data together suggest that the p63+ Krt5+ Krt6a+ pods observed in the lung during repair period were actively proliferating and also had clonogenic ability *in vitro*.

Interestingly, it was also observed that while Krt6a was not detected in the normal airways and during repair (post 11 dpi), it was preferentially observed only in the interstitial damaged regions expressing p63. Considering Krt6a knock-out mice

do not have severe developmental effects we propose Krt6a to be a novel marker specific to Krt5+ pods and could be used for several important studies in the future.

After establishing the proliferation capability of the p63+ Krt5+ cells, we assayed the differentiation potential of the p63+ Krt5+ cells *in vitro*. Since the colonies obtained from adult mouse lungs were generally differentiated, we developed a novel culture system to obtain small populations of p63+ Krt5+ cells from 3-4 week old mouse lungs. Although the lungs develop even after birth, by 3-4 weeks the development is almost complete (Costa et al., 2001). We validated the immature state of the cloned cells by up-regulation of stem cell markers like p63, Krt5, and Krt14 and down-regulation of differentiated cell markers in these immature colonies. We then transferred the p63+ Krt5+ stem cells to a differentiation system to obtain hollow spherical epithelial structures that had markers of bronchial and alveolar cell types up-regulated. These data suggest a multipotent differentiation potential of the p63+ cells into cell types of upper and lower airways. We also prove that these cells in the differentiation system do not contribute to squamous differentiation.

It has been reported that p63+ Krt5+ stem cells from tracheal epithelium can differentiate into cell types of upper airways (Rock et al., 2009), but the ability of these cells in the lung to differentiate into alveolar cell types was not known. These results were confirmed by cloning lung stem cells from mouse and rat

lungs in our system. The cloned p63+ cells from rat lungs also differentiated into hollow spheres that stained positive for alveolar specific hybridomas developed in the Xian-McKeon lab. These results confirmed that p63+ cells cloned from mouse and rat lungs have the potential to differentiate into alveolar cell types.

This work was strongly supported by Dr. Yuanyu Hu's work in the Xian-McKeon lab (Kumar et al., 2011) on cloning human region specific stem cells. Dr.Hu cloned p63+ Krt5+ stem cells from human nasal epithelium, tracheo-bronchial epithelium and distal airway epithelium, and after detailed pedigree analysis concluded that although these stem cells differ in gene expression profile only by a few 100 genes, they have a confirmed fate. The nasal and tracheo-bronchial epithelium in different *in vitro* culture conditions can differentiate into cell types of the upper airways or lead to squamous differentiation. However the p63+ Krt5+ stem cells from the distal airways have a multipotent ability to give rise to cell types of upper and lower airways.

Unlike mouse cells that do not grow very well in this culture system, human cells grow well and can be passaged several times while maintaining the immature state of the colonies. Although we obtained p63+ Krt5+ cells in mouse culture, the clonogenic efficiency was low and they could not be maintained in their immature state for more than two passages, thus making it unsuitable for detailed self-renewal analysis, as possible with human or rat cells. Efforts are currently being made to improve the culture conditions of mouse lung stem cells to enable long-term culture and eventually *in vivo* transplantation experiments. A robust

culture condition is also essential for assays to dissect the underlying mechanisms involved in stem cell renewal and differentiation of the stem cells.

In total, the *in vitro* clonogenic and differentiation assays described in this chapter revealed the stem cell potential of the p63+ Krt5+ cells observed during repair. These cells will be characterized further *in vivo* in the next chapter, to understand their role in repair.

CHAPTER 5: MOLECULAR ANALYSIS OF Krt5+ PODS *IN VIVO*

5.1 INTRODUCTION

In a physiologically relevant lung damage system involving H1N1 infection, we have identified p63+Krt5+ pods during the repair process. This unique population of cells is not detected in normal lungs, or in adverse pathological phenotypes such as fibrosis. Moreover, these Krt5+ pods are actively proliferating *in vivo* and have stem cell potential *in vitro,* in that they are clonogenic and can differentiate into multiple cell types in differentiation assays. To characterize and understand the potential of these cells further we sought to perform detailed molecular analyses of the p63+ Krt5+ pods *in vivo*. Due to the unavailability of surface markers to isolate this population of cells from the entire lung we employed the Laser Capture Microdissection (LCM) technique.

LCM is a technique used for isolating pure populations of cells from a heterogeneous tissue section, cytological preparation, or live cell culture via direct visualization of cells (Bonner et al., 1997; Emmert-Buck et al., 1996). The cells obtained by this method can be used for a variety of applications including DNA genotyping and loss-of-heterozygosity analysis, RNA transcript profiling, cDNA library generation, proteomics discovery and signal-pathway profiling (Espina et al., 2006). There are two general classes of laser-capture microdissection: infrared capture systems (Bonner et al., 1997; Emmert-Buck et al., 1996) and ultraviolet cutting systems (Schütze et al., 1997; Schütze et al., 1998) . In our study we use

the PALM® Robot Microbeam laser microdissection system (P.A.L.M. GmbH, Bernried, Germany) in combination with a Zeiss microscope. This system applies the laser microdissection and pressure catapulting approach which uses an ultraviolet laser (UVA) first to circumscribe the region(s) to be excised, and then, pulses the sample below the focal plane to catapult it into an inverted microfuge tube cap positioned above the sample. For our experiments, the lung could be stained, and desired regions were dissected out using this technology.

Gene expression analysis and pathway analysis were performed to determine the differentiation tendency of the Krt5+ pods dissected using LCM. The PANTHER (Protein ANalysis THrough Evolutionary Relationships) Classification System was used for the pathway analysis. This classification system uses a database of published scientific experimental evidence and evolutionary relationships to predict the functions of genes and classify them based on their functions (Thomas et al., 2003).

In this chapter, we discuss the LCM of samples from mouse lung tissue sections 12 dpi and the gene expression analysis performed on them.

5.2 RESULTS

5.2.1 Dissection of Krt5+ pods at 12 dpi

For the molecular analysis of the Krt5+ populations of cells during repair, mouse lung sections 12 dpi were stained for Krt5. Krt5+ cells could be classified in two

regions namely “Krt5+ interstitial” and “Krt5+ bronchial” regions. Krt5+ interstitial regions consist of the Krt5+ pods detected in the interstitial damaged areas of the lungs during repair. “Krt5+ bronchus” consists of the bronchi or bronchioles lined with Krt5+ cells in the basal layers of the epithelium. Damaged interstitial regions as well as bronchi or bronchioles devoid of Krt5 staining were also observed on the same sections. These “Krt5-interstital” regions and “Krt5-bronchi” or bronchioles served as controls for the molecular analysis (Fig. 24A).

Fig. 24B demonstrates the isolation of a group of just 10-20 cells from the alveolar region of a mouse lung section. These dissected cells can be utilized for several purposes including RNA isolation for gene expression analysis.
For the experiment (Fig. 24C), three mice were infected with a sub-lethal dose of the virus and sacrificed at 12 dpi. Lungs were harvested and embedded immediately in cryo-molds with OCT. Frozen sections were used in this analysis instead of formalin fixed paraffin sections to minimize the degradation of RNA in the tissues.10μm sections were cut on membrane slides under RNAse free conditions. Adjacent sections on normal glass slides were used for Krt5 staining to identify the Krt5+ populations of cells. After imaging the regions to be dissected, we used consecutive sections on membrane slides for the LCM of the desired population of cells (Fig. 25A). Fig. 25B represents dissection of the Krt5+ pods and Krt5+ bronchus from mouse lung sections 12 dpi. All four samples were collected in triplicates in this manner, and RNA was extracted from them and processed to perform gene expression analysis.

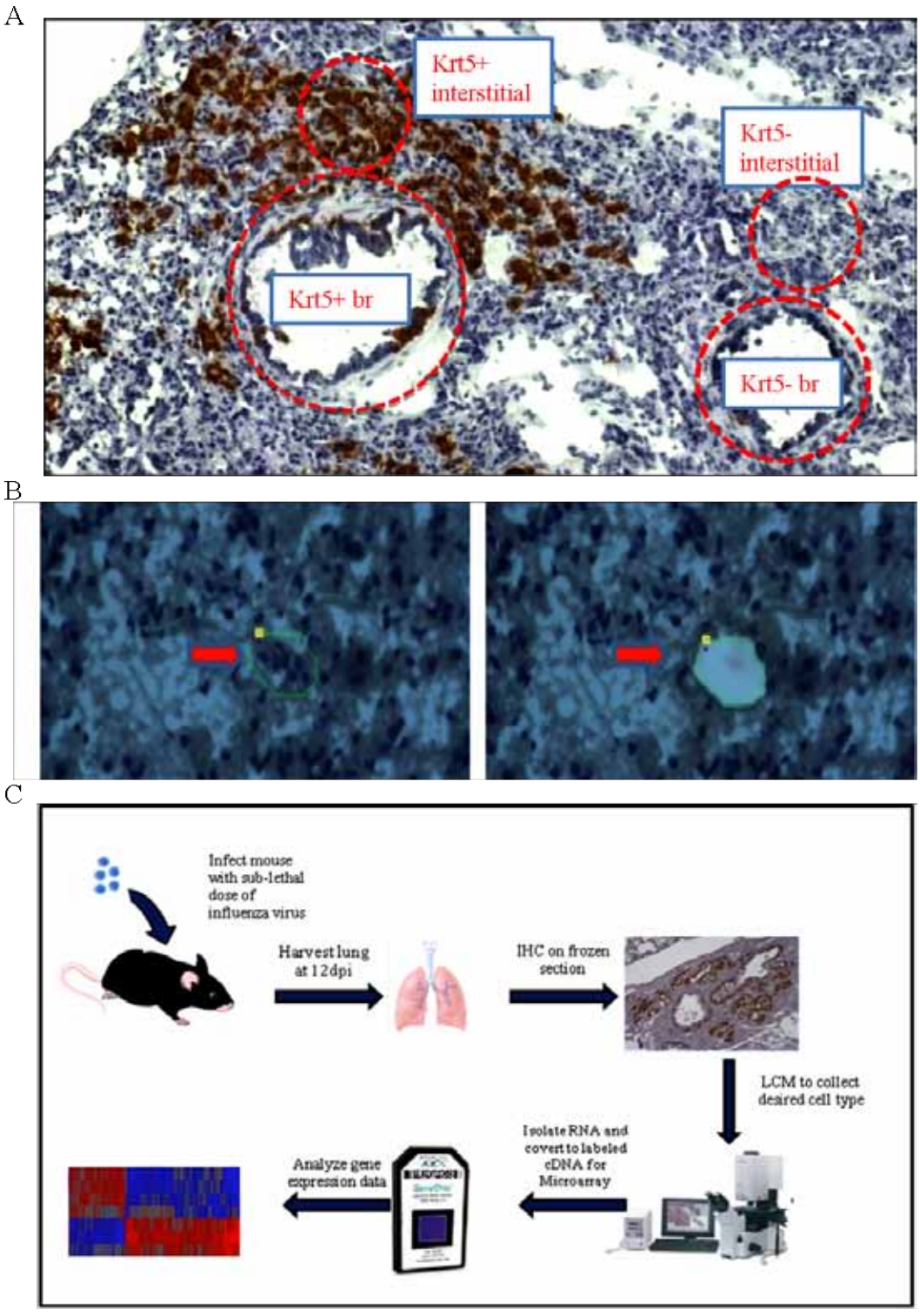

Figure 24 : Krt5+ populations at 12 dpi
A. Different populations identified in mouse lungs 12 dpi based on Krt5 staining on frozen sections namely Krt5+ bronchus (br), Krt5+ interstitial, Krt5- bronchus (br) and Krt5- interstitial. B. Demonstration of LCM of alveolar region from

10μm frozen section of lung before and after the LCM. C. Schematic of workflow for LCM of Krt5+ pods and control regions for gene expression analysis.

5.2.2 Gene expression analysis of Krt5+ pods 12 dpi

Microarray analysis revealed that the biological triplicates for all four samples clustered to each other in spite of being isolated from three different mice with dynamic ongoing repair processes, thus increasing our confidence in the data. The Krt5+ bronchus and Krt5- bronchus clustered together, implicating that they were very similar in expression patterns (Fig. 26A). However Krt5+ interstitial and Krt5-interstitial samples were plotted far away from each other suggesting the Krt5+ pods in the interstitial regions to be a unique population of cells. Unsupervised clustering of the samples with the significantly differentially regulated genes (Fig. 26B) mirrored the PCA map results. Krt5+ bronchus and Krt5- bronchus clustered together, with the distance between the clusters being very small. Interestingly, although Krt5+ interstitial regions had a very different gene expression pattern compared to the other samples by the PCA analysis (Fig. 26A), they clustered together with the Krt5- interstitial regions rather than the two bronchi samples (Fig. 26B). Fig. 26C details the number of differentially expressed genes in each sample which are statistically significant. Krt5+ and Krt5- bronchi are very similar to each other with an overlap of 1746 genes. Only 50 and 43 genes are differentially expressed in the Krt5+ and Krt5- bronchi respectively. Additionally, while Krt5+ interstitial and Krt5- interstitial regions have 1331 genes common they still have 394 and 114 genes respectively, differentially regulated in them.

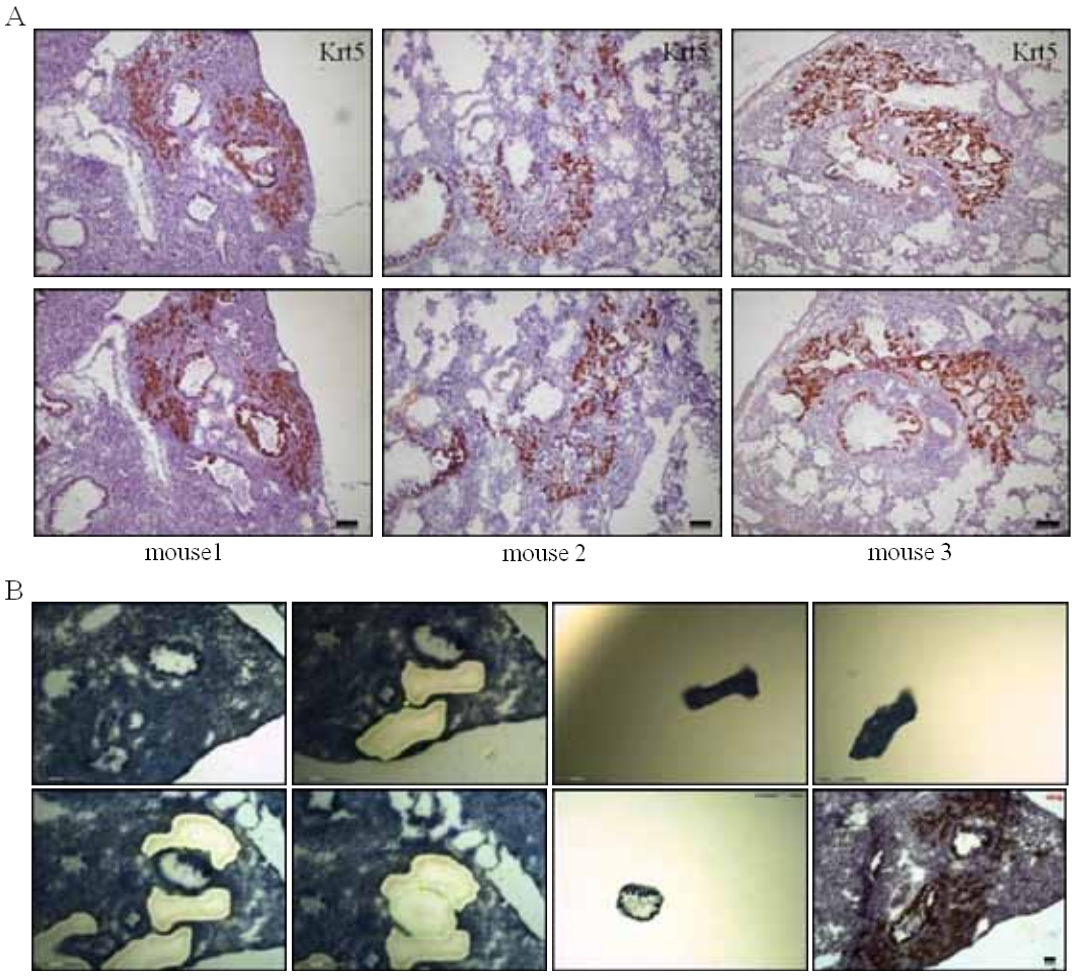

Figure 25 : Laser capture microdissection of Krt5+ pods 12 dpi
A. Left top panel represents Krt5 stained 10µm frozen lung sections of mice 12 dpi. Left bottom panel represents Krt5 stained 10µm frozen lung sections four sections away from the top panel image. The middle and right panel Krt5 stained sections are of similar pattern but from two different mice. Scale bar represents 100µm. B. Top panel represents dissection of Krt5+ interstitial region from mouse lung 12 dpi. Bottom panel represents dissection of Krt5+ bronchus from mouse lung 12 dpi. Bottom right most panel represents Krt5 staining on adjacent section used as reference for the dissection. Scale bar represents 150µm.

These analyses imply that Krt5+ and Krt5- bronchi are very similar to each other. Krt5+ interstitial regions are a unique population of cells with several differentially expressed genes, although in total, they are closer in gene expression pattern to the Krt5- interstitial regions than the bronchi samples. However, this whole genome expression analysis could be misleading as both the Krt5+ and Krt5- interstitial regions, have a common contamination of immune cell populations. This could cause them to cluster together, rather than to the bronchial epithelium. To avoid this bias we analyzed the expression levels of selected bronchial and alveolar genes in the two Krt5+ populations, namely the Krt5+ interstitial region and Krt5+ bronchial epithelium (Fig. 27A). Several alveolar region related genes were up-regulated and bronchial epithelium related genes were down-regulated in Krt5+ interstitial regions compared to the Krt5+ bronchus. For example, ECM proteins important for cell adhesion in alveolar type II cells such as Fn1 and Dpt (Gereke et al., 2007) were up-regulated in Krt5+ interstitial regions. Another ECM protein Tnc (Tenascin C) reported as an important gene involved in lung development and tissue repair (Roth-Kleiner et al., 2004) was also up-regulated in Krt5+ pods. Increased expression of vascular endothelium marker Cdh5 (Monvoisin et al., 2006) and CD34, a marker for alveolar capillaries (Pusztaszeri et al., 2006) also suggested that the endothelium network, which is crucial for alveolar development, is present in Krt5+interstitial regions. Interestingly, CD34+ cells in the lungs have also been reported as a stem cell population during SARS infection(Chen et al., 2007). Other genes up-regulated in Krt5+ interstitial regions include Cfl1 and Sparc. Cfl1 has been

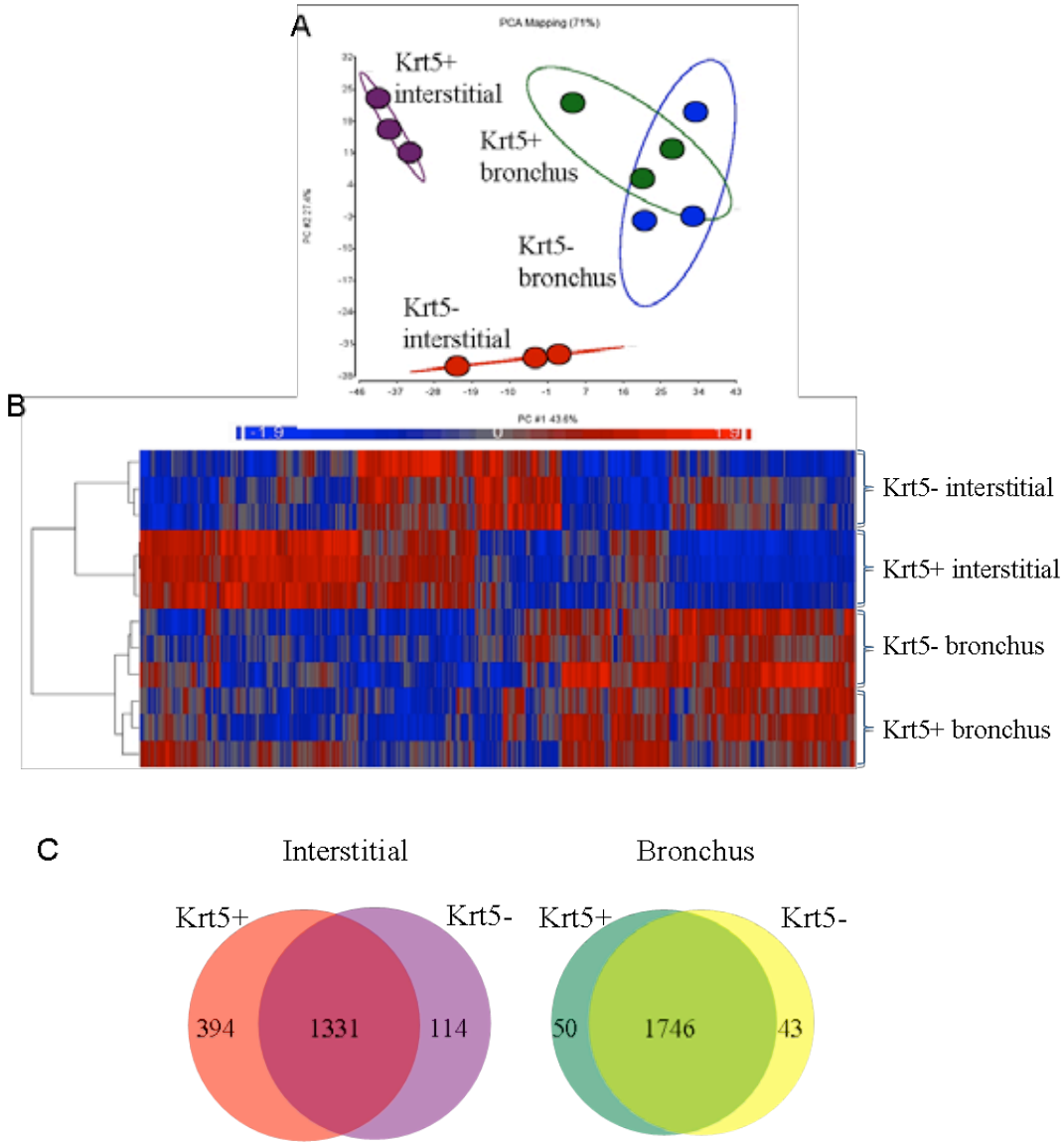

Figure 26 : Gene Expression analysis of Krt5+ pods 12 dpi
A. PCA map based on whole genome expression of four populations of cells. Krt5+ interstitial cells are marked in purple, Krt5+ bronchus cells marked in green, Krt5- bronchus marked in blue and Krt5- interstitial marked in red. Each sample is represented in triplicates. B. Unsupervised clustering of significantly ($p<0.05$) differentially expressed genes in the 4 cell types. Each cell type is in triplicates. C. Venn diagram representing the gene numbers differentially regulated in the four populations of cells. 394 genes and 114 genes are high in Krt5+ and Krt5- interstitial regions respectively while 1331 genes are common between both the regions. 50 genes and 43 genes are high in Krt5+ and Krt5- bronchi respectively while 1746 genes are common between both the regions.

reported to be important for cell invasion and migration (Castro et al., 2010) and is also expressed in alveolar macrophages (Morato-Marques et al., 2011) while Sparc is up-regulated in alveolar fibroblasts during pneumonia (Kuhn and Mason, 1995).

Additionally, several genes that are related to normal alveolar formation were also enriched in Krt5+ interstitial areas compared to Krt5+ bronchi. For example, Pdgfra is an important component of the PDGF signaling, which is important for the formation and compartmentalization of alveoli in lungs (Boström et al., 2002). Msn1 is normally localized to the distal epithelium in the airways and has also been studied vastly in the airways. Researchers have shown that Msn1 knock-out mice have abnormal alveolar architecture, and have more severe lung damage and inflammation upon bleomycin treatment (Hashimoto et al., 2008). Another example of genes involved in the lower airways could be Fbn1, a matrix component of extracellular microfibrils, which is also important for normal alveolar septation (Neptune et al., 2003). Along with the up-regulation of several alveolar region related genes, we also observed a down-regulation of bronchial epithelium related genes in the Krt5+ interstitial regions compared to the Krt5+ bronchus. For example, Muc1, a mucous marker for pseudo-stratified epithelium in proximal airways (Buisine et al., 1999), as well as other tracheobronchial markers such as Retnla (Doherty et al., 2012), are down-regulated in Krt5+ pods. Surfactant proteins such as Sftpa1 (Endo and Oka, 1991), and enzymatic proteins including Pon1 (paraoxonase 1), (Rodrigo et al., 2001) involved in the

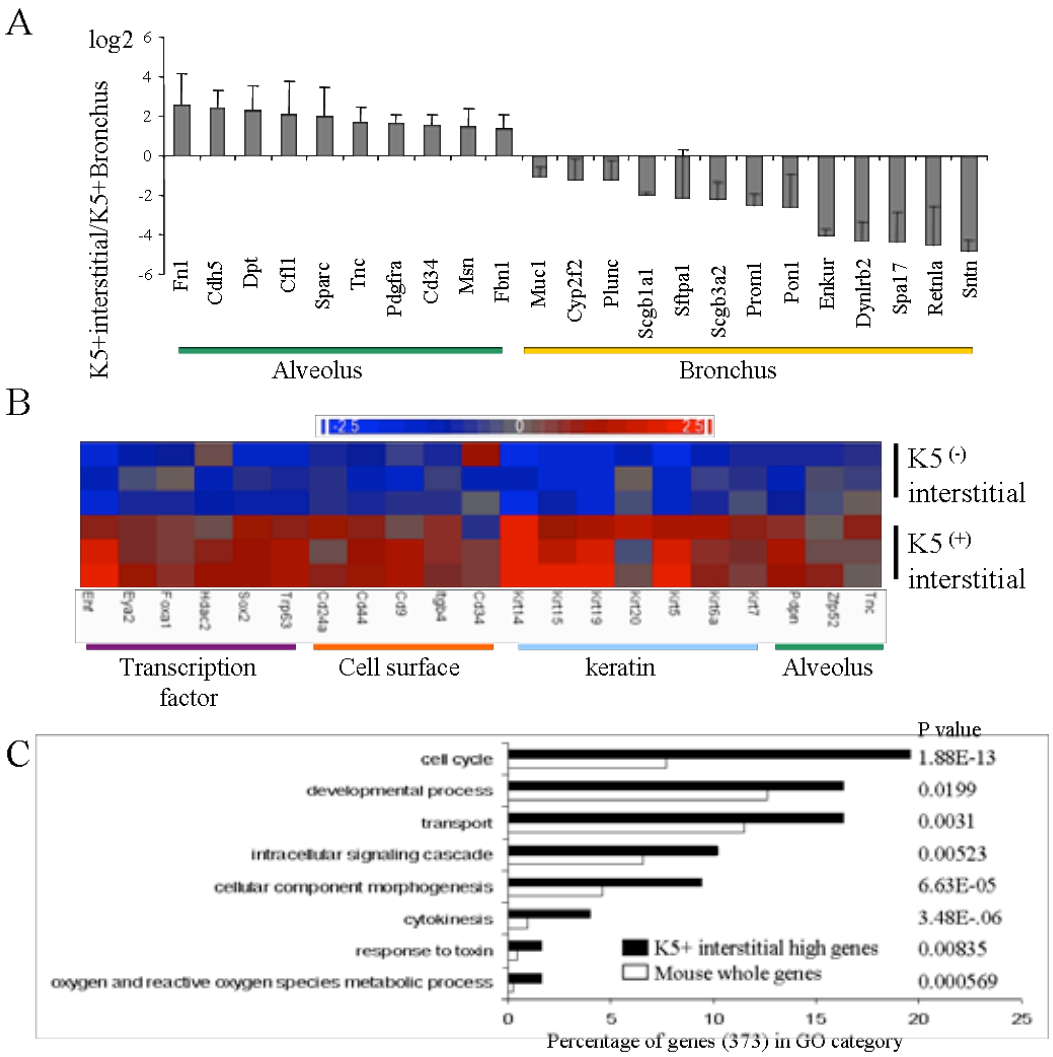

Figure 27 : Alveolar genes up-regulated in Krt5+ pods at 12 dpi
A. Ratio of alveolar and bronchus related gene expression between Krt5+ interstitial and Krt5+ bronchial epithelium. Error bar represents standard deviation from the mean. B. Expression patterns of specific transcription factors, cell surface markers, keratin markers and alveolar markers in Krt5+ interstitial and Krt5- interstitial regions. Each sample is in triplicates. C. Pathway analysis of 373 genes enriched in Krt5+ interstitial region. $p < 0.05$. Black bar represents genes from the Krt5+ interstitial regions while white bars represent genes from the entire mouse genome (26185 genes).

detoxification of toxins in the upper airways are down-regulated in Krt5+pods compared to Krt5+ bronchus. Another interesting marker Prom1 or CD133 stains hematopoietic stem cells, as well as a subset of bronchial epithelial cells, have some stem cell potential in bleomycin damage models (Germano et al., 2009) and are also up-regulated in Krt5+ bronchus but not in the Krt5+ interstitial areas. Clara cell markers such as Scgb1a1 (Rawlins et al., 2009b), Scgb3a2 (Reynolds et al., 2002) as well as Cyp2f2 a member of the Cytochrome p450 family of proteins expressed in bronchial epithelium (Fanucchi et al., 1997) are down-regulated in Krt5+ interstitial regions. Ciliated cell related genes including Enkur (Ross et al., 2007), Dynlrb2 (Geremek et al., 2011), Spa17 (McClintock et al., 2008), Sntn (Kubo et al., 2008) are also up-regulated only in Krt5+ bronchus but not in the Krt5+ interstitial areas. In summary, an up-regulation of alveolar related genes and down-regulation of bronchial epithelium related genes was observed in Krt5+ pods.

We next compared the Krt5+ and Krt5- interstitial regions to identify important genes under several categories that could be important markers for future studies (Fig. 27B). Interestingly, we saw an up-regulation of alveolar type I marker Pdpn in the Krt5+ interstitial area compared to the Krt5- regions. In addition, we observed an enrichment of Tnc in these Krt5+ regions. As mentioned earlier, Tnc is an ECM glycoprotein not expressed in normal adult lung, but is important for branching morphogenesis and is expressed at the tips of the newly forming septa during the alveolarization phase of lung development (Roth-Kleiner et al., 2004).

Zfp52, a gene involved in the lung bud formation in development (Millien et al., 2008) was also up-regulated in Krt5+ interstitial regions compared to Krt5- interstitial region. Several surface markers including Cd34, Cd44, Cd24a, Cd9, Itgb4 and Keratin markers like Krt5, Krt14, Krt6a, Krt19 and Krt20 were also enriched in the Krt5+ regions.

Transcription factors up-regulated in the Krt5+ interstitial regions include p63, Ehf, Sox2, Hdac2 and Foxa1. Ehf, a transcriptional repressor involved in asthma susceptibility in humans was also enriched in Krt5+ pods (Silverman et al., 2002). Interestingly, Sox2 and Krt6a which were up-regulated in the colonies obtained from lungs post infection (Fig. 18, 19) were also up-regulated in the Krt5+ pods compared to the Krt5- interstitial regions. Careful analyses of Krt6a expression levels in the four populations of cells dissected revealed maximum up-regulation in the Krt5+ interstitial regions (Fig. 28A). At 15 dpi, Krt6a + cells preferentially localized in the interstitial regions, unlike Krt5,which stained the basal cells in bronchial epithelium as well as the pods in the interstitial regions (Fig. 28B).

After gene level analysis, we studied the pathways enriched in the Krt5+ interstitial regions. The most significant pathways included those related to cell cycle, developmental processes, cytokinesis and cellular component morphogenesis, indicative of a region actively proliferating in the process of tissue regeneration (Fig. 27C). Moreover, pathways related to response to toxin and oxygen and reactive oxygen species metabolic processes were also enriched

in the Krt5+ interstitial regions.

5.3 CONCLUSIONS AND DISCUSSION

The aim of the experiments described in this chapter was to understand the novel Krt5+ population of cells in the interstitial region, also called Krt5+ pods. We successfully performed LCM for desired population of cells from frozen tissues and collected sufficient RNA for gene expression analysis. We showed that the biological triplicates from three mice were comparable, thus giving us a high level of confidence about the data obtained. The molecular analysis revealed that while Krt5+ and Krt5- bronchial epithelium were very similar in gene expression pattern, the Krt5+ pods were closer to the Krt5- interstitial regions. Thus we showed that Krt5+ pods are not similar to Krt5+ bronchial epithelium in whole genome expression analysis. In addition, we also illustrated an up-regulation of alveolar related genes and down-regulation of bronchial epithelium related genes in the Krt5+ pods. These data are very important because they exclude the possibility that Krt5+ pods in interstitial region lead to abnormal bronchiolization.

The up-regulation of alveolar type I cell marker Pdpn, along with other alveolar cell type markers of endothelial cells and macrophages, as well as markers important for alveolar construction during development, suggested a regeneration process of the damaged regions by Krt5+ pods to form alveolar epithelium. Pathway analysis also pointed out that the Krt5+ pods are actively proliferating

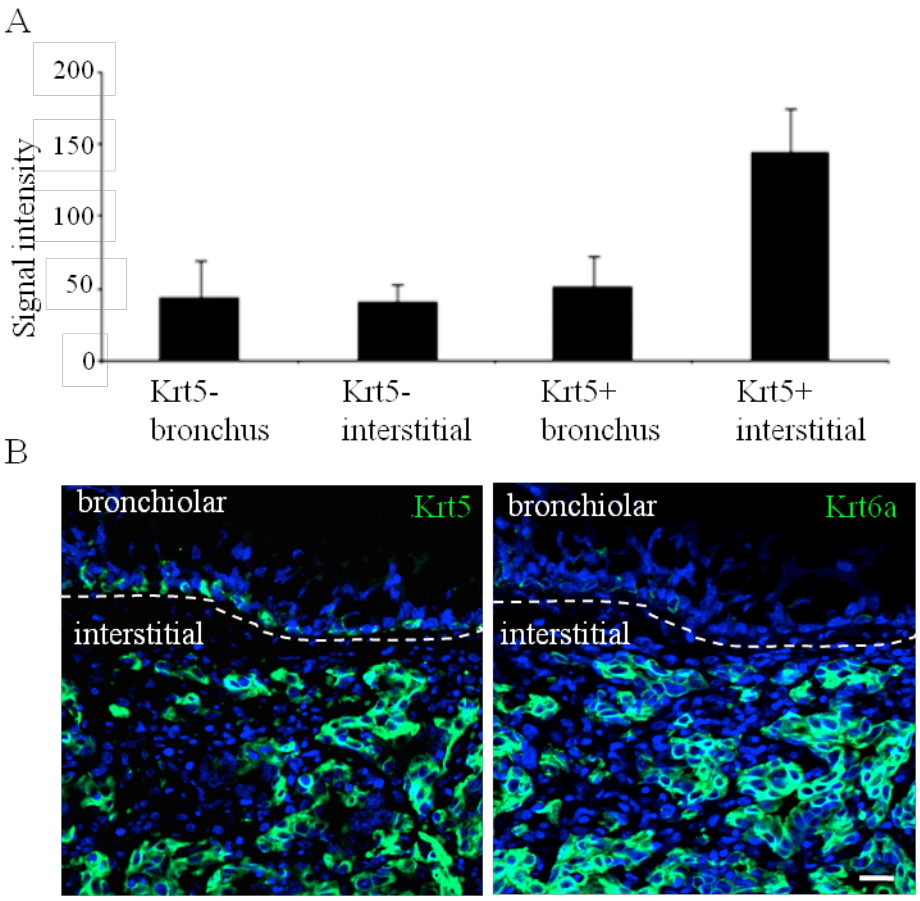

Figure 28 : Krt6a expression in lungs during repair post infection
A. Signal intensity of Krt6a expression across four dissected populations 12 dpi. Error bar represents standard deviation of the mean. B. Krt5 (green, left panel) and Krt6a staining (green, right panel) on consecutive sections 15 dpi in bronchiolar and interstitial regions. Scale bar represents 20μm.

for tissue development further supporting the BrdU studies as well as the clonogenic assays *in vitro*. Interestingly, an enrichment of oxygen metabolism process was also observed in regions of Krt5+ pods further suggesting a probable alveolar fate of these cells. Up-regulation of markers like Krt6a, Krt14 and Sox2 in Krt5+ pods provided us with a strong link between the Krt5+ pods observed *in vivo* and the increase in clonogenic cells obtained *in vitro* which are also high in Krt6a, Sox2, Krt14, and also had pathways related to tissue development and wound healing up-regulated. Further, the preferential expression Krt6a in the Krt5+ pods could be utilized for future studies targeting Krt5+ pods.

All the above data at 12 dpi indicate that Krt5+ pods may participate in alveolar regeneration. Thus we analyze later time points in the coming chapters to confirm the ultimate fate of the Krt5+ pods.

CHAPTER 6: ANALYSES OF DIFFERENTIATION POTENTIAL OF Krt5+ PODS *IN VIVO*

6.1 INTRODUCTION

We have established that Krt5+ pods appear in the damaged interstitial regions during repair post H1N1 influenza infection. We also demonstrated that they are clonogenic and have multipotent differentiation potential *in vitro*. One of the key features of UIP in humans is major alveolar injury due to the chronic inflammation. This results in deranged tissue renewal with abnormal parenchymal remodeling including exaggerated bronchiolar proliferation (Chilosi et al., 2002). Gene expression analysis of the Krt5+ pods isolated by LCM at 12 dpi suggested that the p63+ Krt5+ pods were not only involved in a mere bronchiolization process, but a possible regeneration process of the alveolar epithelium.

In the alveoli, the cuboidal type II cells have the capacity to self renew as well as differentiate into flat type I cells and are considered as the progenitor population of the alveolar epithelium (Brody and Williams, 1992; Mason and Williams, 1977). This model was established in the 1970s using primary culture systems as well as *in vivo* thymidine incorporation studies post lung injury models like NO_2 exposure and bleomycin treatment (Adamson and Bowden, 1974, 1979; Evans et al., 1973, 1975). More recently, Liu and colleagues (Liu et al., 2011), reported that alveolar type II cells mediated alveolar repair post bacterial infection. Besides alveolar type II cells, BASCs at the BADJ (Kim et al., 2005), as well as a unique

population of cells at the duct junction identified by laminin receptor α6β4 have been proposed to have alveolar differentiation potential (Chapman et al., 2011).

In this chapter, we explore the possibility of Krt5+ pods contributing to the regeneration process of the lower airways using known and novel alveolar markers as well as powerful gene expression and pathway analysis.

6.2 RESULTS

6.2.1 Morphological appearance of Krt5+ pods across time

Mice were infected with a sub-lethal dose of the H1N1 influenza virus to harvest lungs at later time points such as 21 dpi. At 21 dpi, lungs appeared relatively normal compared to the massively damaged lungs at 11 dpi, though few areas of dense nuclei and damaged regions still remained (Fig.5B). Fig. 29A depicts a low magnification, stitched representative image of lungs 21 dpi. Though most of the regions in the lungs look normal, several areas of Krt5+ pods surrounding bronchi or bronchioles in the damaged areas were still observed. Krt5 staining and histology of lungs at higher magnification revealed Krt5 + pods were absent in normal regions of the lungs (uninfected or repaired), and were also not detected in extremely damaged regions characterized by dense nuclei (Fig. 29B). Krt5+ pods were only observed in the intermediately dense regions (as observed by H&E).

Another interesting aspect of the Krt5+ pods is their morphological appearance

A

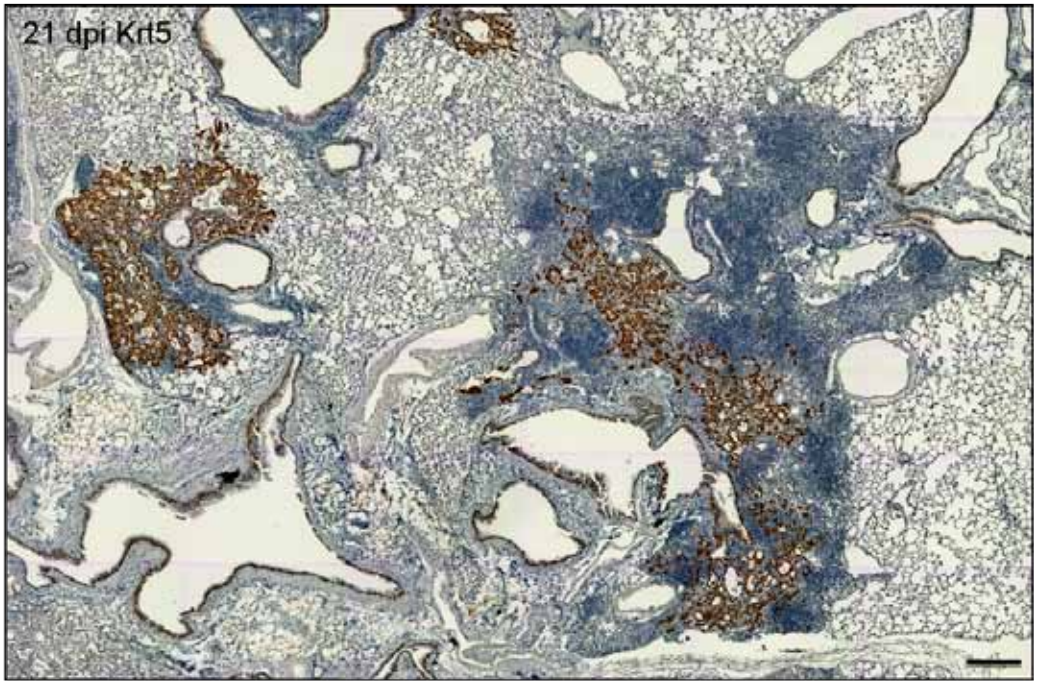

B

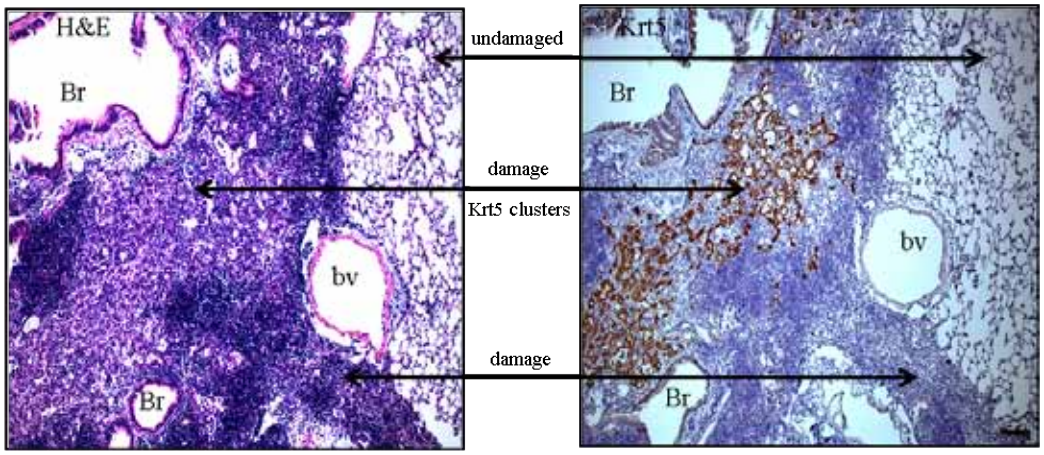

Figure 29 : Krt5+ pods at 21 dpi
A. Low magnification image of Krt5 staining on mouse lung section 21 dpi. Scale bar represents 200µm. B. H&E and Krt5 staining on consecutive sections 21 dpi. Undamaged (or repaired) regions, damaged regions and Krt5+ pods in damaged regions are marked. Br: bronchus, Bv: blood vessel. Scale bar represents 100µm.

with time. At 21 dpi the size of the Krt5+ pods was not homogeneous and included small tight clusters as seen at 11 dpi and also bigger hollow clusters. We quantified the size of the pods across time by classifying them as small tight pods with few cells, medium sized pods which start to hollow out and large pods which are single layered and have hollow lumen (Fig. 30A). The Krt5+ pods on lung sections from 11 dpi, 15 dpi and 21 dpi were quantified based on this size classification (Fig. 30B). At 11 dpi, most of the pods were small and tightly packed (84.5%) and only about 14.5% of pods were of medium size. The percentage of medium sized pods increased with time and by 15 dpi, 44% of the Krt5+ pods were medium sized while about 15% of the pods were larger and hollow. With time, by 21 dpi although the small and medium sized pods remained (15% and 29% respectively), majority of the pods were large and hollow in appearance resembling alveoli structures (56%). While still speculative, together these data could be interpreted as a regeneration process of the moderately dense area by the Krt5+ pods to form *de novo* alveoli.

6.2.2 Krt5+ pods co-staining with lung epithelial markers

After understanding the progressive morphology of the Krt5+ pods, to determine the nature of differentiation of these pods, they were co-stained with markers for differentiated epithelial cell types of the airways such as Clara cells, alveolar type I and II cells. Co-staining of Krt5+ pods with Clara cell marker CC10 at 11, 15 and 21 dpi revealed no significant co-staining with CC10 (Fig. 31). As expected, CC10 was detected in the bronchial epithelium at 11, 15 and 21 dpi. At

A

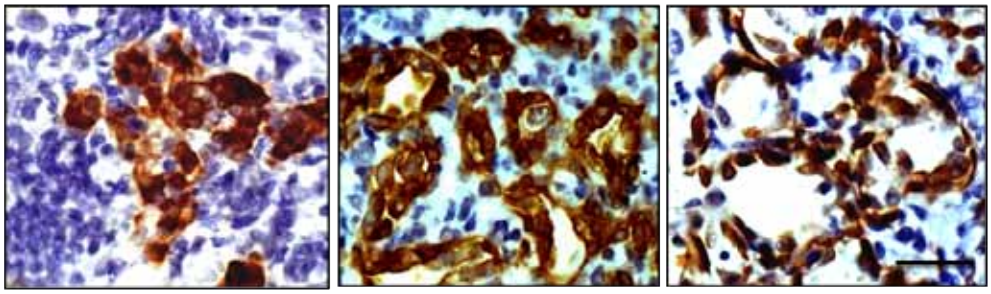

B

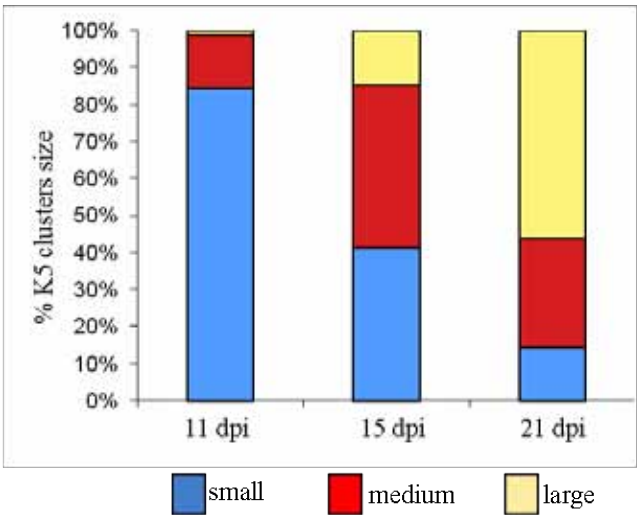

Figure 30 : Kinetics of Krt5+ pods post H1N1 infection
A. Representative images of small, medium and large Krt5+ pods observed at 21 dpi. Scale bar represents 20µm. B. Quantification of small (blue), medium (red), and large (yellow) Krt5+ pods observed at 11, 15 and 21 dpi. Number of clusters (n) counted at 11, 15 and 21 dpi are 200, 424 and 572, respectively.

11 dpi none of the Krt5+ pods co-stained with CC10. However, at 15 dpi some of the cells towards the hollow lumen in the larger multilayered Krt5+ pods were positive for CC10, suggesting that a subset of the Krt5+ pods could be contributing to de-novo bronchioles. Interestingly, by 21 dpi when majority of the Krt5+ pods are single layered, hollow structures, CC10 was not detected on any live cells in the Krt5+ pods. The hollow lumen containing debris of cells resulted in non-specific signal of CC10 while only the bronchial and bronchiolar epithelium retained clear cytoplasmic signal. Thus we concluded that few large Krt5+ pods could be contributing to bronchioles during repair, but all the hollow lumen Krt5+ pods observed at 21 dpi do not contain CC10+ Clara cells.

The next step was to determine if p63+ Krt5+ cells contribute to alveolar type I cells. At 15 dpi, many p63+ Krt5+ cells were observed in the interstitial regions. We co-stained these p63+ cells at 15 dpi with alveolar type I cell marker PDPN. PDPN was detected in alveolar type I cells in normal lung which constitute about 95% of the alveolar epithelium (Fig. 32A). However, at 15 dpi in damaged regions there was a loss of alveolar type I cells as observed by loss of PDPN expression. Interestingly, in interstitial regions where p63+ clusters were observed, PDPN was also expressed. 34% of stained cells were double positive for PDPN and p63, while 63% of the stained cells were PDPN single positive (Fig. 32B). These data suggested that p63+ cells could contribute to PDPN + type I cells in the interstitial regions of the lungs during repair.

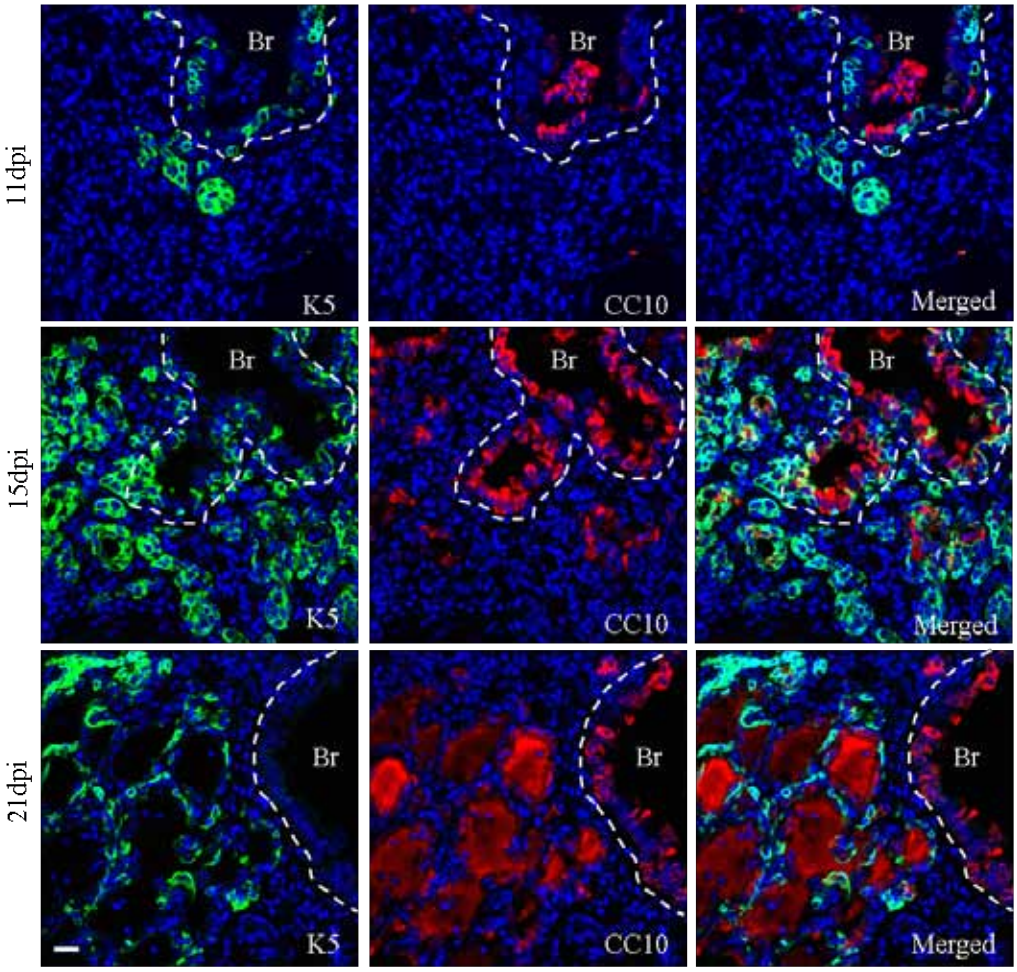

Figure 31 : Krt5 and CC10 across time-points post infection
Krt5 (green) and Clara cell staining with CC10 (red) at 11, 15 and 21 dpi. White dotted line separates bronchiolar epithelium (Br) and alveolar epithelium. Scale bar represents 20μm.

One of the biggest setbacks in the field has been the shortage of specific alveolar markers. In efforts to identify novel cell specific markers, two novel hybrodomas 1H8 and 11B6 were developed in the Xian-McKeon lab. These two hybridomas react specifically to alveolar type I cells (Fig. 32C, D). Krt5+ pods were co-stained with the two hybridomas at 21 dpi when many hollow Krt5+ pods were observed (Fig. 32C, D). Both the hybridomas co-stained with cells in the large hollow Krt5+ pods but not with the small tightly clustered pods. Quantification of Krt5+ 11B6+ cells across time also revealed an increasing trend of double positive cells with maximum overlap of the cells observed at 21 dpi (Fig. 32E) when majority of the Krt5+ pods were big and hollow (Fig. 30B). These data suggested that Krt5+ pods in interstitial areas contribute to the regeneration of the alveolar type I cells because of the morphological phenotype as well as the correlation in alveolar marker staining.

Next, we investigated the possibility of Krt5+ pods differentiating into alveolar type II cells that contribute to about 5% of the alveolar epithelium. Infected lung sections at 21 dpi were co-stained for Krt5 and alveolar type II cell marker SPC. As observed in the low magnification images in Fig. 33A, Krt5 stained the basal cells in the bronchial epithelium and the pods around the bronchus. When co-stained with SPC it was observed that Krt5 and SPC regions were independent of each other and did not overlap. High magnification images, (Fig. 33A lower panel) clearly revealed a separation between Krt5+ pods and SPC+ cells with no overlap between them. This result was consistent across sections form most of the

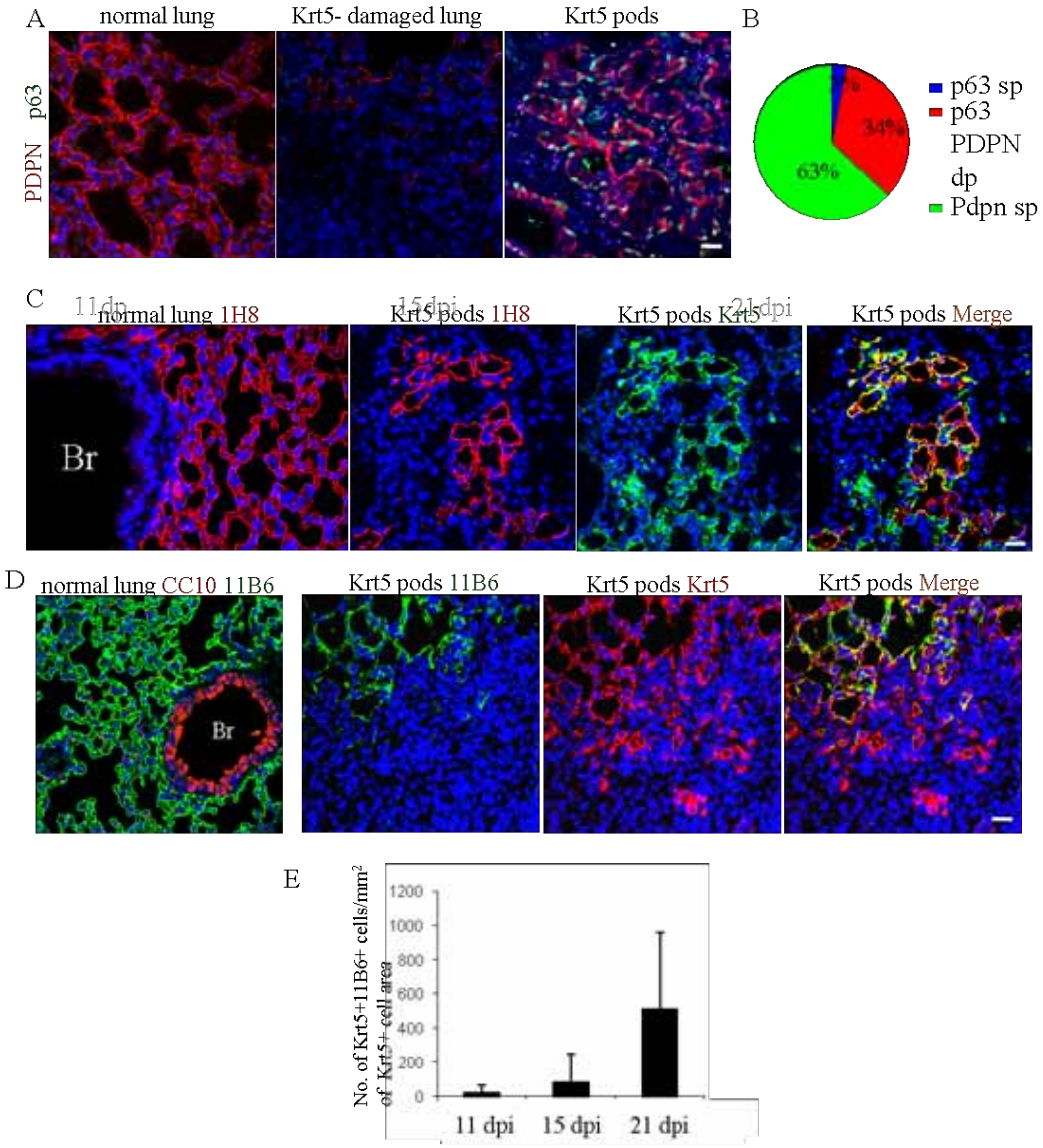

Figure 32 : Krt5+ pods with alveolar type I cells markers during repair post H1N1 infection

A. p63 (green) and PDPN (red) staining on mouse lung sections 15 dpi. p63 and PDPN staining in normal regions of lungs (left panel), damaged regions of the lung (middle panel) and regions of p63+ Krt5+ cells (Right panel) at 15dpi. Scale bar represents 50µm. B. Quantification of p63 and PDPN staining in mouse lungs 15 dpi. 3% of the stained cells are p63 single positive (p63 sp, blue), 34% stained cells are p63 and PDPN double positive (p63 PDPN dp, red) and 63% of stained cells are PDPN single positive (PDPN sp, green). Sections from three mice at 15 dpi were used for the quantification. C. Left panel shows 1H8 hybridoma (red) in bronchial and alveolar regions of normal lung. Second third and fourth panel shows staining of 1H8 hybridoma (red), Krt5 (green) and merged image of 1H8 and Krt5 staining respectively on mouse lung sections 21 dpi. Scale bar represents 50µm. D. Left panel shows 11B6 hybridoma (green) staining with Clara cell

marker CC10 (red) in bronchial and alveolar regions of normal lung. Second third and fourth panel shows staining of 11B6 hybridoma (green), Krt5 (red) and merged image of 11B6 and Krt5 staining respectively on mouse lung sections 21 dpi. Scale bar represents 50μm. E. Trend of number of Krt5+11B6+ cells/mm^2 of Krt5+ cell area at 11, 15 and 21 dpi. Error bar represents standard deviation from the mean. Sections from four mice/ time point were used for the quantification.

mice used for infection for time points until 50 dpi (data not shown). In summary, we saw that Krt5 and SPC + cells did not overlap in most of the lungs, favoring the hypothesis that they are two independent populations. Whether the scattered Krt5+ cells in the large pods eventually give rise to alveolar type II cells is debatable and will require more efficient tracing systems to confirm.

6.2.3 Gene expression profiling of Krt5+ pods 25 dpi

After examining the morphological and phenotypic properties of Krt5+ pods we went on to understand the gene expression profile of different population of cells, 25 dpi. Our studies had clearly shown that the Krt5+ pods after 21 dpi were very different in their morphology as well as differentiation status compared to the immature pods at 12 dpi. Hence we decided to isolate four populations of cells from mouse lung sections 25 dpi (Fig. 34), to further confirm the fate of the Krt5+ pods. Krt5+ pods (region 2) and normal alveoli regions marked by normal SPC staining pattern (region 4) were marked out for the LCM. Additionally, SPC+ clusters observed in damaged areas (region 1) of the lung were also intriguing and could be of interest, given the literature which supports the model of SPC+ cells differentiating into alveolar type I cells in homeostasis in the lungs.

A

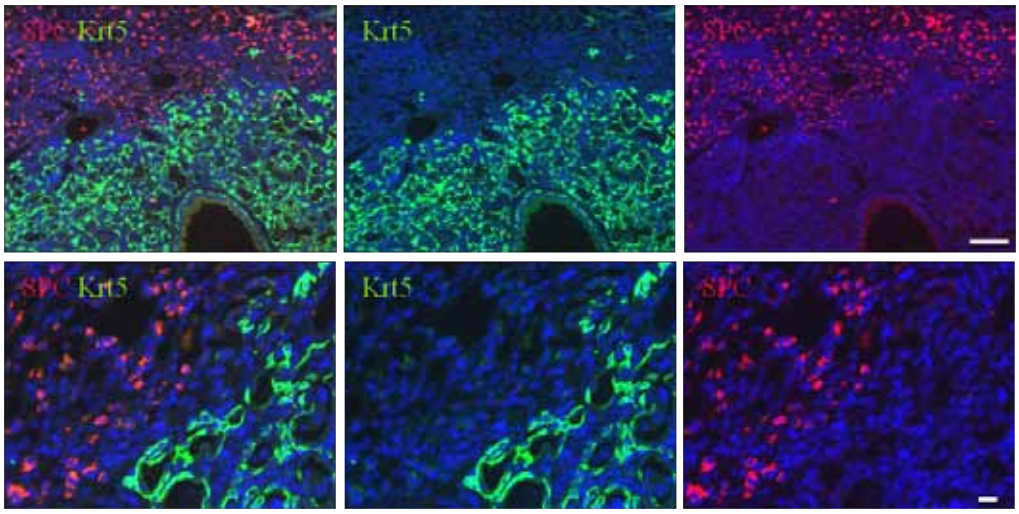

Figure 33 : Krt5+ pods with alveolar type II cell marker during repair post H1N1 infection

A. Low magnification image of Krt5 (green) and SPC (red) staining on mouse lung sections 21 dpi. Scale bar represents 50µm. Lower panel represents high magnification image of Krt5 (green) and SPC (red) staining on mouse lung sections 21 dpi. Scale bar represents 20µm

Hence, we isolated the SPC+ clusters and as a control, also marked out Krt5-SPC- damaged regions post infection (region 3). To confirm the nature of all the populations of cells we co-stained the SPC or Krt5 regions with alveolar type 1 hybridomas namely, 1H8 and 11B6 (Fig. 35A, B). Region 1 with SPC+ clusters in damaged lungs were not positive for normal alveoli markers such as 1H8 or 11B6, confirming that those regions were not normal alveoli regions but SPC+ damaged alveoli regions. Region 2, consisting of Krt5+ pods had some co-staining with alveolar markers mirroring results at 21 dpi (Fig. 32C, D). Region 3, which was SPC- and Krt5- was also negative for alveolar markers 1H8 or 11B6 thus validating the damaged alveoli status. Lastly, region 4, which was characterized as SPC+ normal alveoli region were also positive for alveolar hybridomas confirming they were normal alveoli regions.

After the LCM of the four populations of cells, from three mouse lungs, the RNA extracted was amplified and hybridized on gene chip arrays as described earlier (Chapter 2, 5). Preliminary molecular analysis revealed that the biological triplicates for all four samples were consistent with each other (Fig. 36A). Also, from the PCA map it was observed that the normal alveoli samples were far away from the damaged alveoli region, based on whole transcriptome analysis as expected. Interestingly, the Krt5+ pods were closer to normal alveoli region in whole genome expression pattern compared to the damaged alveoli regions. Further, the SPC+ damaged alveoli (DA) were closer to the damaged regions

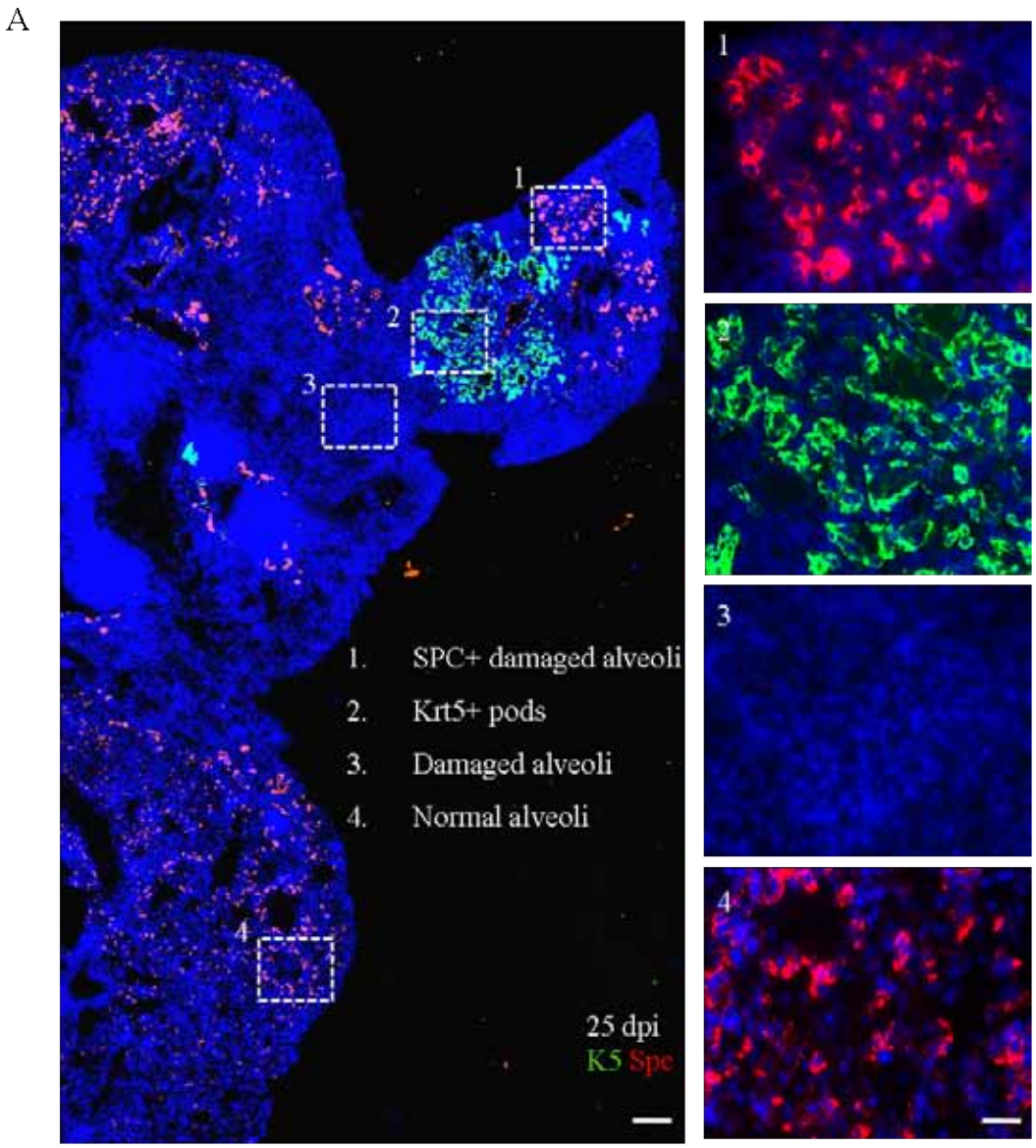

Figure 34 : Krt5 and SPC in mouse lungs 25 dpi
A. Representative image of SPC (red) and Kr5 (green) staining on mouse lung frozen sections 25 dpi. Scale bar represents 200µm. Regions marked are SPC+ damaged alveoli (1), Krt5+ pods (2), damaged alveoli (3) and normal alveoli (4). Scale bar represents 200µm. Inset on right shows higher magnification of four regions of cells to be dissected. Scale bar represents 50µm.

compared to the normal alveoli in whole genome expression. Next, we performed unsupervised clustering analysis on significantly differentially expressed genes (Fig. 36B). The normal alveoli and Krt5+ pods clustered together, while the damaged alveoli and SPC+ DA formed a separate cluster. Majority of the genes were commonly expressed in the damaged alveolar regions as well as the SPC+ DA regions and were not expressed in normal alveoli as well as Krt5+ pods (809 genes, Cluster D). Similarly, several genes were commonly expressed in normal alveoli and Krt5+ pods (281 genes, Cluster B) compared to the damaged regions. There were also a large number of genes that were expressed only in normal alveoli (600 genes, Cluster C) or only specific to Krt5+ pods (515 genes, Cluster A).

We scrutinized the Cluster B set of genes that consisted of genes commonly high in Krt5+ pods and normal alveoli (Fig. 36C). Alveolar type I markers such as Pdpn and Aqp5 were detected to be commonly high in normal alveolar regions and Krt5+ pods. Atp1b1, a Na-K-ATPase localized on alveolar type I cells (Borok et al., 2002) as well as Scnn1g, an amiloride-sensitive epithelial sodium channel which has been reported to be important for alveolar fluid clearance were up-regulated in Krt5+ pods (Hummler and Planès, 2010; Machado-Aranda et al., 2005). Other interesting genes include Caveolin-1 (Cav1), a major scaffolding protein constituent of caveolae (Ryter and Choi, 2008). In adult lung, Cav1 is detected in alveolar endothelium and type I epithelial cells (Ramirez et al., 2002).

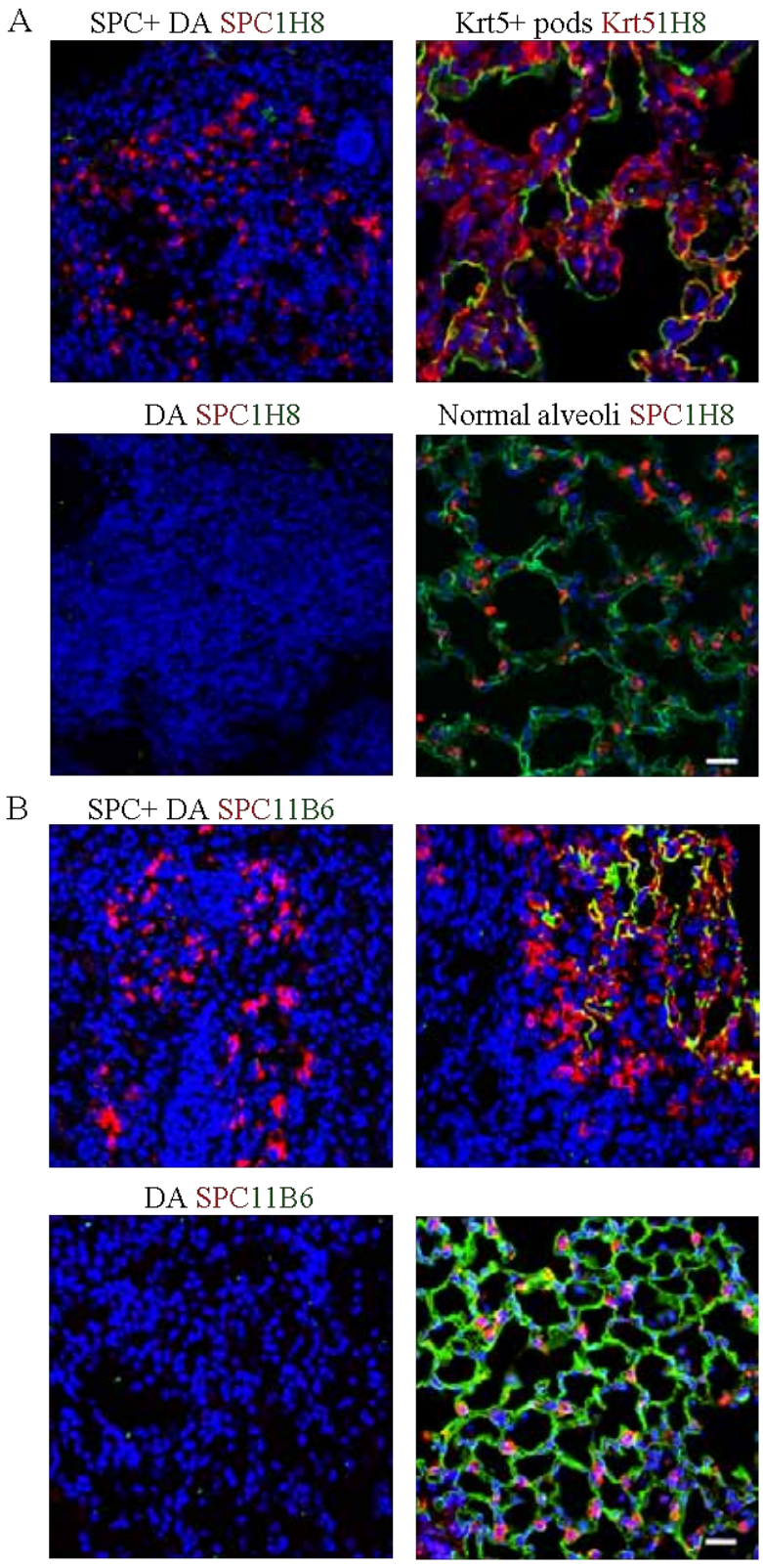

Figure 35 : Alveolar type I cell marker with Krt5 and SPC at 25 dpi

A. Left top panel represents region 1: SPC+ damaged alveoli stained with SPC (red) and 1H8 (green). Right top panel represents region 2: Krt5+ pods stained with Krt5 (red) and 1H8 (green). Left bottom panel represents region 3: SPC- Krt5-damaged alveoli (DA) stained with SPC red and 1H8 green. Right bottom panel represents region 4: normal lung with SPC (red) and 1H8 (green). All sections are from mouse lungs at 25 dpi. Scale bar represents 20μm. B. Left top panel represents region 1: SPC+ damaged alveoli stained with SPC (red) and 11B6 (green). Right top panel represents region 2: Krt5+ pods stained with Krt5 (red) and 11B6 (green). Left bottom panel represents region3: SPC- Krt5- damaged alveoli (DA) stained with SPC red and 11B6 green. Right bottom panel represents region 4: normal lung SPC (red) and 11B6 (green). All sections are from mouse lungs at 25 dpi. Scale bar represents 20μm.

Laminin γ2 (*Lamc2*), which is prominently expressed in the basement membrane of alveolar walls and airways of developing and adult lung (Nguyen et al., 2006) was enriched in normal and Krt5+ pods. Cul7, (Huber et al., 2011; Petroski and Deshaies, 2005) and Pdgfra, important genes involved in normal alveolar development were also prominently observed in the Krt5+ pods and normal alveoli.

Next, we performed detailed pathway analysis of the four clusters of genes using the PANTHER pathway database discussed earlier (Fig. 37). Gene ontology analysis of Cluster B representing genes commonly elevated in normal alveoli and Krt5+ pods revealed several interesting pathways including, 5-Hydroxytryptamine degradation and Phenylethylamine degradation. Degradation of amines such as 5-hydroxytryptamine (5-HT), or serotonin, a vasoconstrictor and phenylethylamine by monoamine oxidase (MAO) in the lungs (Bakhle and Youdim, 1979; Gillis and Pitt, 1982; Junod, 1985) are part of normal alveolar function. Furthermore,

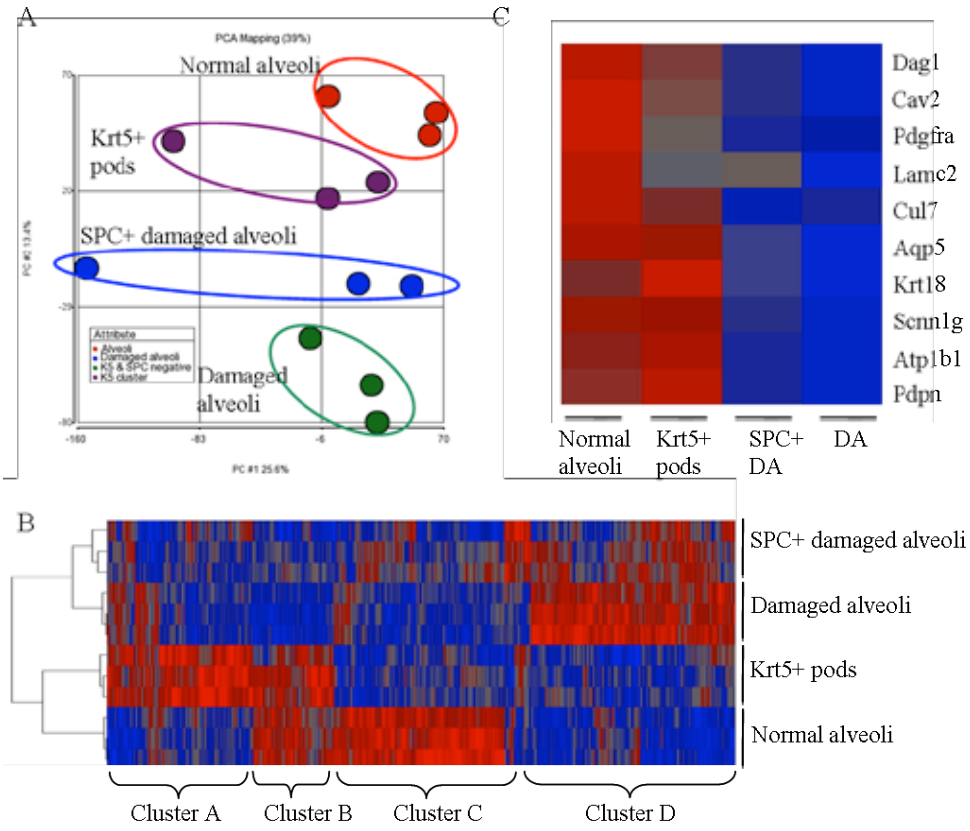

Figure 36 : Gene expression analysis of Krt5+ pods at 25 dpi
PCA analysis of different populations of cells dissected out at 25 dpi. The four regions dissected out are SPC+ normal alveoli region (region 4, red), Krt5+ pods (region 2, purple), SPC+ damaged alveoli (region 1, blue), Damaged alveolar regions (region 3, green). B. Unsupervised clustering of the four dissected regions at 25 dpi namely SPC+ damaged alveoli, damaged alveoli, Krt5+ pods and normal alveoli with $p<0.05$ including 2205 genes. Cluster of genes marked out in the heatmap. Cluster A consists of 515 genes specifically up-regulated in Krt5+ pods. Cluster B consists of 281 genes commonly expressed in Krt5+ pods and normal alveoli, Cluster C consists of 600 genes specifically expressed in normal alveoli while Cluster D consists of 809 genes commonly expressed in SPC+ damaged alveoli as well as damaged alveoli. C. Expression pattern of alveolar region related genes in four dissected regions 25 dpi namely Normal alveoli, Krt5+ pods, SPC+ damaged alveoli (DA) and Damaged alveoli (DA).

endothelium signaling and angiogenesis pathways which are essential for functional alveoli units of gas exchange (Khimji and Rockey, 2010) were also enriched in Cluster B genes (Fig. 37B). Over-representation of genes involved in Wnt, Hedgehog, and nicotinic acetylcholine receptor signaling were also observed in the Cluster B genes (Table 3).

The pathways significantly enriched in Cluster A genes, which was specific to Krt5+ pods included pathways such as axonal guidance by netrins. While netrins are known to regulate axonal guidance in multiple systems, they have also been reported to have crucial effects on epithelial and endothelial cells during lung development (Liu et al., 2004). Besides these, several metabolic pathways such as fructose galactose metabolism and glutamine to glutamate conversion were also enriched in Krt5+ pods. Reports state that since lungs have high flow of blood owing to pulmonary circulation, they express the glutamine synthetase enzyme for glutamine metabolism to catalyze *de novo* glutamine biosynthesis (Karinch et al., 2001). Additionally, it has also been speculated that in severe pulmonary dysfunction, due to metabolic failure, the damaged lungs are unable to release sufficient amounts of glutamine (Souba et al., 1990). Glutamine is also a key source of energy in the developing lung (Fox et al., 1996). Insulin/IGF pathway, and the PI3 kinase pathway (Thomas and Owen, 2008), also enriched in Krt5+pods have been implicated to play an important role in lung diseases and are also important for survival and proliferation of many cells (Choi et al., 2009).

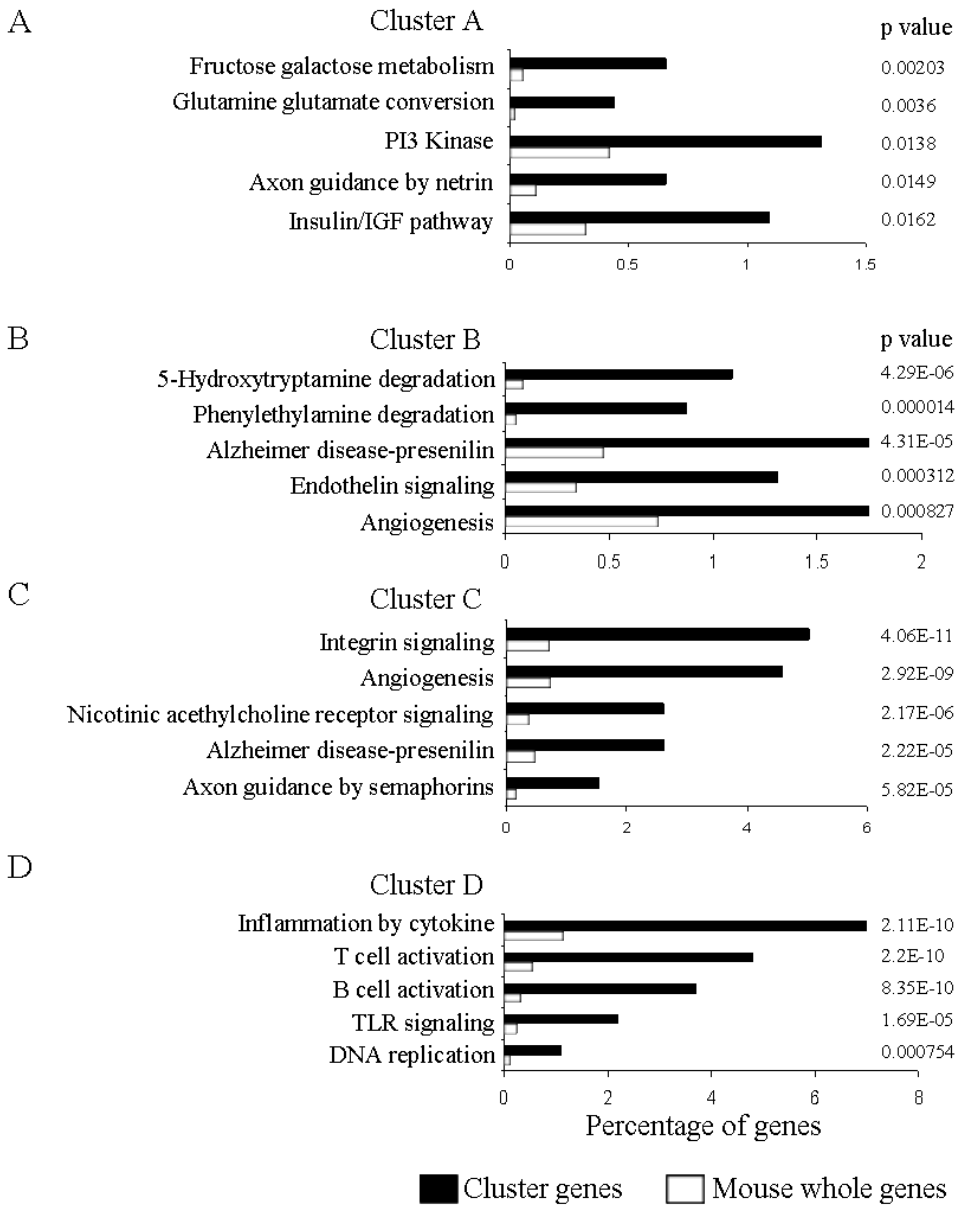

Figure 37 : Pathway analysis of clusters 25 dpi
A. Gene ontology analysis of genes in Cluster A with respective p-values. B. Gene ontology analysis of genes in Cluster B with respective p-values. C. Gene ontology analysis of genes in Cluster C with respective p-values. D. Gene ontology analysis of genes in Cluster D with respective p-values. $p<0.05$. Black bar represents genes from the marked clusters while white bars represent genes from the entire mouse genome (26185 genes).

Together, these data suggested that the Krt5+ pods, in association with elements involved in capillary formation were attempting to reconstruct a functional alveolar network.

Cluster C, which consisted of genes enriched in normal alveoli included Integrin signaling, angiogenesis, Nicotinic acethylcholine receptor signaling and Axon guidance by semaphorins pathways (Fig. 37C). Cluster D, which represented genes from damaged alveoli had mostly immune response and proliferation pathways up-regulated including T and B cell activation, Inflammation by cytokines, TLR signaling and DNA replication.

6.3 CONCLUSIONS AND DISCUSSION

In this chapter, we demonstrated that Krt5+ pods, which were observed in the moderately damaged regions, individually expanded in size with time, and by 21 dpi formed large hollow structures reminiscence of alveoli. Some Krt5+ pods may have developed into *de novo* bronchioles as suggested by CC10 staining at 15 dpi but by 21 dpi the hollow lumen Krt5+ pods developed into alveolar type I cells. The general problem in the field has been the lack of specific markers for all differentiated cell types in the lung. Amongst the hybridomas developed in the Xian-McKeon lab, the 1H8 and 11B6 hybridomas reacted specifically to alveolar type I cells. Post infection, the damaged alveolar region was detected by the loss of the hybridoma staining. However, in regions with Krt5 signal in large hollow pods, co-staining of alveolar markers was observed again. While the Krt5+ pods

Pathways enriched in cluster A (515) genes by GO with p<0.02
Cluster A

Pathways	% of cluster A	% of whole genome	P value
Fructose galactose metabolism	0.66	0.05	0.00203
Glutamine glutamate conversion	0.44	0.02	0.0036
PI3 kinase pathway	1.31	0.42	0.0138
Axon guidance mediated by netrin	0.66	0.11	0.0149
Insulin/IGF pathway-protein kinase B signaling cascade	1.09	0.32	0.0162
Flavin biosynthesis	0.22	0.00	0.0173

Pathways enriched in cluster B (281) genes by GO with p<0.02
Cluster B

Pathways	% of cluster B	% of whole genome	P value
5-Hydroxytryptamine degredation	1.91	0.09	4.29E-06
Phenylethylamine degradation	1.53	0.05	0.000014
Alzheimer disease-presenilin pathway	3.05	0.47	4.31E-05
Endothelin signaling pathway	2.29	0.34	0.000312
Angiogenesis	3.05	0.74	0.000827
Cadherin signaling pathway	2.67	0.64	0.00163
Hedgehog signaling pathway	1.15	0.10	0.00214
Wnt signaling pathway	3.44	1.33	0.00908
GABA-B_receptor_II_signaling	1.15	0.16	0.00957
EGF receptor signaling pathway	1.91	0.53	0.0132
Beta2 adrenergic receptor signaling pathway	1.15	0.19	0.0136
Beta1 adrenergic receptor signaling pathway	1.15	0.19	0.0136
Heterotrimeric G-protein signaling pathway-Gq alpha and Go alpha mediated pathway	1.91	0.53	0.0136
TCA cycle	0.76	0.07	0.0144
Nicotinic acetylcholine receptor signaling pathway	1.53	0.37	0.0176
Metabotropic glutamate receptor group II pathway	1.15	0.21	0.0184
Succinate to proprionate conversion	0.38	0.01	0.0198

Pathways enriched in cluster C (600) genes by GO with p<0.02
Cluster C

Pathways	% of cluster C	% of whole genome	P value
Integrin signalling pathway	4.08	0.71	4.06E-11
Angiogenesis	3.72	0.74	2.92E-09
Nicotinic acetylcholine receptor signaling pathway	2.13	0.37	2.17E-06
Alzheimer disease-presenilin pathway	2.13	0.47	2.22E-05
Axon guidance mediated by semaphorins	1.24	0.17	5.82E-05
VEGF signaling pathway	1.24	0.29	0.00149
Inflammation mediated by chemokine and cytokine signaling pathway	2.66	1.14	0.00247
PDGF signaling pathway	1.60	0.62	0.00946
Axon guidance mediated by Slit/Robo	0.53	0.08	0.011
B cell activation	1.06	0.33	0.0123

Pathways enriched in cluster D (809) genes by GO with p<0.02
Cluster D

Pathways	% of cluster D	% of whole genome	P value
Inflammation mediated by chemokine and cytokine signaling pathway	4.40	1.14	2.11E-10
T cell activation	3.02	0.54	2.2E-10
B cell activation	2.34	0.33	8.35E-10
Toll receptor signaling pathway	1.37	0.24	1.69E-05
DNA replication	0.69	0.10	0.000754
PDGF signaling pathway	1.79	0.62	0.000775
Integrin signalling pathway	1.79	0.71	0.00246
JAK/STAT signaling pathway	0.55	0.08	0.00255
p53 pathway feedback loops 2	0.82	0.19	0.00336
EGF receptor signaling pathway	1.37	0.53	0.00604
Heterotrimeric G-protein signaling pathway-Gq alpha and Go alpha mediated pathway	1.37	0.53	0.00633
Apoptosis signaling pathway	1.37	0.54	0.00696
Axon guidance mediated by netrin	0.55	0.11	0.00927
FGF signaling pathway	1.24	0.48	0.00929
Interferon-gamma signaling pathway	0.55	0.11	0.0104
Thyrotropin-releasing hormone receptor signaling pathway	0.82	0.27	0.0155

Table 3 : Pathway analysis of clusters 25 dpi
List of pathways enriched in cluster A, B, C and D with $p<0.02$.

co-stained well with alveolar type I cell markers they were most of the times not co-expressed with alveolar type II marker SPC. These results were against the norm in the field which believes that SPC+ cells give rise to alveolar type I cells. While this course of repair was not completely excluded in the regeneration process, the Krt5+ pods seemed to give rise to alveolar type I cells without differentiating into alveolar type II cells first. Further, these results did not exclude the possibility that the scattered Krt5+ cells in the large Krt5+ pods could eventually convert to SPC+ alveolar type II cells. The transitional phase when Krt5 and SPC were co-expressed in the same cells might be very short and thus it was a very rare phenomenon to observe. Whether or not the Krt5+ cells can eventually differentiate into alveolar type II cells requires further investigation using more sophisticated model systems like lineage tracing or carefully monitored *in vivo* differentiation assays.

Gene expression profiling of four different regions of the lungs at 25 dpi provided the most intriguing evidence favoring a role for Krt5+ pods in alveolar regeneration. The 25 dpi LCM data further validated the notion obtained from the LCM data of Krt5+ pods at 12 dpi, that they were involved in alveolar regeneration. While some markers such as Krt6a involved in wound healing and Pdgfra involved in normal lung development were commonly high in Krt5+ pods across time, the molecular analysis at a later time point opened up a whole new

avenue to explore. We observed that Krt5+ pods and normal alveoli shared common cluster of genes (Cluster B), which were enriched in several biochemical pathways typical of normal alveolar function. Moreover, a potential role of nicotinamide acetylcholine receptor signaling common to normal alveoli and Krt5+ pods also suggested development of neuronal signaling in the lungs (Coughlin, 1975; Knox et al., 2010; Proctor and Carpenter, 2007; Wongtrakool et al., 2007) . Krt5+ pods were also enriched in signaling pathways involving PI-3Kinase and insulin as well as metabolic pathways involving glutamine-glutamate conversion. Although speculative, these pathways could be fulfilling the high metabolic demand of the Krt5+ pods actively involved in the regeneration process, the same way these pathways are actively involved in lung development (Fox et al., 1996).

During lung development, the alveolar budding and development of vascular capillaries occur in parallel (Cardoso, 2001; Metzger et al., 2008; White et al., 2007). The lungs are the functional gas exchange units of the respiratory system and the alveolar capillary interface is pivotal for transfer of oxygen to the blood for circulation (Huh et al., 2010; Petersen et al., 2010; Vaporciyan et al., 1993). Recently, Ding and colleagues (Ding et al., 2011) demonstrated that during regeneration, pulmonary endothelial cells sprout to initiate angiogenesis and fulfill the gas exchange requirements of the lungs. They are also capable of facilitating alveolarization in the lungs via angiocrine signals involving MMP14 or activation of VEGFR2 and FGFR1. The enrichment of pathways related to

angiogenesis and endothelium signaling in the Krt5+ pods supported this notion that capillaries are a functional unit of the alveoli and the pulmonary endothelial cells may also be involved in guiding de-novo alveolar regeneration.

Interestingly, SPC+ clusters in damaged alveoli were closer to the damaged alveoli compared to the normal alveoli in terms of staining with alveolar hybridomas as well as gene expression profiles. They shared similar gene expression patterns with pathways enriched in TLR signaling, and immune cell activation including T and B cells, while alveolar region specific markers like PDPN and Aqp5 were down-regulated in these regions. However we cannot exclude the possibility that the SPC+ clusters in damaged alveoli could also be contributing to a delayed regeneration process in the lungs.

On the broadest level, we concluded that regions with Krt5 pods expressed genes similar to apparently normal or repaired lung, and were very different from regions marked by severe damage. The data suggested that a dynamic regeneration process with a host of interesting pathways could be involved in the recovery of lungs from ARDS. The study of these pathways will require extensive empirical validation to determine their clinical significance.

CHAPTER 7:GENETIC TRACING OF Krt5+ PODS DURING REPAIR

7.1 INTRODUCTION

We have identified Krt5+ pods during the repair process post H1N1 infection that contribute to the regeneration of the alveolar epithelium. The next question we addressed was the origin of these p63+ Krt5+ pods. p63+ Krt5+ cells in the normal lungs are detected only in the basal layer of the bronchial epithelium. During regeneration however, these cells were observed in bronchiolar epithelium as well as in the interstitial damaged regions in the distal airways. To determine the origin of these cells, we adopted a lineage tracing system that genetically tags cells. The labeled cells and their daughter cells can then be traced at a later time point even if the cells shut down the expression of the specific promoter, or have differentiated into other cell types.

The Cre-loxp recombination is a site-specific recombination system in which Cre, a 38-kDa protein, is both necessary and sufficient to catalyze recombination between two loxp sites, each of which is 34 bp in length (Abremski et al., 1983; Hoess and Abremski, 1985; Sternberg et al., 1981). This system was initially used for activating gene expression in yeast and mammalian cell lines (Sauer, 1987; Sauer and Henderson, 1988). Subsequently, Orban and colleagues (Orban et al., 1992) showed that Cre-lox recombination could be used to delete loxP-flanked chromosomal DNA sequences at high efficiency in selected cell types of

transgenic animals, suggesting this approach as a means to define gene function in specific cell types, indelibly mark progenitors in cell fate determination studies, induce specific chromosomal rearrangements for biological and disease modeling, and determine the roles of early genetic lesions in disease (and phenotype) maintenance. To control the temporal activity of the Cre excision reaction, forms of Cre which take advantage of various ligand-binding domains have been developed. One successful strategy for inducing temporally specific Cre activity involves fusing the enzyme with a mutated ligand-binding domain of the human estrogen receptor (ERt), (Littlewood et al., 1995). This system was fused together with the promoter driven Cre system to generate promoter driven Cre-ERt mice.

In this chapter, we demonstrate that the p63+Krt5+ pods observed during repair are also positive for Krt14 and hence the Krt14 promoter driven CreERt mouse (Vasioukhin et al., 1999) was used for genetic tracing of these cells. The Krt14 promoter specific CreERt mouse, was crossed with a reporter mouse, which could be induced to have constitutive expression of β galactosidase because of its location in the constitutively expressed Rosa26 locus (Mao et al., 1999). In these mice ERt binds endogenous estrogens, which allows Cre-ERt to remain cytoplasmic in animals untreated with tamoxifen. However upon tamoxifen (an estrogen receptor antagonist) injection, the Cre-ERt construct is able to penetrate the nucleus and induce recombination at loxp-flanked sites. This leads to the removal of the stop codon flanked by the loxp sites thus resulting in constitutive expression of β galactosidase under the Rosa26 locus.

Using this genetic tracing system we trace the p63+ Krt5+ Krt14+ cells during repair in the lungs to determine the origin of these pods in alveolar regions.

7.2 RESULTS

7.2.1 Kinetics of Krt5+ Krt14+ pods post infection

p63+ Krt5+ pods are observed in interstitial regions from 11 dpi. Interestingly, in damaged regions where bronchioles were not Krt5+ there were no Krt5+ pods surrounding them. Krt5+ pods were associated with Krt5+ bronchioles (Fig. 38A) about 95% of the times. These data suggested that Krt5+ pods in the interstitial areas could be the result of the migration of Krt5+ cells from the basal layer of the bronchial epithelium.

Interesting, Krt5+ pods also expressed other Keratin markers like Krt14 (Fig.27B, Fig.38 B), 15 dpi. We analyzed the kinetics of Krt14 staining in mouse lungs post infection. Unlike Krt5, which stained a few basal cells in the bronchial epithelium of normal lungs, Krt14 was nearly absent by staining in normal lungs (Fig. 39A). However, by 7 dpi, Krt14+ cells were observed in the bronchial epithelium, which increased in number at 9 dpi. Until 9 dpi, the Krt14+ cells were only restricted to the bronchial epithelium and by 11 dpi, small pods of Krt14+ cells were observed in the damaged alveolar regions which progressed in size with time and by 21 dpi scattered Krt14+ cells in large alveolar like networks were detected. We quantified this expression pattern across many sections. Fig. 39B further

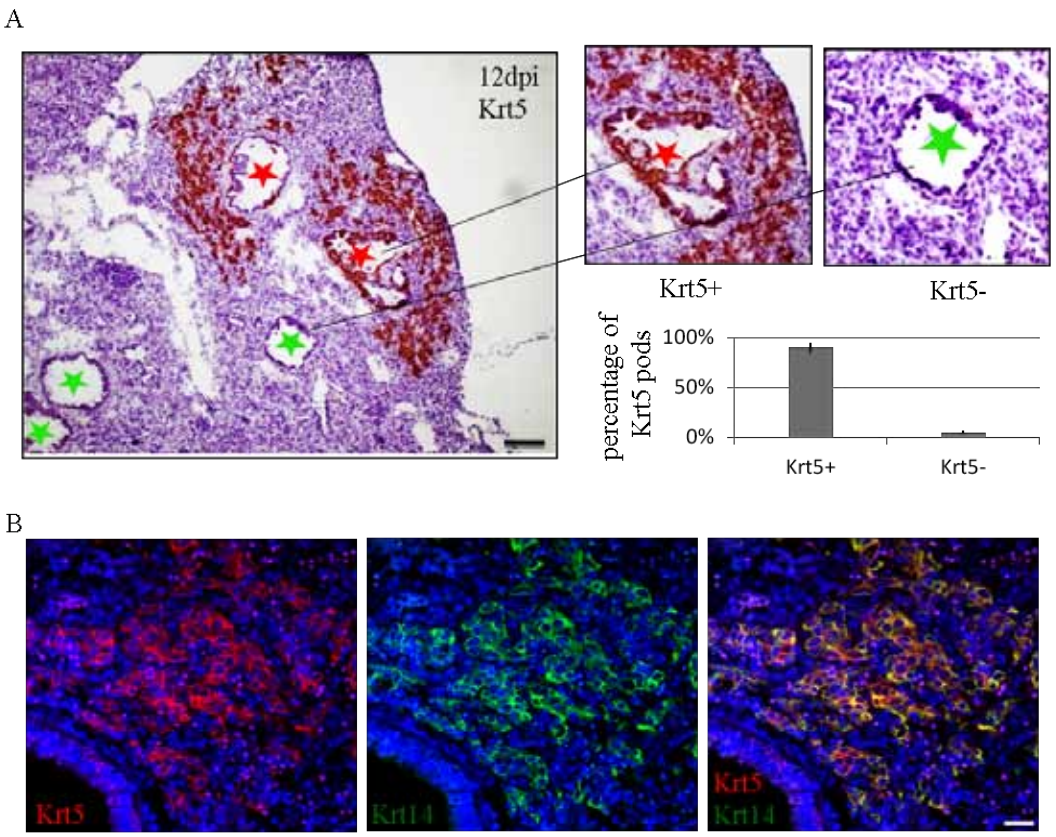

Figure 38 : Association of Krt5+ pods with bronchi
A. Krt5 IHC on mouse lung section 12 dpi. Red star marks bronchioles with Krt5+ cells. Green star marks bronchioles without Krt5+ cells. Scale bar represents 100µm. Right panel shows high magnification of Krt5+ bronchiole with Krt5+ pods around it and Krt5- bronchioles without Krt5+ pods around it. Right bottom panel represents quantification of the % of times the regions with Krt5+ pods are associated with a Krt5+ bronchus. Number of regions, n=32. Error bar represents standard deviation from mean. B. Krt5 (red) and Krt14 (green) co-staining on mouse lung sections 13 dpi. Scale bar represents 20µm.

illustrated the presence of Krt14+ cells being restricted to the bronchial epithelium at 7 and 9 dpi, and from 11 dpi, Krt14+ cells were also observed in alveolar regions. We decided to genetically trace these Krt5+ Krt14+ cells using the Krt14+ promoter to determine the origin and fate of the pods.

7.2.2 Lineage tracing of Krt14+ cells post infection

To trace the Krt5+ Krt14+ cells during repair post infection we crossed the Krt14 promoter driven CreERt mouse with the loxp-flanked LacZ mice under the constitutive Rosa26 locus. (Fig. 40A) Off-spring from matings were genotyped using standard primers to check for the 110 bp CreErT2 insert, and 340 bp and 650 bp inserts for heterozygous mice for the LacZ transgene (Fig. 40B). Experiments were performed on mice heterozygous for both the alleles.

From the kinetics of Krt14 expression in lungs during repair (Fig. 39) we planned to inject tamoxifen at day 5, 6 and 7 post infection (Fig.40C). At these time points, the Krt14+ cells were restricted to the basal layer of the bronchial epithelium only. The tamoxifen injections would induce Cre recombination in Krt14+ cells, which were restricted to the bronchial epithelium only until 9 dpi (Fig. 39). Our hypothesis was that if the Krt14+ cells migrated from the bronchial epithelium to the interstitial region during repair the Krt14+ cells labeled by β galactosidase expression on tamoxifen injection would also be observed in the alveolar region at later time points (25 dpi).

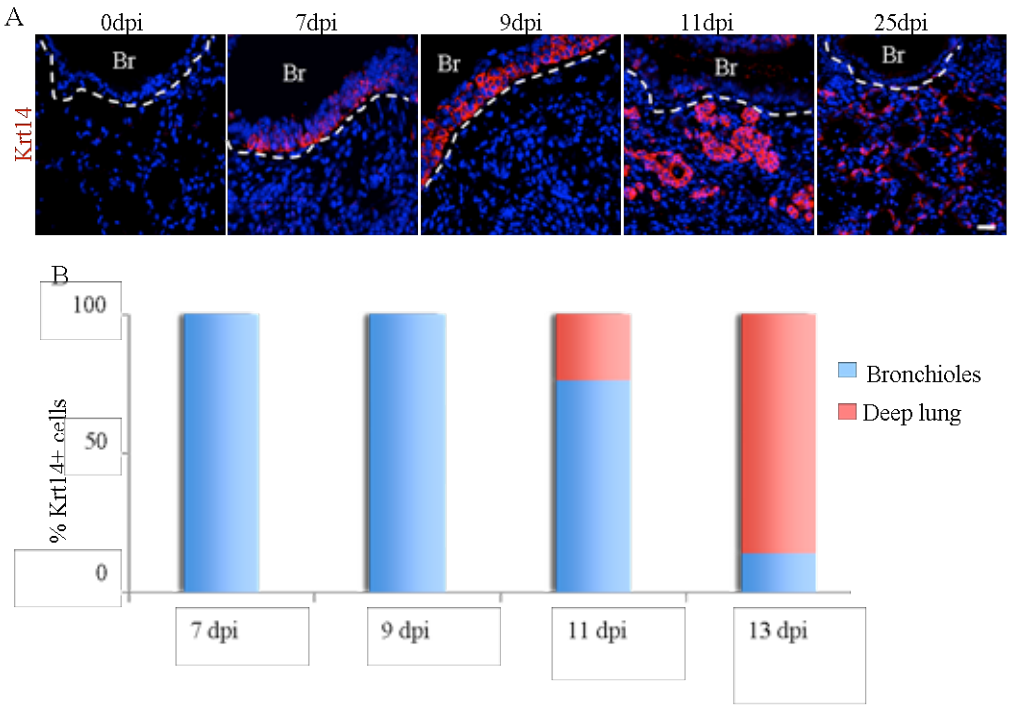

Figure 39 : Krt14 staining pattern over time post infection
A Krt14 (red) staining at 0, 7, 9, 11 and 25 dpi. White dotted line separates bronchial (Br) and alveolar regions. Scale bar represents 20µm. B. Quantification of % of Krt14+ cells in bronchioles (blue) and interstitial regions (red) at 7, 9, 11 and 13 dpi. Sections from three mice were used for the quantification.

Infected mice were injected with tamoxifen or oil 5-7 dpi and sacrificed at 25 dpi to harvest lungs and skin (positive control). Fig. 41A shows that while the lungs from oil (vector control) injected mice had no blue regions after X-gal staining, small blue regions were observed in lungs from tamoxifen injected mice (Fig. 41B). Skin was used as a positive control for all experiments. Krt14 promoter is highly active in the basal layer of the epidermis and obtaining blue color in the skin provided us with confirmation about the genotype of the mouse, as well as confirmed the tamoxifen activity and X-gal staining procedures. We observed that this system is leaky in the skin, as even in oil-injected mice the skin contained blue cells. This could be attributed to the extremely high Krt14 promoter activity in the skin as well as the intrinsic leaky nature of the CreERt system. However, no leakage in β galactosidase expression in the lungs was observed confirming the blue regions observed in lungs in tamoxifen injected, infected mice were due to induced expression of β galactosidase due to tamoxifen inductions from 5-7 dpi.

Fig. 42A shows high magnification of X-gal stained blue regions in a lobe of the infected lungs at 25 dpi. Sections through these regions revealed X-gal stained β galactosidase+ blue cells in the small bronchiolar epithelium, as well as in interstitial areas (Fig. 42B). To confirm that the X-gal staining is observed in regions of Krt5+ pods we co-stained X-gal treated lungs with Krt5. Fig. 42C shows a low magnification image of X-gal stained cells. The stained cells were detected in the zone between normal (or repaired) appearing alveoli regions and regions with Krt5+ pods in intermediately damaged regions. High magnification

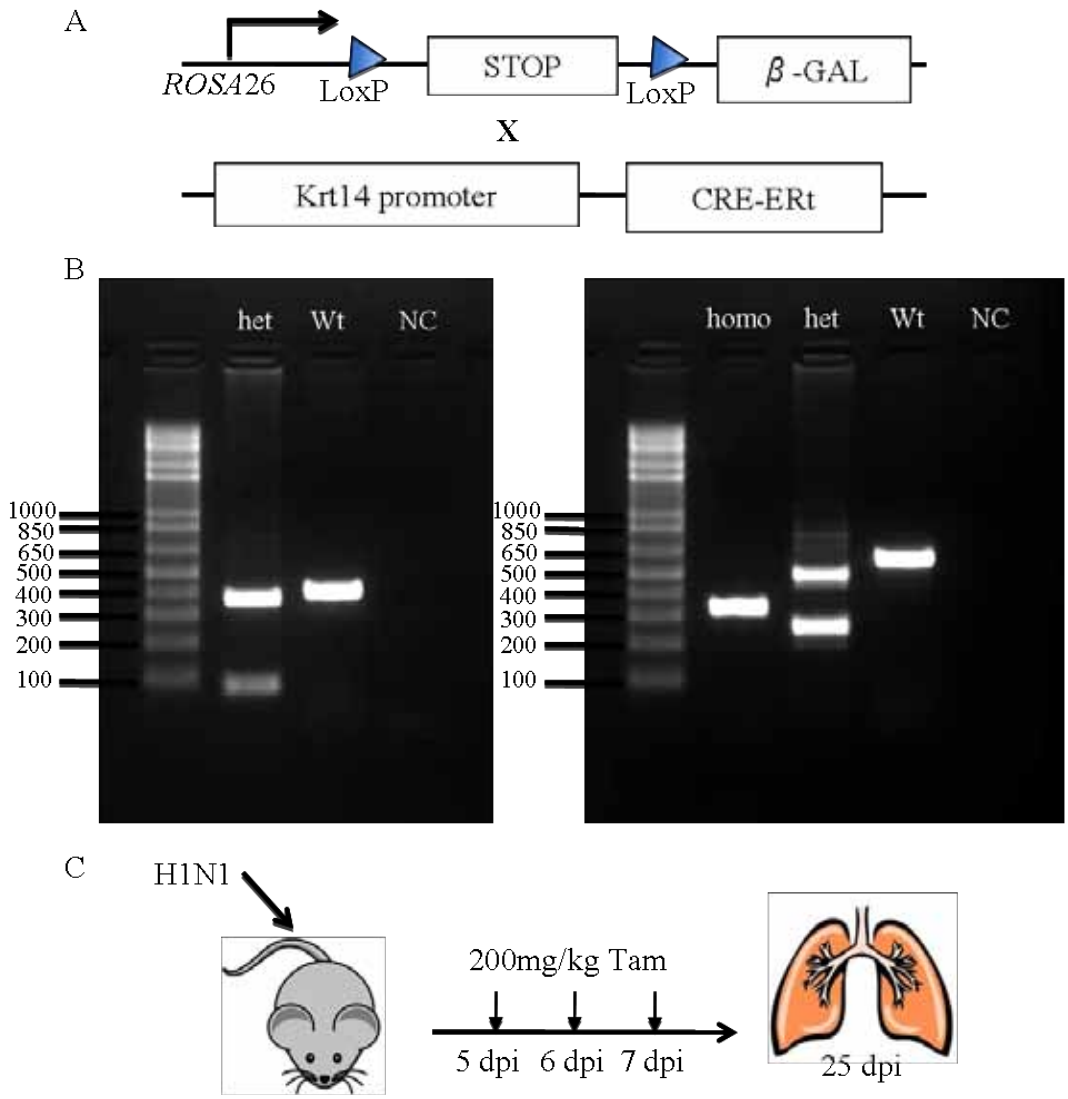

Figure 40 : Mice used for lineage tracing of Krt5+ pods
A. Krt14 promoter driven CreERt mice (KRT14-cre/ERt) were mated with Rosa26 LacZ mice (Gt(ROSA)26Sortm1Sor). B. Genotyping results of KRT14-cre/ERt mice (left panel) and Gt(ROSA)26Sortm1Sor (right panel). Left panel represents the genotyping result of heterozygous Krt14CreERt mice with Cre insert at 104 bp and internal positive control band at 400 bp. Wild type mice only have the 400 bp internal positive control band while negative control (NC) has no amplification band. Right panel represents the genotyping result of Rosa26 Lacz mice from lane one to four. Homozygous insert band is at 340 bp, heterozygous bands at 340 and 650 bp, wild type band is at 650 bp and negative control has no amplification band. C. Schematic of experimental design for lineage tracing experiments. Mice infected with a sub-lethal dose of the H1N1 influenza virus were injected with 200mg/kg tamoxifen (IP) at 5,6 and 7 dpi. Mice were sacrificed at 25 dpi and lungs harvested were used for X-gal staining.

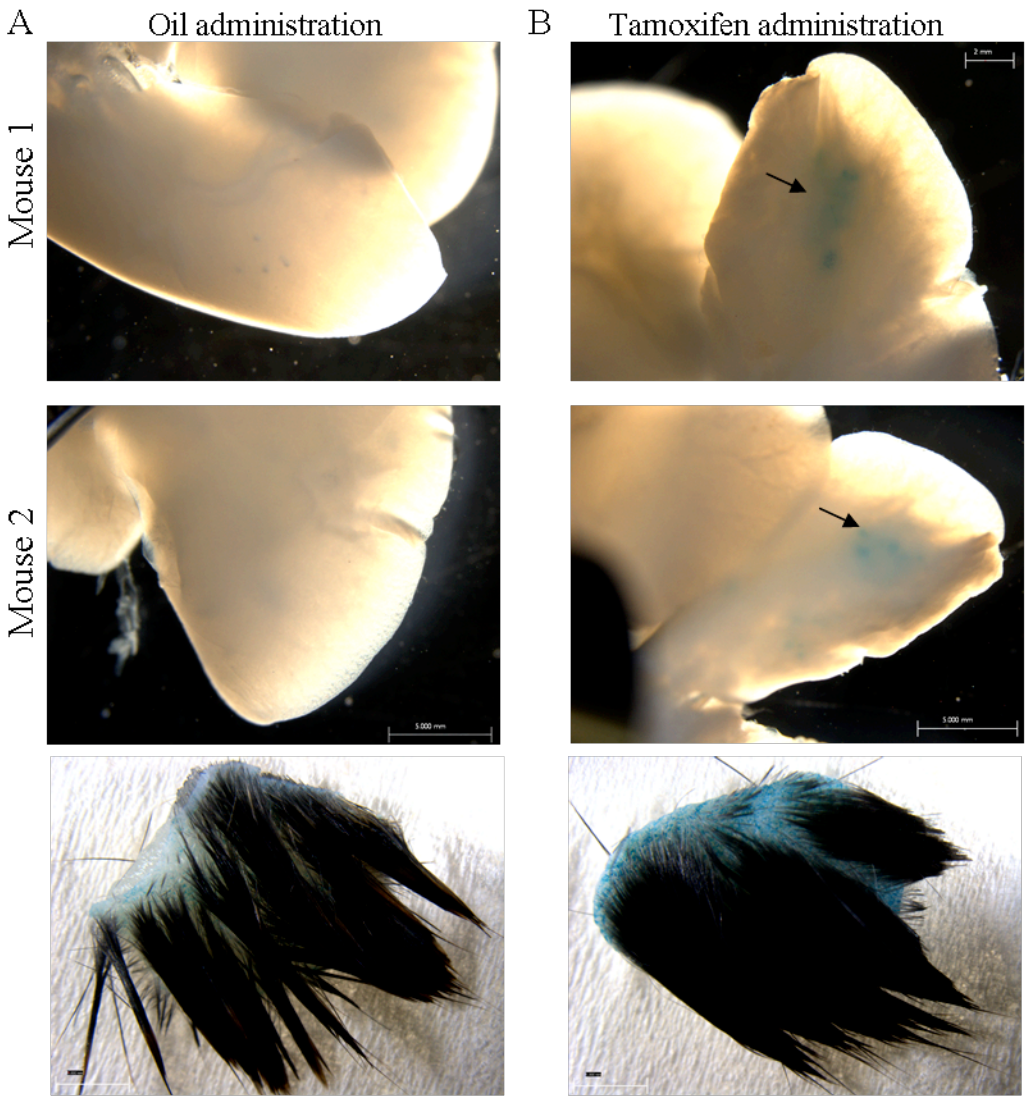

Figure 41 : Whole mount X-gal staining of tissues post infection
A. Left panel represents X-gal stained lungs from two different (Krt14 CreERt x Rosa lacz) mice that were infected with sub-lethal dose of H1N1 and injected with oil at 5, 6 and 7 dpi. Bottom left panel represents skin from oil-injected mice, which were also stained with X-gal. A. Right panel represents X-gal stained lungs from two different (Krt14 CreERt x Rosa lacz) mice, which were infected with sub-lethal dose of H1N1 and injected with 200mg/kg tamoxifen at 5, 6 and 7 dpi. Arrow marks blue regions in the lungs post X-gal staining. Bottom left panel represents skin from mice, which were also stained with X-gal.

image of the X-gal stained region in the small bronchiolar epithelium as well as in the alveolar regions was clearly observed (Fig. 42D). Few cells in the bronchiolar epithelium and some blue cells in the interstitial regions still retained their Krt5 staining. These data support our hypothesis that Krt14+ cells labeled in the bronchial or bronchiolar epithelium migrate out to adjacent damaged alveolar regions during repair. Co-staining of these small X-gal positive regions with alveolar makers such as 1H8 revealed faint overlap in the staining patterns (Fig. 42E). These data, all though not conclusive, further supports an alveolar fate of the lineage labeled cells.

7.3 CONCLUSIONS AND DISCUSSION

In this chapter, we address the question of the origin of the Krt5+ pods during repair. The close association of Krt5+ pods with Krt5+ bronchi throughout infection, the clear absence of Krt5+ cells in normal alveolar regions, as well as expression of metallo-protease proteins in the Krt5+ pods lead us to our hypothesis that, the p63+ Krt5+ Krt14+ cells from the bronchial epithelium migrate out to the damaged interstitial region when needed, to participate in the repair of the alveolar epithelium. To confirm this hypothesis, we used genetic tracing systems using the Cre-loxp system under the Krt14 promoter. The recombination event to initiate the genetic tracing was induced by tamoxifen injections from 5-7 dpi. The Krt14+ cells in bronchial and bronchiolar epithelium were labeled, and these cells were traced until 25 dpi. Interestingly at 25 dpi, X-gal positive blue cells were observed in the bronchiolar epithelium as well as in

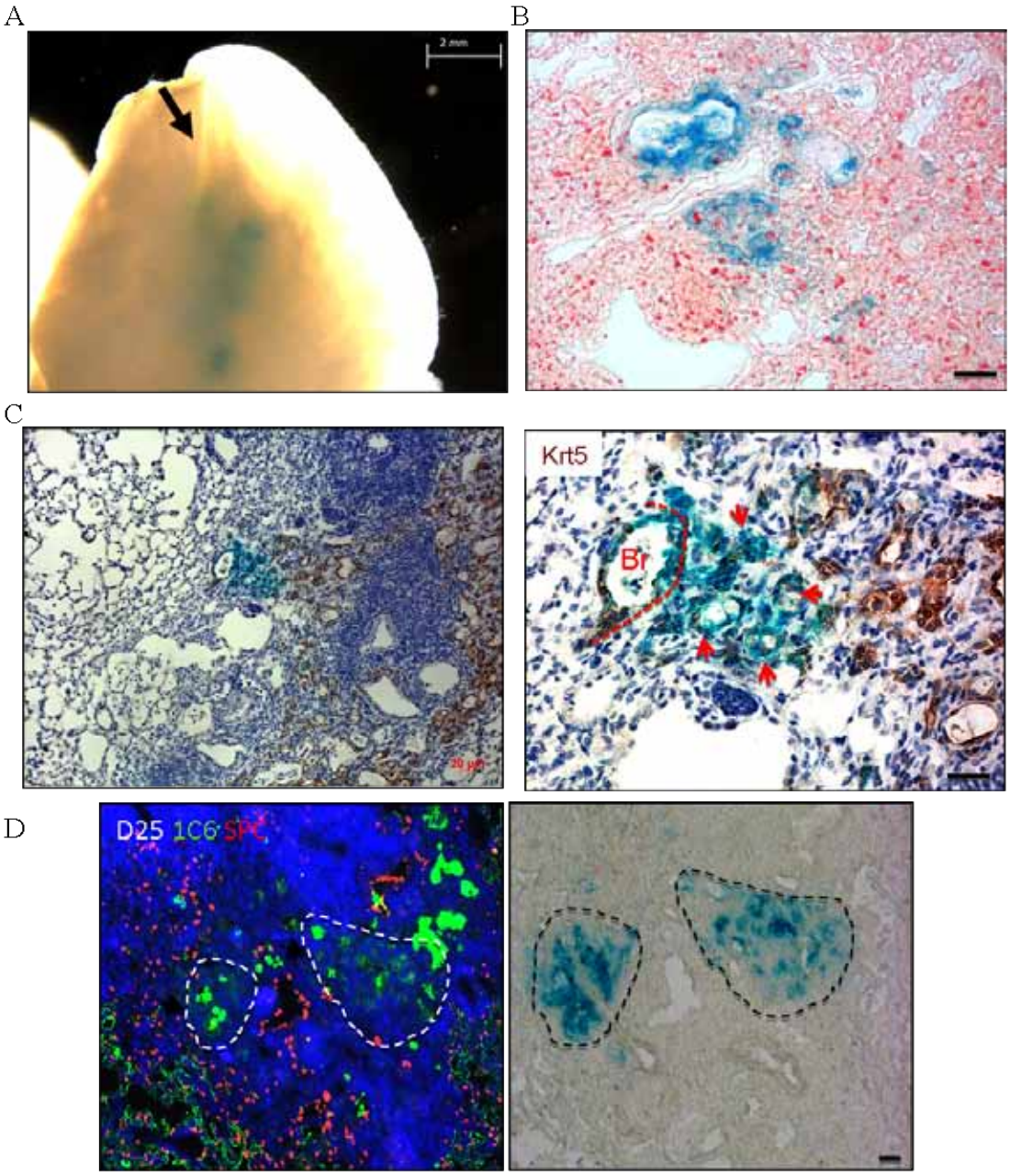

Figure 42 : Genetic tracing of Krt5+ Krt14+ pods post infection
A. High magnification image of X-gal stained lung 25 dpi. B. X-gal stained mouse lung section 25 dpi counter-stained with nuclear fast red. Scale bar represents 20µm. C. Left panel represents low magnification image of X-gal (blue) and Krt5 (brown) on mouse lung section 25 dpi. Right panel represents higher magnification image of the same area with X-gal and Krt5+ cells. Br: bronchiole. Arrows point to X-gal positive regions in the interstitial areas. Scale bar represents 20µm. D. Left panel represents staining of 1H8 and SPC on mouse lung sections 25 dpi. Right panel represents X-gal staining pattern on the same section. Scale bar represents 20µm.

interstitial regions. This experiment thus confirmed our hypothesis of p63+ Krt5+ Krt14+ cells migrating into damaged interstitial regions to enable alveolar regeneration (Fig. 43).

While some of the lineage labeled cells still retained Krt5 expression, many of the blue cells in the interstitial areas were observed in zones between Krt5+ regions and normal/repaired alveoli regions. Staining of these cells with differentiation alveolar markers revealed a possible co-stain. Although these experiments conformed the origin of the Krt5+ pods observed during repair, the ultimate fate of the pods to normal alveoli still requires confirmation using more efficient lineage tracing systems with better promoters such as Krt5 or Krt6a. The inherent limitation of the Krt14 promoter driven CreERt system in the airways leads to not so frequent recombination events in the lung during repair. Whether this is due to the low promoter activity in the airways or inherent chromatin structure problems is unknown. This low recombination efficiency does not allow us to determine the ultimate fate of the large Krt5+ pods observed during repair. Ongoing experiments hope to address these unanswered questions pertaining to the ultimate fate of the pods to develop into normal functional alveoli.

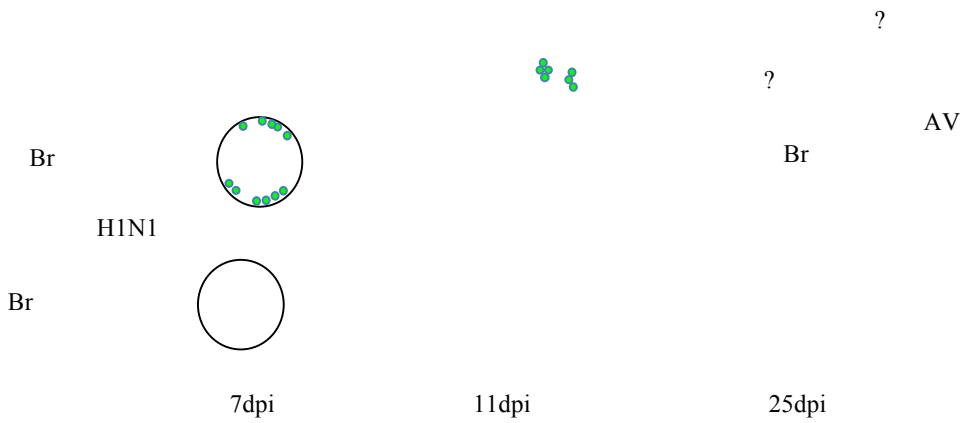

Figure 43 : Model for distal airway regeneration post H1N1 infection
p63+ Krt5+ basal cells (green) are present in the basal layer of bronchial epithelium in normal lungs. 7 dpi, massive damage is observed in bronchial and alveolar epithelium. In some bronchi and bronchioles the p63+Krt5+ basal cells proliferate to regenerate the damaged epithelium. By 11 dpi when the interstitial alveolar damage is at its peak, the p63+ Krt5+ basal cells migrate out into the damaged regions to form discreet pods. With time these pods differentiate into alveolar cell types to regenerate the alveolar epithelium. Mechanisms underlying this migration process as well as differentiation process remain an interesting area of study.

CHAPTER 8: IMPLICATIONS AND FUTURE DIRECTIONS

In this study, we identify and characterize a novel population of p63+ Krt5+ cells in the distal airways during repair post H1N1 influenza virus induced ARDS. We illustrate that p63+ Krt5+ cells, normally residing in the basal layer of bronchial epithelium, migrate into the interstitial regions during extreme alveolar damage and form discreet p63+ Krt5+ pods that contribute to proposed alveolar reconstruction during repair. While p63+ Krt5+ cells have been designated as the stem cells for the upper airways, their role in the regeneration of lower airways was not known. Further, no robust stem cell population has been identified for the lower airways of the respiratory system. In our study, by using an *in vivo* infection induced ARDS model, in parallel with an *in vitro* pedigree system for cloning and molecular analysis of regio-specific human airway stem cells (work by Dr. Yuanyu Hu, Xian-McKeon lab) we demonstrate that p63+ Krt5+ distal airway stem cells contribute to alveolar regeneration (Kumar et al., 2011).

A sub-lethal dose of the virus was used in our system to induce lung damage while also allowing a repair process. The kinetics of damage and repair in our study were predicted based on parameters such as bodyweight kinetics and histology in different mice across time. Although these experiments provided us with the fundamental time-line of the damage and repair process, a better system for precise spatial and temporal kinetics would be greatly beneficial. Probably a more efficient and accurate method of probing for inflammation, injury and

epithelial repair across time in the H1N1 infected mouse lungs could be possible using modern imaging technologies like Positron Emission Tomography (PET) imaging of small animals in combination with transgenic animals or specific biomarkers. Live imaging of lungs in small animals has been a challenge in the past but researchers now use different forms of PET imaging in lungs for several applications, including probing for particular cell types in inflammatory diseases, as well as to detect or target lung cancers (Locke et al., 2009; Nielsen et al., 2010). These tools could be utilized to conduct high-resolution analysis of pulmonary populations of cells, which would reveal a better temporal understanding of the entire damage and repair process in the same mouse and also uncover possible repair mechanisms.

Further, our analyses on lung damage and repair are based on histology and marker expression. Our detailed study ruled out the possibility of abnormal bronchiolization and fibrosis, which are typical pathological conditions in airway diseases including pneumonia. A possible alveolar fate of the Krt5+ pods was concluded based on known alveolar markers in the field as well as novel hybridomas against alveolar cell types for mouse and rat developed in the Xian-McKeon lab. Gene expression analysis also revealed an orchestrated alveolar development phase with enrichment of several genes involved in alveolar epithelium development along with endothelial capillary bed formation. More sophisticated lineage tracing systems with better promoters will confirm this proposed alveolarization process.

While these data point to an alveolar reconstruction process, the true functionality of alveolar region post regeneration in the lungs of these mice remains unknown. Several invasive and non-invasive methods of lung function assessment routinely used for human studies have now also been adapted to mouse models (Glaab et al., 2007; Verhoeven et al., 2009). One of the classical methods of monitoring lung function involves an invasive orotracheal intubation procedure to measure parameters such as pulmonary resistance (R_L) or dynamic compliance (C_{dyn}) for accurate and specific determination of pulmonary mechanics. Low-frequency forced oscillation technique (LFOT) estimates lung impedance (Z), which provides more detailed measurements of pulmonary mechanics. Several noninvasive methods for monitoring pulmonary function have also been developed for long-term experiments which allow continuous evaluation of pulmonary function of a large number of animals across time. For example, in humans, non-invasive pulse-oximeter readings provide an important clinical readout of morbidity in respiratory diseases (Sidwell et al., 1992). This technique involves the spectrophotometric analysis of the percent of oxygenated hemoglobin in the blood, a direct measure of lung function and blood oxygenation (Wahr et al., 1995). These different assays individually, or in combination could be utilized in our experiments in the future to understand the physiologic significance of respiratory phenotypes including damage and repair. Further, the functionality of regenerated alveolar epithelium can also be quantified using these lung function techniques.

In this work we characterized the unique epithelial population of p63+ Krt5+ pods in the interstitial region. All though these cells are actively proliferating *in vivo* and also have clonogenic potential *in vitro,* they are not linked to other stem cell populations such as BASCs. Further, the norm in the field has been that alveolar type II cells differentiate into alveolar type I cells in the lungs. In our experiments we speculate that Krt5+ pods differentiate into type I cells first, independent of an alveolar type II cell transition phase. Whether the Krt5+ pods ultimately differentiate into type II cells is still debatable. Further, we do not exclude the possibility that alveolar type II cells or even BASCs may be involved in an independent, delayed regenerative process. Detailed studies involving *in vitro* differentiation assays as well as multiple lineage tracing systems will be required to understand the contributions of these different populations of cells during repair.

In-depth gene expression analysis of Krt5+ pods in lung regeneration provides a very rich and previously unavailable database of molecular factors and pathways participating in the damage and repair process *in vivo*. Efforts will have to be made to maximize the knowledge that we can extract from these datasets. Several chemokines, MMPs, transcription factors, surface receptors and pathways have been identified in our study. Many of these markers could be used to develop powerful tools for further experimentation and validation. Further, large scale *in vitro* validation experiments will be required to dissect out the underlying mechanisms of the migration and differentiation of Krt5+ pods. For this, the

mouse *in vitro* stem cell culture will have to be optimized to develop a robust system to obtain large number of cells for several migration, invasion and differentiation assays *in vitro*. Ultimately these cells could also be used for potential transplantation experiments *in vivo*.

Adult human stem cells that are intrinsic to various tissues have been described and characterized over the years. Stem cells are defined as cells that have clonogenic and self-renewing capabilities and that differentiate into multiple cell lineages (Weissman, 2000). These cells are capable of maintaining, generating, and replacing terminally differentiated cells within their own specific tissue as a consequence of physiologic cell turnover or tissue damage due to injury (Slack, 2000). Because the normal reparative mechanisms seems to be overwhelmed when clinically significant airway injury occurs, a logical next step would be to aid the regenerative process during recovery. One approach is based on identifying and expanding *in vitro* multipotent adult progenitor cells that are capable of regenerating the airway epithelium. The other approach is based on harnessing the *in vivo* availability of endogenous adult stem cells that can be manipulated to improve the efficiency of the regeneration process (Körbling and Estrov, 2003).

Adult stem cell transplantation is a novel therapeutic path being developed to treat various medical conditions. The most common area for adult stem cell transplantation has been in the hematopoetic stem cell (HSCs) field. HSCs are

well defined and characterized and are used clinically to treat patients with hematologic and lymphoid cancers as well as many other hematopetic disorders such as anemia and Thalassemia major (Copelan, 2006). Several clinical trials to treat patients with myocardial infarctions with the use of mononuclear bone marrow cells also seem promising (Strauer et al., 2002). *In vitro* cultured p63+ human keratinocytes using Dr. Howard Green's culture system used to treat burn patients in 1984 (Gallico III et al., 1984) was probably amongst the first adult epithelial stem cell therapy developed and approved for human use. This system has also been adapted for corneal epithelium and has met with huge success. Culture of corneal and limbal stem cells from normal eye yielded p63+ holoclones which are engrafted to treat the burnt eye of patients. The clinical results for these kinds of corneal transplantations were successful at up to 10 years in more than 75% of the patients treated (Rama et al., 2010). This culture system with several improvements has been used worldwide since the 1980s and during the past 30 years, no adverse effects have been reported and is approved for clinical use in the United States, Japan, Italy, and South Korea (De Luca et al., 2006; Green, 2008) .

No adult stem cells therapeutic system has been developed for the airways to date. Owing to the low turn-over rate of stem cells in the lung and the fatally damaged lung tissue post several airway diseases; the only way to replace lung tissue to restore normal function currently is to perform lung transplantations. As one can imagine, lung transplantation is an expensive procedure that achieves only 10 to 20% survival at 10 years and one that is hampered by a severe shortage of donor

organs (Orens and Garrity Jr, 2009). In the recent years, researchers have been working on obtaining a cellular, tissue-engineered airway with mechanical properties that allow normal functioning, and which is free from the risks of rejection. They have adapted tissue engineering techniques along with basic biology to reconstruct trachea and bronchi by allotransplantation of recipient's epithelial and mesenchymal cells on tissue engineered scaffolds without the use of immunosuppressive therapy (Delaere et al., 2010; Macchiarini et al., 2008) . These findings suggest that autologous cells combined with appropriate biomaterials might provide successful treatment for patients with serious clinical disorders of the airways. While transplantation of the upper airways in humans seems favorable, three-dimensional modeling of the lungs has been a challenge because the engineered lung should contain lung-specific cells, display the branching geometry of the airways and contain a perfusing microvasculature, provide barrier function to separate blood from air, and have mechanical properties that allow ventilation at physiological pressures. Recently, researchers have been working on the construction of a functional, tissue-engineered lung with all these properties by employing a scaffold of rat lungs denuded of all cellular components. The retained extracellular matrix scaffold provides the hierarchical branching structures of airways and vasculature (Petersen et al., 2010). Seeding cultured, pulmonary epithelium and vascular endothelium cells on the acellular lung matrix leads to the formation of native-like lungs capable of gas exchange *in vivo* in the rat model. These novel tissue engineering approaches when combined with our knowledge and understanding of stem cells (Kumar et

al., 2011) could be developed into a potential treatment strategy for patients with severe airway diseases who are awaiting lung transplantations as a mean of survival. While still speculative, this mode of treatment could enable allotransplantation of human lungs stem cells to improve survival of patients.

Combining stem cell therapy with other treatments may increase therapeutic options in the future. Gene therapy has shown encouraging results in promoting angiogenesis, but the safety of gene delivery by means of viral vectors has become of increasing public concern (Iwaguro et al., 2002). Further, hESC-derived retinal pigment epithelium (RPE) transplantation in patients with Stargardt's macular dystrophy and dry age-related macular degeneration look promising with restoration of vision and no abnormal hyperproliferation, tumorigenicity, ectopic tissue formation, or apparent rejection after 4 months (Schwartz et al., 2012). The long-term effects of such experiments remain unknown and the field of ES cells as therapy in humans has to be pursued with extreme caution.

While stem cell therapy is a promising option to treat patients with chronic airway diseases, several concerns are yet to be addressed including, cell numbers used for transplantation, stem cell survival, delivery route and homing issues, long term adverse affects such as uncontrollable growth, tumor initiation, host rejection, etc . The second approach of harnessing existing stem cells to improve the regenerative capacity of the lungs may be a more feasible and commonly used

therapeutic intervention considering the time constraint and urgency for the need of improved lung function in severe forms of ARDS as well as unresolved issues with adult stem cell transplantations.

Studies in the past have focused on identifying immune modulators that are key to limiting the devastating effects of infection. These studies have been very useful in developing novel therapeutics to control the extent of lung damage post infections. For example, IFITM3 was identified in a functional genomic screen as mediating resistance to Influenza A virus, dengue virus and West Nile virus infection *in vitro* (Brass et al., 2009). By potently restricting the replication of multiple pathogenic viruses, this key factor of the innate immune response protects the hosts from severe forms of infection. Suppression of another interesting effecter of early innate immune response, S1P1 on endothelial cells results in reduced mortality during infection with a human pathogenic strain of influenza virus in mouse models (Teijaro et al., 2011). Researchers have also shown that some patients have an increased susceptibility to normal-moderate infections because of their genetic predisposition. For example, IFITM3-compromised individuals are more vulnerable to the initial establishment and spread of a H1N1 (2009) virus which results in morbidity (Everitt et al., 2012). These results illustrate that modulation of host immune response which play a key role in inducing the cytokine storm resulting in a significant pathological component of the disease, could be top candidates for pharmacological treatment as the first line of defense against fatal infections.

While these studies are extremely beneficial in developing therapeutics they may not be very useful for end-stage patients where extensive lung damage has impaired lung function of the individuals. We propose that in addition to modulating key intrinsic immune effectors, targeting molecules or pathways that affect adult stem cells directly, may provide a better and more immediate relief strategy (Xian and McKeon, 2012). Systemic and local growth factors almost certainly influence stem cells homing and biology. For example, in the airways, pulmonary capillary endothelial cells (PCECs) produce angiocrine growth factors that induce proliferation of epithelial progenitor cells supporting alveologenesis (Ding et al., 2011). In our studies using mouse models we have identified several pathways which can be targeted after better understanding to improve the *in vivo* stem cell potential. For example, identifying chemokines that induce the migration of the p63+ Krt5+ pods in the damaged alveolar regions, determining the mechanism of differentiation of Krt5+ pods into alveolar epithelium and more importantly understanding the interaction between the alveolar epithelium and micro-vasculature to form potentially functional units of gas exchange could provide important modulators for medical intervention.

The combination of basic biology knowledge on airway stem cells and key modulators in combination with novel tissue engineering approaches will open up a whole new avenue of clinical treatment for patients with fatal infections resulting in ARDS.

REFERENCES

Abremski, K., Hoess, R., and Sternberg, N. (1983). Studies on the properties of P1 site-specific recombination: evidence for topologically unlinked products following recombination. Cell *32*, 1301.

Adamson, I., and Bowden, D.H. (1974). The type 2 cell as progenitor of alveolar epithelial regeneration. A cytodynamic study in mice after exposure to oxygen. Laboratory investigation; a journal of technical methods and pathology *30*, 35.

Adamson, I., and Bowden, D.H. (1979). Bleomycin-induced injury and metaplasia of alveolar type 2 cells. Relationship of cellular responses to drug presence in the lung. The American journal of pathology *96*, 531.

Albiger, B., Dahlberg, S., Sandgren, A., Wartha, F., Beiter, K., Katsuragi, H., Akira, S., Normark, S., and Henriques‐Normark, B. (2007). Toll‐like receptor 9 acts at an early stage in host defence against pneumococcal infection. Cellular microbiology *9*, 633-644.

Ali, N.N., Edgar, A.J., Samadikuchaksaraei, A., Timson, C.M., Romanska, H.M., Polak, J.M., and Bishop, A.E. (2002). Derivation of type II alveolar epithelial cells from murine embryonic stem cells. Tissue engineering *8*, 541-550.

Ashbaugh, D.G., Boyd Bigelow, D., Petty, T.L., and Levine, B.E. (1967). Acute respiratory distress in adults. The Lancet *290*, 319-323.

Aso, Y., Yoneda, K., and Kikkawa, Y. (1976). Morphologic and biochemical study of pulmonary changes induced by bleomycin in mice. Laboratory investigation; a journal of technical methods and pathology *35*, 558.

Atkinson, J.J., and Senior, R.M. (2003). Matrix metalloproteinase-9 in lung remodeling. American journal of respiratory cell and molecular biology *28*, 12.

Bakhle, Y., and Youdim, M. (1979). The metabolism of 5-hydroxytryptamine and beta-phenylethylamine in perfused rat lung and in vitro. British journal of pharmacology *65*, 147.

Balkissoon, R., Lommatzsch, S., Carolan, B., and Make, B. (2011). Chronic obstructive pulmonary disease: a concise review. The Medical clinics of North America *95*, 1125.

Baron, R.M., Choi, A.J.S., and Owen, C.A. (2011). Genetically Manipulated Mouse Models of Lung Disease: Potential and Pitfalls. American Journal of Physiology-Lung Cellular and Molecular Physiology.

Barrandon, Y., and Green, H. (1985). Cell size as a determinant of the clone-forming ability of human keratinocytes. Proceedings of the National Academy of Sciences *82*, 5390.

Berthiaume, Y., Lesur, O., and Dagenais, A. (1999). Treatment of adult respiratory distress syndrome: plea for rescue therapy of the alveolar epithelium. Thorax *54*, 150-160.

Blanc, P.D., Iribarren, C., Trupin, L., Earnest, G., Katz, P.P., Balmes, J., Sidney, S., and Eisner, M.D. (2009). Occupational exposures and the risk of COPD: dusty trades revisited. Thorax *64*, 6-12.

Bonner, R.F., Emmert-Buck, M., Cole, K., Pohida, T., Chuaqui, R., Goldstein, S., and Liotta, L.A. (1997). Laser capture microdissection: molecular analysis of tissue. Science *278*, 1481.

Borok, Z., Liebler, J.M., Lubman, R.L., Foster, M.J., Zhou, B., Li, X., Zabski, S.M., Kim, K.J., and Crandall, E.D. (2002). Na transport proteins are expressed by rat alveolar epithelial type I cells. American Journal of Physiology-Lung Cellular and Molecular Physiology *282*, L599-L608.

Borthwick, D.W., Shahbazian, M., Krantz, Q.T., Dorin, J.R., and Randell, S.H. (2001). Evidence for stem-cell niches in the tracheal epithelium. American journal of respiratory cell and molecular biology *24*, 662.

Boström, H., Gritli‐Linde, A., and Betsholtz, C. (2002). PDGF‐a/PDGF alpha‐receptor signaling is required for lung growth and the formation of alveoli but not for early lung branching morphogenesis. Developmental dynamics *223*, 155-162.

Bowden, D. (1983). Cell turnover in the lung. The American review of respiratory disease *128*, S46.

Brass, A.L., Huang, I., Benita, Y., John, S.P., Krishnan, M.N., Feeley, E.M., Ryan, B.J., Weyer, J.L., Van Der Weyden, L., and Fikrig, E. (2009). The IFITM proteins mediate cellular resistance to influenza A H1N1 virus, West Nile virus, and dengue virus. Cell *139*, 1243-1254.

Breuer, R., Zajicek, G., Christensen, T., Lucey, E., and Snider, G. (1990). Cell kinetics of normal adult hamster bronchial epithelium in the steady state. American journal of respiratory cell and molecular biology *2*, 51.

Brody, J.S., and Williams, M.C. (1992). Pulmonary alveolar epithelial cell differentiation. Annual review of physiology *54*, 351-371.

Buisine, M.P., Devisme, L., Copin, M.C., Durand-Reville, M., Gosselin, B., Aubert, J.P., and Porchet, N. (1999). Developmental mucin gene expression in the human respiratory tract. American journal of respiratory cell and molecular biology *20*, 209.

Burri, P.H. (1984). Fetal and postnatal development of the lung. Annual review of physiology *46*, 617-628.

Cardoso, W.V. (2001). Molecular regulation of lung development. Annual review of physiology *63*, 471-494.

Cardoso, W.V., and Lü, J. (2006). Regulation of early lung morphogenesis: questions, facts and controversies. Development *133*, 1611-1624.

Castro, M.A.A., Dal‐Pizzol, F., Zdanov, S., Soares, M., Müller, C.B., Lopes, F.M., Zanotto‐Filho, A., Fernandes, M.C., Moreira, J.C.F., and Shacter, E. (2010). CFL1 expression levels as a prognostic and drug resistance marker in nonsmall cell lung cancer. Cancer *116*, 3645-3655.

Chapman, H.A., Li, X., Alexander, J.P., Brumwell, A., Lorizio, W., Tan, K., Sonnenberg, A., Wei, Y., and Vu, T.H. (2011). Integrin α6β4 identifies an adult distal lung epithelial population with regenerative potential in mice. The Journal of clinical investigation *121*, 2855.

Chen, S.C., Mehrad, B., Deng, J.C., Vassileva, G., Manfra, D.J., Cook, D.N., Wiekowski, M.T., Zlotnik, A., Standiford, T.J., and Lira, S.A. (2001). Impaired pulmonary host defense in mice lacking expression of the CXC chemokine lungkine. The Journal of Immunology *166*, 3362.

Chen, Y., Chan, V.S.F., Zheng, B., Chan, K.Y.K., Xu, X., To, L.Y.F., Huang, F.P., Khoo, U.S., and Lin, C.L.S. (2007). A novel subset of putative stem/progenitor CD34+ Oct-4+ cells is the major target for SARS coronavirus in human lung. The Journal of experimental medicine *204*, 2529-2536.

Chilosi, M., Poletti, V., Murer, B., Lestani, M., Cancellieri, A., Montagna, L., Piccoli, P., Cangi, G., Semenzato, G., and Doglioni, C. (2002). Abnormal Re-epithelialization and Lung Remodeling in Idiopathic Pulmonary Fibrosis: The Role of &Dgr; N-p63. Laboratory investigation *82*, 1335-1345.

Choi, J.E., Lee, S., Sunde, D.A., Huizar, I., Haugk, K.L., Thannickal, V.J., Vittal, R., Plymate, S.R., and Schnapp, L.M. (2009). Insulin-like growth factor-I receptor blockade improves outcome in mouse model of lung injury. American journal of respiratory and critical care medicine *179*, 212-219.

Copelan, E.A. (2006). Hematopoietic stem-cell transplantation. New England Journal of Medicine *354*, 1813-1826.

Coraux, C., Nawrocki-Raby, B., Hinnrasky, J., Kileztky, C., Gaillard, D., Dani, C., and Puchelle, E. (2005). Embryonic stem cells generate airway epithelial tissue. Am J Respir Cell Mol Biol *32*, 87-92.

Costa, R.H., Kalinichenko, V.V., and Lim, L. (2001). Transcription factors in mouse lung development and function. American Journal of Physiology-Lung Cellular and Molecular Physiology *280*, L823-L838.

Coughlin, M.D. (1975). Target organ stimulation of parasympathetic nerve growth in the developing mouse submandibular gland. Developmental biology *43*, 140-158.

Daniely, Y., Liao, G., Dixon, D., Linnoila, R.I., Lori, A., Randell, S.H., Oren, M., and Jetten, A.M. (2004). Critical role of p63 in the development of a normal esophageal and tracheobronchial epithelium. American Journal of Physiology-Cell Physiology *287*, C171-C181.

De Luca, M., Pellegrini, G., and Green, H. (2006). Regeneration of squamous epithelia from stem cells of cultured grafts. Regenerative medicine *1*, 45-57.

De Vries, J., Visser, G., and Prechtl, H.F.R. (1982). The emergence of fetal behaviour. I. Qualitative aspects. Early human development *7*, 301-322.

Delaere, P., Vranckx, J., Verleden, G., De Leyn, P., and Van Raemdonck, D. (2010). Tracheal allotransplantation after withdrawal of immunosuppressive therapy. New England Journal of Medicine *362*, 138-145.

DiFiore, J., and Wilson, J. (1994). Lung development.

Ding, B.S., Nolan, D.J., Guo, P., Babazadeh, A.O., Cao, Z., Rosenwaks, Z., Crystal, R.G., Simons, M., Sato, T.N., and Worgall, S. (2011). Endothelial-Derived Angiocrine Signals Induce and Sustain Regenerative Lung Alveolarization. Cell *147*, 539-553.

Doherty, P.C., Turner, S.J., Webby, R.G., and Thomas, P.G. (2006). Influenza and the challenge for immunology. Nature immunology *7*, 449-455.

Doherty, T.A., Khorram, N., Sugimoto, K., Sheppard, D., Rosenthal, P., Cho, J.Y., Pham, A., Miller, M., Croft, M., and Broide, D.H. (2012). Alternaria Induces STAT6-Dependent Acute Airway Eosinophilia and Epithelial FIZZ1 Expression That Promotes Airway Fibrosis and Epithelial Thickness. The Journal of Immunology *188*, 2622-2629.

Dovey, J.S., Zacharek, S.J., Kim, C.F., and Lees, J.A. (2008). Bmi1 is critical for lung tumorigenesis and bronchioalveolar stem cell expansion. Proceedings of the National Academy of Sciences *105*, 11857.

Dulbecco, R., and Vogt, M. (1953). Some problems of animal virology as studied by the plaque technique (Cold Spring Harbor Laboratory Press).

Emmert-Buck, M.R., Bonner, R.F., Smith, P.D., Chuaqui, R.F., Zhuang, Z., Goldstein, S.R., Weiss, R.A., and Liotta, L.A. (1996). Laser capture microdissection. Science *274*, 998-1001.

Endo, H., and Oka, T. (1991). An immunohistochemical study of bronchial cells producing surfactant protein A in the developing human fetal lung. Early human development *25*, 149-156.

Espina, V., Wulfkuhle, J.D., Calvert, V.S., VanMeter, A., Zhou, W., Coukos, G., Geho, D.H., Petricoin, E.F., and Liotta, L.A. (2006). Laser-capture microdissection. Nature Protocols *1*, 586-603.

Evans, M., Cabral-Anderson, L., and Freeman, G. (1978). Role of the Clara cell in renewal of the bronchiolar epithelium. Laboratory investigation; a journal of technical methods and pathology *38*, 648.

Evans, M., Cox, R., Shami, S., and Plopper, C. (1990). Junctional adhesion mechanisms in airway basal cells. American journal of respiratory cell and molecular biology *3*, 341.

Evans, M., Johnson, L., Stephens, R., and Freeman, G. (1976). Renewal of the terminal bronchiolar epithelium in the rat following exposure to NO2 or O3. Laboratory investigation; a journal of technical methods and pathology *35*, 246.

Evans, M.J., Cabral, L.J., Stephens, R.J., and Freeman, G. (1973). Renewal of alveolar epithelium in the rat following exposure to NO2. The American journal of pathology *70*, 175.

Evans, M.J., Cabral, L.J., Stephens, R.J., and Freeman, G. (1975). Transformation of alveolar type 2 cells to type 1 cells following exposure to NO2. Experimental and molecular pathology *22*, 142-150.

Evans, M.J., and Plopper, C.G. (1988). The role of basal cells in adhesion of columnar epithelium to airway basement membrane. American journal of respiratory and critical care medicine *138*, 481-483.

Everitt, A.R., Clare, S., Pertel, T., John, S.P., Wash, R.S., Smith, S.E., Chin, C.R., Feeley, E.M., Sims, J.S., and Adams, D.J. (2012). IFITM3 restricts the morbidity and mortality associated with influenza. Nature.

Fanucchi, M.V., Murphy, M.E., Buckpitt, A.R., Philpot, R.M., and Plopper, C.G. (1997). Pulmonary cytochrome P450 monooxygenase and Clara cell

differentiation in mice. American journal of respiratory cell and molecular biology *17*, 302.

Fehrenbach, H. (2001). Alveolar epithelial type II cell: defender of the alveolus revisited. Respir Res *2*, 33-46.

Fellrath, J., and Bois, R.M. (2003). Idiopathic pulmonary fibrosis/cryptogenic fibrosing alveolitis. Clinical and experimental medicine *3*, 65-83.

Ford, J.R., and Terzaghi-Howe, M. (1992a). Basal cells are the progenitors of primary tracheal epithelial cell cultures. Experimental cell research *198*, 69-77.

Ford, J.R., and Terzaghi-Howe, M. (1992b). Characteristics of magnetically separated rat tracheal epithelial cell populations. American Journal of Physiology-Lung Cellular and Molecular Physiology *263*, L568-L574.

Forkert, P.G., and Reynolds, E.S. (1982). 1, 1-Dichloroethylene-induced pulmonary injury. Experimental lung research *3*, 57-68.

Fox, R.E., Hopkins, I.B., Cabacungan, E.T., and Tildon, J.T. (1996). The Role of Glutamine and Other Alternate Substrates as Energy Sources in the Fetal Rat Lung Type II Cell1. Pediatric research *40*, 135-141.

Fuchs, E., and Segre, J.A. (2000). Stem cells: Review a new lease on life. Cell *100*, 143-155.

Fuchs, E., Tumbar, T., and Guasch, G. (2004). Socializing with the neighbors: stem cells and their niche. Cell *116*, 769-778.

Gallico III, G.G., O'Connor, N.E., Compton, C.C., Kehinde, O., and Green, H. (1984). Permanent coverage of large burn wounds with autologous cultured human epithelium. New England Journal of Medicine *311*, 448-451.

Gereke, M., Gröbe, L., Prettin, S., Kasper, M., Deppenmeier, S., Gruber, A.D., Enelow, R.I., Buer, J., and Bruder, D. (2007). Phenotypic alterations in type II alveolar epithelial cells in CD4+ T cell mediated lung inflammation. Respir Res *8*, 47.

Geremek, M., Bruinenberg, M., Ziętkiewicz, E., Pogorzelski, A., Witt, M., and Wijmenga, C. (2011). Gene expression studies in cells from primary ciliary dyskinesia patients identify 208 potential ciliary genes. Human genetics *129*, 283-293.

Germano, D., Blyszczuk, P., Valaperti, A., Kania, G., Dirnhofer, S., Landmesser, U., Lüscher, T.F., Hunziker, L., Zulewski, H., and Eriksson, U. (2009). Prominin-

1/CD133+ lung epithelial progenitors protect from bleomycin-induced pulmonary fibrosis. American journal of respiratory and critical care medicine *179*, 939-949.

Ghedin, E., Sengamalay, N.A., Shumway, M., Zaborsky, J., Feldblyum, T., Subbu, V., Spiro, D.J., Sitz, J., Koo, H., and Bolotov, P. (2005). Large-scale sequencing of human influenza reveals the dynamic nature of viral genome evolution. Nature *437*, 1162-1166.

Giangreco, A., Reynolds, S.D., and Stripp, B.R. (2002). Terminal bronchioles harbor a unique airway stem cell population that localizes to the bronchoalveolar duct junction. The American journal of pathology *161*, 173-182.

Gill, J.R., Sheng, Z.M., Ely, S.F., Guinee Jr, D.G., Beasley, M.B., Suh, J., Deshpande, C., Mollura, D.J., Morens, D.M., and Bray, M. (2010). Pulmonary pathologic findings of fatal 2009 pandemic influenza A/H1N1 viral infections.

Gillis, C., and Pitt, B. (1982). The fate of circulating amines within the pulmonary circulation. Annual review of physiology *44*, 269-281.

Glaab, T., Taube, C., Braun, A., and Mitzner, W. (2007). Invasive and noninvasive methods for studying pulmonary function in mice. Respir Res *8*, 63.

Gontan, C., de Munck, A., Vermeij, M., Grosveld, F., Tibboel, D., and Rottier, R. (2008). Sox2 is important for two crucial processes in lung development: branching morphogenesis and epithelial cell differentiation. Developmental biology *317*, 296-309.

Grande, N.R., Peão, M.N.D., de Sá, C.M., and Águas, A.P. (1998). Lung fibrosis induced by bleomycin: structural changes and overview of recent advances. Scanning Microscopy *12*, 487-494.

Green, H. (2008). The birth of therapy with cultured cells. Bioessays *30*, 897-903.
Gribbin, J., Hubbard, R.B., Le Jeune, I., Smith, C.J.P., West, J., and Tata, L.J. (2006). Incidence and mortality of idiopathic pulmonary fibrosis and sarcoidosis in the UK. Thorax *61*, 980-985.

Grose, C. (2004). Avian influenza virus infection of children in Vietnam and Thailand. The Pediatric infectious disease journal *23*, 793.

Gubareva, L.V., McCullers, J.A., Bethell, R.C., and Webster, R.G. (1998). Characterization of influenza A/HongKong/156/97 (H5N1) virus in a mouse model and protective effect of zanamivir on H5N1 infection in mice. Journal of Infectious Diseases *178*, 1592-1596.

Haschek, W.M., Boyd, M.R., Hakkinen, P.J., Owenby, C.S., and Witschi, H. (1984). Acute inhalation toxicity of 3-methylfuran in the mouse: pathology, cell

kinetics, and respiratory rate effects. Toxicology and applied pharmacology *72*, 124-133.

Hashimoto, S., Amaya, F., Matsuyama, H., Ueno, H., Kikuchi, S., Tanaka, M., Watanabe, Y., Ebina, M., Ishizaka, A., and Tsukita, S. (2008). Dysregulation of lung injury and repair in moesin-deficient mice treated with intratracheal bleomycin. American Journal of Physiology-Lung Cellular and Molecular Physiology *295*, L566-L574.

Hay, A.J., Gregory, V., Douglas, A.R., and Lin, Y.P. (2001). The evolution of human influenza viruses. Philos Trans R Soc Lond B Biol Sci *356*, 1861-1870.

Herridge, M.S., Cheung, A.M., Tansey, C.M., Matte-Martyn, A., Diaz-Granados, N., Al-Saidi, F., Cooper, A.B., Guest, C.B., Mazer, C.D., and Mehta, S. (2003). One-year outcomes in survivors of the acute respiratory distress syndrome. New England Journal of Medicine *348*, 683-693.

Hilleman, M.R. (2002). Realities and enigmas of human viral influenza: pathogenesis, epidemiology and control. Vaccine *20*, 3068-3087.

Hoess, R.H., and Abremski, K. (1985). Mechanism of strand cleavage and exchange in the Cre-lox site-specific recombination system. Journal of molecular biology *181*, 351-362.

Hong, K.U., Reynolds, S.D., Giangreco, A., Hurley, C.M., and Stripp, B.R. (2001). Clara cell secretory protein-expressing cells of the airway neuroepithelial body microenvironment include a label-retaining subset and are critical for epithelial renewal after progenitor cell depletion. American journal of respiratory cell and molecular biology *24*, 671.

Hong, K.U., Reynolds, S.D., Watkins, S., Fuchs, E., and Stripp, B.R. (2004a). Basal cells are a multipotent progenitor capable of renewing the bronchial epithelium. The American journal of pathology *164*, 577-588.

Hong, K.U., Reynolds, S.D., Watkins, S., Fuchs, E., and Stripp, B.R. (2004b). In vivo differentiation potential of tracheal basal cells: evidence for multipotent and unipotent subpopulations. American Journal of Physiology-Lung Cellular and Molecular Physiology *286*, L643-L649.

Hosford, G.E., Fang, X., and Olson, D.M. (2004). Hyperoxia decreases matrix metalloproteinase-9 and increases tissue inhibitor of matrix metalloproteinase-1 protein in the newborn rat lung: association with arrested alveolarization. Pediatric research *56*, 26-34.

Huber, C., Munnich, A., and Cormier-Daire, V. (2011). The 3M syndrome. Best Practice & Research Clinical Endocrinology & Metabolism *25*, 143-151.

Huh, D., Matthews, B.D., Mammoto, A., Montoya-Zavala, M., Hsin, H.Y., and Ingber, D.E. (2010). Reconstituting organ-level lung functions on a chip. Science *328*, 1662-1668.

Hummler, E., and Planès, C. (2010). Importance of ENaC-mediated sodium transport in alveolar fluid clearance using genetically-engineered mice. Cellular Physiology and Biochemistry *25*, 63-70.

Ibricevic, A., Pekosz, A., Walter, M.J., Newby, C., Battaile, J.T., Brown, E.G., Holtzman, M.J., and Brody, S.L. (2006). Influenza virus receptor specificity and cell tropism in mouse and human airway epithelial cells. Journal of virology *80*, 7469-7480.

Inayama, Y., Hook, G., Brody, A., Cameron, G., Jetten, A., Gilmore, L., Gray, T., and Nettesheim, P. (1988). The differentiation potential of tracheal basal cells. Laboratory investigation; a journal of technical methods and pathology *58*, 706.

Inayama, Y., Hook, G., Brody, A., Jetten, A., Gray, T., Mahler, J., and Nettesheim, P. (1989). In vitro and in vivo growth and differentiation of clones of tracheal basal cells. The American journal of pathology *134*, 539.

Iwaguro, H., Yamaguchi, J., Kalka, C., Murasawa, S., Masuda, H., Hayashi, S., Silver, M., Li, T., Isner, J.M., and Asahara, T. (2002). Endothelial progenitor cell vascular endothelial growth factor gene transfer for vascular regeneration. Circulation *105*, 732-738.

Jackson, E.L., Willis, N., Mercer, K., Bronson, R.T., Crowley, D., Montoya, R., Jacks, T., and Tuveson, D.A. (2001). Analysis of lung tumor initiation and progression using conditional expression of oncogenic K-ras. Genes & development *15*, 3243.

Jeffery, P.K. (1998). The development of large and small airways. American journal of respiratory and critical care medicine *157*, S174-S180.

Johnson, N., and Mueller, J. (2002). Updating the accounts: global mortality of the 1918-1920" Spanish" influenza pandemic. Bulletin of the History of Medicine *76*, 105-115.

Johnson, N., Wilson, J., Habbersett, R., Thomassen, D., Shopp, G., and Smith, D. (1990a). Separation and characterization of basal and secretory cells from the rat trachea by flow cytometry. Cytometry *11*, 395-405.

Johnson, N.F., Hubbs, A.F., and Thomassen, D.G. (1990b). Epithelial progenitor cells in the rat respiratory tract. Biology, toxicology and carcinogenesis of respiratort epithelium Washington, DC, Hemisphere, 88-98.

Junod, A.F. (1985). 5‐Hydroxytryptamine and Other Amines in the Lungs. Comprehensive Physiology.

Kajstura, J., Rota, M., Hall, S.R., Hosoda, T., D'Amario, D., Sanada, F., Zheng, H., Ogórek, B., Rondon-Clavo, C., and Ferreira-Martins, J. (2011). Evidence for human lung stem cells. New England Journal of Medicine *364*, 1795-1806.

Karinch, A.M., Pan, M., Lin, C.M., Strange, R., and Souba, W.W. (2001). Glutamine metabolism in sepsis and infection. The Journal of nutrition *131*, 2535S-2538S.

Kavet, R.I., and Brain, J.D. (1974). Minireview reaction of the lung to air pollutant exposure. Life sciences *15*, 849-861.

Khimji, A., and Rockey, D.C. (2010). Endothelin—Biology and disease. Cellular signalling *22*, 1615-1625.

Kim, C.F.B., Jackson, E.L., Woolfenden, A.E., Lawrence, S., Babar, I., Vogel, S., Crowley, D., Bronson, R.T., and Jacks, T. (2005). Identification of bronchioalveolar stem cells in normal lung and lung cancer. Cell *121*, 823-835.

Knobler, S. (2005). The threat of pandemic influenza: are we ready?: workshop summary (Natl Academy Pr).

Knox, S., Lombaert, I., Reed, X., Vitale-Cross, L., Gutkind, J., and Hoffman, M. (2010). Parasympathetic innervation maintains epithelial progenitor cells during salivary organogenesis. Science's STKE *329*, 1645.

Köhler, G., and Milstein, C. (1975). Continuous cultures of fused cells secreting antibody of predefined specificity. Nature *256*, 495-497.

Körbling, M., and Estrov, Z. (2003). Adult stem cells for tissue repair—a new therapeutic concept? New England Journal of Medicine *349*, 570-582.

Krane, C.M., Fortner, C.N., Hand, A.R., McGraw, D.W., Lorenz, J.N., Wert, S.E., Towne, J.E., Paul, R.J., Whitsett, J.A., and Menon, A.G. (2001). Aquaporin 5-deficient mouse lungs are hyperresponsive to cholinergic stimulation. Proceedings of the National Academy of Sciences *98*, 14114.

Kubo, A., Yuba-Kubo, A., Tsukita, S., and Amagai, M. (2008). Sentan: a novel specific component of the apical structure of vertebrate motile cilia. Molecular biology of the cell *19*, 5338-5346.

Kuhn, C., and Mason, R.J. (1995). Immunolocalization of SPARC, tenascin, and thrombospondin in pulmonary fibrosis. The American journal of pathology *147*, 1759.

Kumar, P.A., Hu, Y., Yamamoto, Y., Hoe, N.B., Wei, T.S., Mu, D., Sun, Y., Joo, L.S., Dagher, R., and Zielonka, E.M. (2011). Distal Airway Stem Cells Yield Alveoli In Vitro and during Lung Regeneration following H1N1 Influenza Infection. Cell *147*, 525-538.

Lamb, D., and Reid, L. (1968). Mitotic rates, goblet cell increase and histochemical changes in mucus in rat bronchial epithelium during exposure to sulphur dioxide. The Journal of pathology and bacteriology *96*, 97-111.

Littlewood, T.D., Hancock, D.C., Danielian, P.S., Parker, M.G., and Evan, G.I. (1995). A modified oestrogen receptor ligand-binding domain as an improved switch for the regulation of heterologous proteins. Nucleic acids research *23*, 1686-1690.

Liu, J.Y., Nettesheim, P., and Randell, S.H. (1994). Growth and differentiation of tracheal epithelial progenitor cells. American Journal of Physiology-Lung Cellular and Molecular Physiology *266*, L296-L307.

Liu, X., Driskell, R.R., and Engelhardt, J.F. (2006). Stem cells in the lung. Methods in enzymology *419*, 285-321.

Liu, Y., Sadikot, R.T., Adami, G.R., Kalinichenko, V.V., Pendyala, S., Natarajan, V., Zhao, Y., and Malik, A.B. (2011). FoxM1 mediates the progenitor function of type II epithelial cells in repairing alveolar injury induced by Pseudomonas aeruginosa. The Journal of experimental medicine *208*, 1473-1484.

Liu, Y., Stein, E., Oliver, T., Li, Y., Brunken, W.J., Koch, M., Tessier-Lavigne, M., and Hogan, B.L.M. (2004). Novel role for Netrins in regulating epithelial behavior during lung branching morphogenesis. Current biology *14*, 897-905.

Locke, L.W., Chordia, M.D., Zhang, Y., Kundu, B., Kennedy, D., Landseadel, J., Xiao, L., Fairchild, K.D., Berr, S.S., and Linden, J. (2009). A novel neutrophil-specific PET imaging agent: cFLFLFK-PEG-64Cu. Journal of Nuclear Medicine *50*, 790-797.

Lowy, R.J. (2003). Influenza virus induction of apoptosis by intrinsic and extrinsic mechanisms. International reviews of immunology *22*, 425-449.

Lu, X., Tumpey, T.M., Morken, T., Zaki, S.R., Cox, N.J., and Katz, J.M. (1999). A mouse model for the evaluation of pathogenesis and immunity to influenza A (H5N1) viruses isolated from humans. Journal of virology *73*, 5903-5911.

Lu, Y., Futtner, C., Rock, J.R., Xu, X., Whitworth, W., Hogan, B.L.M., and Onaitis, M.W. (2010). Evidence that SOX2 overexpression is oncogenic in the lung. PLoS One *5*, e11022.

Macchiarini, P., Jungebluth, P., Go, T., Asnaghi, M., Rees, L.E., Cogan, T.A., Dodson, A., Martorell, J., Bellini, S., and Parnigotto, P.P. (2008). Clinical transplantation of a tissue-engineered airway. The Lancet *372*, 2023-2030.

Machado-Aranda, D., Adir, Y., Young, J.L., Briva, A., Budinger, G.R.S., Yeldandi, A.V., Sznajder, J.I., and Dean, D.A. (2005). Gene transfer of the Na+, K+-ATPase β1 subunit using electroporation increases lung liquid clearance. American journal of respiratory and critical care medicine *171*, 204-211.

Mahvi, D., Bank, H., and Harley, R. (1977). Morphology of a naphthalene-induced bronchiolar lesion. The American journal of pathology *86*, 558.

Mancebo, J., Fernández, R., Blanch, L., Rialp, G., Gordo, F., Ferrer, M., Rodríguez, F., Garro, P., Ricart, P., and Vallverdú, I. (2006). A multicenter trial of prolonged prone ventilation in severe acute respiratory distress syndrome. American journal of respiratory and critical care medicine *173*, 1233-1239.

Mao, X., Fujiwara, Y., and Orkin, S.H. (1999). Improved reporter strain for monitoring Cre recombinase-mediated DNA excisions in mice. Proceedings of the National Academy of Sciences *96*, 5037.

Mason, R., and Williams, M. (1977). Type II alveolar cell. Defender of the alveolus. The American review of respiratory disease *115*, 81.

Massion, P.P., Taflan, P.M., Rahman, S.M.J., Yildiz, P., Shyr, Y., Edgerton, M.E., Westfall, M.D., Roberts, J.R., Pietenpol, J.A., and Carbone, D.P. (2003). Significance of p63 amplification and overexpression in lung cancer development and prognosis. Cancer research *63*, 7113-7121.

Mathers, C.D., and Loncar, D. (2006). Projections of global mortality and burden of disease from 2002 to 2030. PLoS medicine *3*, e442.

Matuschak, G., and Lechner, A. (2010). Acute lung injury and the acute respiratory distress syndrome: pathophysiology and treatment. Missouri medicine *107*, 252.

Matute-Bello, G., Frevert, C.W., and Martin, T.R. (2008). Animal models of acute lung injury. American Journal of Physiology-Lung Cellular and Molecular Physiology *295*, L379-L399.

McClintock, T.S., Glasser, C.E., Bose, S.C., and Bergman, D.A. (2008). Tissue expression patterns identify mouse cilia genes. Physiological genomics *32*, 198-206.

McQualter, J.L., Yuen, K., Williams, B., and Bertoncello, I. (2010). Evidence of an epithelial stem/progenitor cell hierarchy in the adult mouse lung. Proceedings of the National Academy of Sciences *107*, 1414-1419.

Meltzer, E.B., and Noble, P.W. (2008). Idiopathic pulmonary fibrosis. Orphanet J Rare Dis *3*.

Metzger, R.J., Klein, O.D., Martin, G.R., and Krasnow, M.A. (2008). The branching programme of mouse lung development. Nature *453*, 745-750.

Miao, H., Hollenbaugh, J.A., Zand, M.S., Holden-Wiltse, J., Mosmann, T.R., Perelson, A.S., Wu, H., and Topham, D.J. (2010). Quantifying the early immune response and adaptive immune response kinetics in mice infected with influenza A virus. Journal of virology *84*, 6687-6698.

Millien, G., Beane, J., Lenburg, M., Tsao, P.N., Lu, J., Spira, A., and Ramirez, M.I. (2008). Characterization of the mid-foregut transcriptome identifies genes regulated during lung bud induction. Gene Expression Patterns *8*, 124-139.

Mills, A.A., Zheng, B., Wang, X.J., Vogel, H., Roop, D.R., and Bradley, A. (1999). p63 is a p53 homologue required for limb and epidermal morphogenesis. Nature *398*, 708-713.

Moeller, A., Ask, K., Warburton, D., Gauldie, J., and Kolb, M. (2008). The bleomycin animal model: a useful tool to investigate treatment options for idiopathic pulmonary fibrosis? The international journal of biochemistry & cell biology *40*, 362-382.

Monvoisin, A., Alva, J.A., Hofmann, J.J., Zovein, A.C., Lane, T.F., and Iruela‐Arispe, M.L. (2006). VE‐cadherin‐CreERT2 transgenic mouse: A model for inducible recombination in the endothelium. Developmental dynamics *235*, 3413-3422.

Mori, I., Komatsu, T., Takeuchi, K., Nakakuki, K., Sudo, M., and Kimura, Y. (1995). In vivo induction of apoptosis by influenza virus. Journal of general virology *76*, 2869-2873.

Morrisey, E.E., and Hogan, B.L.M. (2010). Preparing for the first breath: genetic and cellular mechanisms in lung development. Developmental cell *18*, 8-23.

Moyron-Quiroz, J.E., Rangel-Moreno, J., Kusser, K., Hartson, L., Sprague, F., Goodrich, S., Woodland, D.L., Lund, F.E., and Randall, T.D. (2004). Role of inducible bronchus associated lymphoid tissue (iBALT) in respiratory immunity. Nature medicine *10*, 927-934.

Mozdzanowska, K., Furchner, M., Zharikova, D., Feng, J.Q., and Gerhard, W. (2005). Roles of CD4+ T-cell-independent and-dependent antibody responses in the control of influenza virus infection: evidence for noncognate CD4+ T-cell activities that enhance the therapeutic activity of antiviral antibodies. Journal of virology *79*, 5943-5951.

Narasaraju, T., Ng, H., Phoon, M., and Chow, V.T.K. (2010). MCP-1 antibody treatment enhances damage and impedes repair of the alveolar epithelium in influenza pneumonitis. American journal of respiratory cell and molecular biology *42*, 732.

Neptune, E.R., Frischmeyer, P.A., Arking, D.E., Myers, L., Bunton, T.E., Gayraud, B., Ramirez, F., Sakai, L.Y., and Dietz, H.C. (2003). Dysregulation of TGF-β activation contributes to pathogenesis in Marfan syndrome. Nature genetics *33*, 407-411.

Neuringer, I.P., and Randell, S.H. (2004). Stem cells and repair of lung injuries. Respir Res *5*.

Nguyen, N.M., Pulkkinen, L., Schlueter, J.A., Meneguzzi, G., Uitto, J., and Senior, R.M. (2006). Lung development in laminin γ2 deficiency: abnormal tracheal hemidesmosomes with normal branching morphogenesis and epithelial differentiation. Respiratory research *7*, 28.

Nielsen, C.H., Kimura, R.H., Withofs, N., Tran, P.T., Miao, Z., Cochran, J.R., Cheng, Z., Felsher, D., Kjær, A., and Willmann, J.K. (2010). PET imaging of tumor neovascularization in a transgenic mouse model with a novel 64Cu-DOTA-knottin peptide. Cancer research *70*, 9022-9030.

Nielsen, S., King, L.S., Christensen, B.M., and Agre, P. (1997). Aquaporins in complex tissues. II. Subcellular distribution in respiratory and glandular tissues of rat. American Journal of Physiology-Cell Physiology *273*, C1549-C1561.

Nishida, K., Yamato, M., Hayashida, Y., Watanabe, K., Yamamoto, K., Adachi, E., Nagai, S., Kikuchi, A., Maeda, N., and Watanabe, H. (2004). Corneal reconstruction with tissue-engineered cell sheets composed of autologous oral mucosal epithelium. New England Journal of Medicine *351*, 1187-1196.

Orban, P.C., Chui, D., and Marth, J.D. (1992). Tissue-and site-specific DNA recombination in transgenic mice. Proceedings of the National Academy of Sciences *89*, 6861.

Orens, J.B., and Garrity Jr, E.R. (2009). General overview of lung transplantation and review of organ allocation. Proceedings of the American Thoracic Society *6*, 13-19.

Perez-Padilla, R., de la Rosa-Zamboni, D., Ponce de Leon, S., Hernandez, M., Quiñones-Falconi, F., Bautista, E., Ramirez-Venegas, A., Rojas-Serrano, J., Ormsby, C.E., and Corrales, A. (2009). Pneumonia and respiratory failure from swine-origin influenza A (H1N1) in Mexico. New England Journal of Medicine *361*, 680-689.

Petersen, T.H., Calle, E.A., Zhao, L., Lee, E.J., Gui, L., Raredon, M.S.B., Gavrilov, K., Yi, T., Zhuang, Z.W., and Breuer, C. (2010). Tissue-engineered lungs for in vivo implantation. Science *329*, 538-541.

Petroski, M.D., and Deshaies, R.J. (2005). Function and regulation of cullin–RING ubiquitin ligases. Nature Reviews Molecular Cell Biology *6*, 9-20.

Post, M., and Copland, I. (2002). Overview of lung development. ACTA PHARMACOLOGICA SINICA *23*, 4-7.

Potter, C.W. (2001). A history of influenza. Journal of applied microbiology *91*, 572-579.

Proctor, G.B., and Carpenter, G.H. (2007). Regulation of salivary gland function by autonomic nerves. Autonomic Neuroscience *133*, 3-18.

Pusztaszeri, M.P., Seelentag, W., and Bosman, F.T. (2006). Immunohistochemical expression of endothelial markers CD31, CD34, von Willebrand factor, and Fli-1 in normal human tissues. Journal of Histochemistry & Cytochemistry *54*, 385-395.

Rama, P., Matuska, S., Paganoni, G., Spinelli, A., De Luca, M., and Pellegrini, G. (2010). Limbal stem-cell therapy and long-term corneal regeneration. New England Journal of Medicine *363*, 147-155.

Ramirez, M.I., Pollack, L., Millien, G., Cao, Y.X., Hinds, A., and Williams, M.C. (2002). The alpha-isoform of caveolin-1 is a marker of vasculogenesis in early lung development. The journal of histochemistry and cytochemistry : official journal of the Histochemistry Society *50*, 33-42.

Ramsey, C., and Kumar, A. (2011). H1N1: viral pneumonia as a cause of acute respiratory distress syndrome. Current opinion in critical care *17*, 64.

Randell, S.H., Comment, C.E., Ramaekers, F.C., and Nettesheim, P. (1991). Properties of rat tracheal epithelial cells separated based on expression of cell surface alpha-galactosyl end groups. Am J Respir Cell Mol Biol *4*, 544-554.

Rawlins, E.L., Clark, C.P., Xue, Y., and Hogan, B.L.M. (2009a). The Id2+ distal tip lung epithelium contains individual multipotent embryonic progenitor cells. Development *136*, 3741-3745.

Rawlins, E.L., and Hogan, B.L.M. (2006). Epithelial stem cells of the lung: privileged few or opportunities for many? Development *133*, 2455-2465.

Rawlins, E.L., Okubo, T., Xue, Y., Brass, D.M., Auten, R.L., Hasegawa, H., Wang, F., and Hogan, B.L.M. (2009b). The role of Scgb1a1+ Clara cells in the long-term maintenance and repair of lung airway, but not alveolar, epithelium. Cell Stem Cell *4*, 525-534.

Reynolds, S.D., Giangreco, A., Power, J.H.T., and Stripp, B.R. (2000a). Neuroepithelial bodies of pulmonary airways serve as a reservoir of progenitor cells capable of epithelial regeneration. The American journal of pathology *156*, 269-278.

Reynolds, S.D., Hong, K.U., Giangreco, A., Mango, G.W., Guron, C., Morimoto, Y., and Stripp, B.R. (2000b). Conditional clara cell ablation reveals a self-renewing progenitor function of pulmonary neuroendocrine cells. American Journal of Physiology-Lung Cellular and Molecular Physiology *278*, L1256-L1263.

Reynolds, S.D., Reynolds, P.R., Pryhuber, G.S., Finder, J.D., and Stripp, B.R. (2002). Secretoglobins SCGB3A1 and SCGB3A2 define secretory cell subsets in mouse and human airways. American journal of respiratory and critical care medicine *166*, 1498-1509.

Rheinwatd, J.G., and Green, H. (1975). Seria cultivation of strains of human epidemal keratinocytes: the formation keratinizin colonies from single cell is. Cell *6*, 331-343.

Rock, J.R., Onaitis, M.W., Rawlins, E.L., Lu, Y., Clark, C.P., Xue, Y., Randell, S.H., and Hogan, B.L.M. (2009). Basal cells as stem cells of the mouse trachea and human airway epithelium. Proceedings of the National Academy of Sciences *106*, 12771-12775.

Rodrigo, L., Hernández, A.F., López-Caballero, J.J., Gil, F., and Pla, A. (2001). Immunohistochemical evidence for the expression and induction of paraoxonase in rat liver, kidney, lung and brain tissue. Implications for its physiological role. Chemico-biological interactions *137*, 123-137.

Rogers, C.S., Hao, Y., Rokhlina, T., Samuel, M., Stoltz, D.A., Li, Y., Petroff, E., Vermeer, D.W., Kabel, A.C., Yan, Z*., et al.* (2008a). Production of CFTR-null and CFTR-DeltaF508 heterozygous pigs by adeno-associated virus-mediated gene targeting and somatic cell nuclear transfer. The Journal of clinical investigation *118*, 1571-1577.

Rogers, C.S., Stoltz, D.A., Meyerholz, D.K., Ostedgaard, L.S., Rokhlina, T., Taft, P.J., Rogan, M.P., Pezzulo, A.A., Karp, P.H., and Itani, O.A. (2008b). Disruption

of the CFTR gene produces a model of cystic fibrosis in newborn pigs. Science's STKE *321*, 1837.

Ronaghi, M., Erceg, S., Moreno‐Manzano, V., and Stojkovic, M. (2010). Challenges of stem cell therapy for spinal cord injury: human embryonic stem cells, endogenous neural stem cells, or induced pluripotent stem cells? Stem Cells *28*, 93-99.

Ross, A.J., Dailey, L.A., Brighton, L.E., and Devlin, R.B. (2007). Transcriptional profiling of mucociliary differentiation in human airway epithelial cells. American journal of respiratory cell and molecular biology *37*, 169.

Rossman, J.S., Jing, X., Leser, G.P., and Lamb, R.A. (2010). Influenza virus M2 protein mediates ESCRT-independent membrane scission. Cell *142*, 902-913.

Roth-Kleiner, M., Hirsch, E., and Schittny, J.C. (2004). Fetal lungs of tenascin-C-deficient mice grow well, but branch poorly in organ culture. American journal of respiratory cell and molecular biology *30*, 360-366.

Rubenfeld, G.D., Caldwell, E., Peabody, E., Weaver, J., Martin, D.P., Neff, M., Stern, E.J., and Hudson, L.D. (2005). Incidence and outcomes of acute lung injury. New England Journal of Medicine *353*, 1685-1693.

Ryter, S.W., and Choi, A.M.K. (2008). Caveolin-1: a critical regulator of pulmonary vascular architecture and nitric oxide bioavailability in pulmonary hypertension. American Journal of Physiology-Lung Cellular and Molecular Physiology *294*, L862-L864.

Sauer, B. (1987). Functional expression of the cre-lox site-specific recombination system in the yeast Saccharomyces cerevisiae. Molecular and cellular biology *7*, 2087-2096.

Sauer, B., and Henderson, N. (1988). Site-specific DNA recombination in mammalian cells by the Cre recombinase of bacteriophage P1. Proceedings of the National Academy of Sciences *85*, 5166.

Schoch, K.G., Lori, A., Burns, K.A., Eldred, T., Olsen, J.C., and Randell, S.H. (2004). A subset of mouse tracheal epithelial basal cells generates large colonies in vitro. American Journal of Physiology-Lung Cellular and Molecular Physiology *286*, L631-L642.

Schütze, K., Becker, I., Becker, K.F., Thalhammer, S., Stark, R., Heckl, W.M., Böhm, M., and Pösl, H. (1997). Cut out or poke in--the key to the world of single genes: laser micromanipulation as a valuable tool on the look-out for the origin of disease. Genetic analysis: biomolecular engineering *14*, 1-8.

Schütze, K., Pösl, H., and Lahr, G. (1998). Laser micromanipulation systems as universal tools in cellular and molecular biology and in medicine. Cellular and molecular biology (Noisy-le-Grand, France) *44*, 735.

Schwartz, S.D., Hubschman, J.P., Heilwell, G., Franco-Cardenas, V., Pan, C.K., Ostrick, R.M., Mickunas, E., Gay, R., Klimanskaya, I., and Lanza, R. (2012). Embryonic stem cell trials for macular degeneration: a preliminary report. The Lancet.

Senoo, M., Pinto, F., Crum, C.P., and McKeon, F. (2007). p63 Is essential for the proliferative potential of stem cells in stratified epithelia. Cell *129*, 523-536.

Shapiro, S. (2007). Transgenic and gene-targeted mice as models for chronic obstructive pulmonary disease. European Respiratory Journal *29*, 375-378.

Sidwell, R.W., Huffman, J.H., Gilbert, J., Moscon, B., Pedersen, G., Burger, R., and Warren, R.P. (1992). Utilization of pulse oximetry for the study of the inhibitory effects of antiviral agents on influenza virus in mice. Antimicrobial agents and chemotherapy *36*, 473-476.

Silverman, E.S., Baron, R.M., Palmer, L.J., Le, L., Hallock, A., Subramaniam, V., Riese, R.J., McKenna, M.D., Gu, X., and Libermann, T.A. (2002). Constitutive and cytokine-induced expression of the ETS transcription factor ESE-3 in the lung. American journal of respiratory cell and molecular biology *27*, 697.

Singer, P., Theilla, M., Fisher, H., Gibstein, L., Grozovski, E., and Cohen, J. (2006). Benefit of an enteral diet enriched with eicosapentaenoic acid and gamma-linolenic acid in ventilated patients with acute lung injury. Critical care medicine *34*, 1033-1038.

Slack, J.M.W. (2000). Stem cells in epithelial tissues. Science *287*, 1431-1433.
Sminia, T., Van der Brugge-Gamelkoorn, G., and Jeurissen, S. (1989). Structure and function of bronchus-associated lymphoid tissue (BALT). Critical reviews in immunology *9*, 119.

Souba, W.W., Herskowitz, K., and Plumley, D.A. (1990). Lung glutamine metabolism. JPEN Journal of parenteral and enteral nutrition *14*, 68S.
Sternberg, N., Hamilton, D., Austin, S., Yarmolinsky, M., and Hoess, R. (1981). Site-specific recombination and its role in the life cycle of bacteriophage P1 (Cold Spring Harbor Laboratory Press).

Strauer, B.E., Brehm, M., Zeus, T., Köstering, M., Hernandez, A., Sorg, R.V., Kögler, G., and Wernet, P. (2002). Repair of infarcted myocardium by autologous intracoronary mononuclear bone marrow cell transplantation in humans. Circulation *106*, 1913-1918.

Stripp, B.R., Maxson, K., Mera, R., and Singh, G. (1995). Plasticity of airway cell proliferation and gene expression after acute naphthalene injury. American Journal of Physiology-Lung Cellular and Molecular Physiology *269*, L791-L799.

Subramanian, A., Tamayo, P., Mootha, V.K., Mukherjee, S., Ebert, B.L., Gillette, M.A., Paulovich, A., Pomeroy, S.L., Golub, T.R., and Lander, E.S. (2005). Gene set enrichment analysis: a knowledge-based approach for interpreting genome-wide expression profiles. Proceedings of the National Academy of Sciences of the United States of America *102*, 15545.

Tansey, C.M., Louie, M., Loeb, M., Gold, W.L., Muller, M.P., de Jager, J.A., Cameron, J.I., Tomlinson, G., Mazzulli, T., and Walmsley, S.L. (2007). One-year outcomes and health care utilization in survivors of severe acute respiratory syndrome. Archives of internal medicine *167*, 1312.

Teijaro, J.R., Walsh, K.B., Cahalan, S., Fremgen, D.M., Roberts, E., Scott, F., Martinborough, E., Peach, R., Oldstone, M., and Rosen, H. (2011). Endothelial cells are central orchestrators of cytokine amplification during influenza virus infection. Cell *146*, 980-991.

Thomas, M., and Owen, C. (2008). Inhibition of PI-3 kinase for treating respiratory disease: good idea or bad idea? Current opinion in pharmacology *8*, 267-274.

Thomas, P.D., Campbell, M.J., Kejariwal, A., Mi, H., Karlak, B., Daverman, R., Diemer, K., Muruganujan, A., and Narechania, A. (2003). PANTHER: a library of protein families and subfamilies indexed by function. Genome research *13*, 2129-2141.

Thomas, P.G., Keating, R., Hulse-Post, D.J., and Doherty, P.C. (2006). Cell-mediated protection in influenza infection. Emerging infectious diseases *12*, 48.

Tompkins, D.H., Besnard, V., Lange, A.W., Keiser, A.R., Wert, S.E., Bruno, M.D., and Whitsett, J.A. (2011). Sox2 activates cell proliferation and differentiation in the respiratory epithelium. American journal of respiratory cell and molecular biology *45*, 101.

van der Laan, J.W., Herberts, C., Lambkin-Williams, R., Boyers, A., Mann, A.J., and Oxford, J. (2008). Animal models in influenza vaccine testing. Expert review of vaccines *7*, 783-793.

Vaporciyan, A.A., Delisser, H.M., Yan, H.C., Mendiguren, I.I., Thom, S.R., Jones, M.L., Ward, P.A., and Albelda, S.M. (1993). Involvement of platelet-endothelial cell adhesion molecule-1 in neutrophil recruitment in vivo. Science *262*, 1580-1582.

Vasioukhin, V., Degenstein, L., Wise, B., and Fuchs, E. (1999). The magical touch: genome targeting in epidermal stem cells induced by tamoxifen application to mouse skin. Proceedings of the National Academy of Sciences *96*, 8551.

Verhoeven, D., Teijaro, J.R., and Farber, D.L. (2009). Pulse-oximetry accurately predicts lung pathology and the immune response during influenza infection. Virology *390*, 151-156.

Wahr, J.A., Tremper, K.K., and Diab, M. (1995). Pulse oximetry. Respiratory care clinics of North America *1*, 77.

Wang, C., Lamb, R.A., and Pinto, L.H. (1995). Activation of the M2 ion channel of influenza virus: a role for the transmembrane domain histidine residue. Biophysical journal *69*, 1363-1371.

Wang, D., Morales, J.E., Calame, D.G., Alcorn, J.L., and Wetsel, R.A. (2010). Transplantation of human embryonic stem cell–derived alveolar epithelial type II cells abrogates acute lung injury in mice. Molecular Therapy *18*, 625-634.

Weissman, I.L. (2000). Stem Cells: Units of Development, Review Units of Regeneration, and Units in Evolution. Cell *100*, 157-168.

White, A.C., Lavine, K.J., and Ornitz, D.M. (2007). FGF9 and SHH regulate mesenchymal Vegfa expression and development of the pulmonary capillary network. Development *134*, 3743-3752.

Wojcik, S.M., Bundman, D.S., and Roop, D.R. (2000). Delayed wound healing in keratin 6a knockout mice. Molecular and cellular biology *20*, 5248-5255.

Wongtrakool, C., Roser-Page, S., Rivera, H.N., and Roman, J. (2007). Nicotine alters lung branching morphogenesis through the α 7 nicotinic acetylcholine receptor. American Journal of Physiology-Lung Cellular and Molecular Physiology *293*, L611-L618.

Wu, S., Metcalf, J.P., and Wu, W. (2011). Innate immune response to influenza virus. Current Opinion in Infectious Diseases *24*, 235.

Xian, W., and McKeon, F. (2012). Adult stem cells underlying lung regeneration. Cell cycle (Georgetown, Tex) *11*.

Yang, A., Kaghad, M., Wang, Y., Gillett, E., Fleming, M.D., Andrews, N.C., Caput, D., and McKeon, F. (1998). p63, a p53 homolog at 3q27-29, encodes multiple products with transactivating, death-inducing, and dominant-negative activities. Molecular cell *2*, 305-316.

Yang, A., Schweitzer, R., Sun, D., Kaghad, M., Walker, N., Bronson, R.T., Tabin, C., Sharpe, A., Caput, D., and Crum, C. (1999). p63 is essential for regenerative proliferation in limb, craniofacial and epithelial development. Nature *398*, 714-717.

Ye, P., Rodriguez, F.H., Kanaly, S., Stocking, K.L., Schurr, J., Schwarzenberger, P., Oliver, P., Huang, W., Zhang, P., and Zhang, J. (2001). Requirement of interleukin 17 receptor signaling for lung CXC chemokine and granulocyte colony-stimulating factor expression, neutrophil recruitment, and host defense. The Journal of experimental medicine *194*, 519-528.

Yeldandl, A.V., and Colby, T.V. (1994). Pathologic features of lung biopsy specimens from influenza pneumonia cases. Human pathology *25*, 47-53.

Yu, I.J., Song, K.S., Chang, H.K., Han, J.H., Kim, K.J., Chung, Y.H., Maeng, S.H., Park, S.H., Han, K.T., and Chung, K.H. (2001). Lung fibrosis in Sprague-Dawley rats, induced by exposure to manual metal arc–stainless steel welding fumes. Toxicological Sciences *63*, 99-106.

Zacharek, S.J., Fillmore, C.M., Lau, A.N., Gludish, D.W., Chou, A., Ho, J.W.K., Zamponi, R., Gazit, R., Bock, C., and Jäger, N. (2011). Lung stem cell self-renewal relies on Bmi1-dependent control of expression at imprinted loci. Cell Stem Cell *9*, 272-281.

Zambon, M., and Vincent, J.L. (2008). Mortality Rates for Patients With Acute Lung Injury/ARDS Have Decreased Over Time*. Chest *133*, 1120-1127.

Zhou, L., Dey, C.R., Wert, S.E., and Whitsett, J.A. (1996). Arrested Lung Morphogenesis in Transgenic Mice Bearing an SP-C-TGF-[beta] 1 Chimeric Gene. Developmental biology *175*, 227-238.

Bannister, L.H. Respiratory system P.L. Williams, R. Warwick, M. Dyson, L.H. Bannister (Eds.), Gray's Anatomy (Thirty-Eighth Edition), Churchill Livingstone, New York (1999), pp. 1666–1672.

Centers for Disease Control and Prevention, 2004. Cases of influenza A(H5N1): Thailand, 2004. MMWR Morb Mortal Wkly Rep 2004;53:100–103.

National Heart Lung and Blood Institute, 2009.Morbidity and mortality: 2009 chart book on cardiovascular, lung, and blood diseases. Bethesda (MD): National Heart, Lung, and Blood Institute; 2009.

National Institutes of Health. National Heart, Lung and Blood Institute. Diseases and Conditions, 2007: http://www.nhlbi.nih.gov/health/dci/Diseases/Ards/Ards_WhatIs.html

WHO 2005:
http://apps.who.int/csr/disease/influenza/pandemic10things/en/index.html

WHO 2012:
www.who.int/csr/disease/influenza/pandemic10things/en/index.html

National Heart Lung and Blood Institute, 2010:
http://www.nhlbi.nih.gov/health/health-topics/topics/copd/

LIST OF PUBLICATIONS

- Distal Airway Stem Cells Yield Alveoli *In Vitro* and during Lung Regeneration following H1N1 Influenza Infection.
  Kumar PA[*], Hu Y[*], Yamamoto Y, Neo BH, Tay SW, Mu D, Yan S, Lim SJ, Daghers R, Zielonka E, Wang DY, Chow VT, Crum CP, Xian W[£], McKeon F[£]. **Cell**. 2011 Oct 28;147(3):525-38.

- Residual embryonic cells as precursors of a Barrett's-like metaplasia. Wang X[*], Ouyang H[*], Yamamoto Y[*], **Kumar PA**, Wei TS, Dagher R, Vincent M, Lu X, Bellizzi AM, Ho KY, Crum CP, Xian W[£], McKeon F[£]. **Cell**. 2011 Jun 24;145(7):1023-35.

[*] Equally contributing first authors
[£] Corresponding authors